

Designing and Evaluating Carbide-Derived Carbon

As a Novel Biomaterial for Hip Implants

By

Eik-lang Lau

B.S, Tennessee Technological University, 1997

M.S, Tennessee Technological University, 1999

THESIS

Submitted as partial fulfillment of the requirements
for the degree of Doctor of Philosophy in Bioengineering
in the Graduate College of the
University of Illinois at Chicago, 2015

Defense Committees:

Michael McNallan, Chair and Advisor, Department of Material Engineering

Michael Cho, Co-Chair and Co-advisor

Michael Stroschio

Mathew Mathew, Rush University, Department of Orthopedics

Yury Gogotsi, Drexel University, Department of Materials Science & Engineering

Ali Erdemir, Argonne National Laboratory

DEDICATION

This thesis is dedicated to my husband, Yun Sun Lee, without whom it would never have been accomplished.

ACKNOWLEDGMENTS

First of all, I want to thank my advisor, Dr. McNallan, for his guidance and for being so supportive throughout the entire program. He made me realized the power of being supportive and complementary on my desire to want to be a better student. I am going to keep this learning in mind at all time, especially when come to guiding my children.

Secondly, I want to thank Dr. Cho and Dr. Mathew for all the supports they provided me throughout this research. Their support had helped me tremendously in completing the experiments and testing within a timely manner. I sincerely thank them for opening up their labs for me and let me be part of the labs.

Also, I want to thank Dr. Gogotsi for his help with the post chlorination-vacuum treatment and for the very interesting and concise technical discussions during the research. I vividly remember there were numerous times during our skype teleconference calls, I was thinking to myself after Dr. Gogotsi voiced his suggestions “That makes sense and how come I did not think of that”. It is really my pleasure to have a chance to work with someone who is so knowledgeable and astute.

Additionally, I want to thank the following individuals for their supports and assistance in completing this research. Every one of them contributed a piece of the puzzle which allowing me to complete the entire puzzle rather effortlessly. With that, I sincerely thank them and they will always be in my memory:

Dr. Stroschio, Dr. Erdemir, Dr. Sun Shan, Farah Sherif, Kai Yuan Cheng, Jason Wong, Maria-Joao Runa, Maria F. Alfaro, Eric Schmidt, Dr. Alan Nicholls, Sai Desai, Eric Lee, Elias Saltz, and Rex Lip.

TABLE OF CONTENTS

1.0	INTRODUCTION	1
2.0	LITERATURE REVIEW	9
2.1	Carbon.....	9
2.2	Silicon Carbide.....	10
2.3	Carbide Derived Carbon (CDC)	11
2.4	Carbons Used in Biomedical Application.....	13
2.5	Definition of Biocompatibility and Toxicity in Biomedical Engineering	14
2.6	Biocompatibility and Toxicity of CNTs	14
2.7	Bio-tribology with a Focus of Artificial Joints	15
3.0	Experimental Materials	17
3.1	CDC Powder	17
3.2	Polycrystalline Silicon Carbide.....	18
3.3	Reference Materials for Biocompatibility	20
3.4	Bovine Calf Serum Solution for Tribological Test.....	21
3.5	Reference Materials for Tribological Test.....	22
4.0	Experimental Setup and Approaches	24
4.1	CDC Synthesis	24
4.2	Post Synthesis Treatment.....	25
4.3	In-vitro Cytotoxicity Tests and Cell Culture	28

4.4 Indirect Contact Cytotoxicity for CDC Powder.....	29
4.5 Indirect Contact Cytotoxicity for CDC layer.....	33
4.6 Indirect Contact Cell Proliferation for CDC layer.....	34
4.7 Direct Contact Cytotoxicity for CDC layer	35
4.8 Direct Contact Cell Proliferation for CDC layer	36
4.9 Bio-tribological Test	37
4.10 CDC Sample Polishing	40
5.0 Characterization Techniques.....	41
5.1 Raman Spectroscopy.....	41
5.2 Scanning Electron Microscopy	43
5.3 Energy Dispersive X-ray Spectroscopy	44
5.4 Quantitative Cell Viability using CCK-8.....	45
5.5 Qualitative Cell Viability using Live/dead Cell Viability Kit	52
5.6 Protein Adsorption using Pierce™ Bicinchoninic Acid (BCA) Protein Assay Kit.....	54
5.7 Volumetric Wear Rate Determination with Zygo.....	55
6.0 Results and Discussions.....	57
6.1 Determine the Effect of Residual Chlorine and Submicron CDC Particles on the Biocompatibility of CDC Powder.....	57
6.2 Determine the Effects of key CDC Processing Parameters on Tribological Properties of CDC Specimens under Physiological Simulated Conditions	64
6.2.1 Effect of Polishing on Wear Rate	65
6.2.2 Effect of Sliding Frequency on Wear Rate	67

6.2.3	Effect of Sliding Time/Cycle on Wear Rate	69
6.2.4	Effect of Processing Parameters on Friction Coefficient and Wear Rate	71
6.2.5	Effect of Protein on Friction Coefficient and Wear Rate	87
6.2.6	Comparison of 100,000 Sliding Cycles Data between CDC and CoCrMo	93
6.2.7	Wear volume of the Counterpart (alumina ball).....	95
6.3	Determine the Effect of Post Chlorination Treatments on the Biocompatibility of the CDC Specimens.....	96
6.3.1	Effect of Hydrogen Post Treatment on Biocompatibility of CDC Specimens ..	98
6.3.2	Effect of Vacuum Post Treatment on Biocompatibility of CDC Specimens...112	
6.3.3	Effect of Ammonia Post Treatment on Biocompatibility of CDC Specimens	116
7.0	Conclusions.....	120
8.0	References.....	125

LIST OF TABLES

Table 1: Typical Physical Properties of α -SiC Layer Specimen [17] [46]	19
Table 2: Chemical Composition of CoCrMo (Allvac TJA-1537, UNS # R31537) [47].....	23
Table 3: ISO Requirements for Extraction (Solid-to-solvent) Ratio [49].....	30
Table 4: Mechanical Properties and Initial Hertzian Contact Stress Values	39
Table 5: Chemical Composition of CDC Powder.....	57
Table 6: EDS Analysis Result for the CDC Powder Samples Before and After Extraction ..	62
Table 7: Summary of Processing Parameters Studied	64
Table 8: Summary of Polishing Effect Data	66
Table 9: Summary of Sliding Frequency Effect on Wear Rate	68
Table 10: Summary of Sliding Time Effect on Wear Rate.....	70
Table 11: Summary of Processing Parameters Studied and the Respective Experiments.....	72
Table 12: Summary of OFAT Experiments.....	72
Table 13: Summary of Processing Parameters Effect on CDC Wear Rate	73
Table 14: EDS Result for CDC-28	79
Table 15: Summary of Protein Adsorption Test Result.....	88
Table 16: Summary of Protein Concentration Effect on Wear Rate	90
Table 17: Summary of Protein Concentration Effect on Wear Rate (100,000 Cycle)	91
Table 18: Summary of 100,000 Cycle Wear Test Conditions and Results for CDC and CoCrMo	94
Table 19: Summary of Hardness and Wear Result on the Alumina Balls [61]	95

Table 20: Summary of CDC Specimens with and without Post Treatment98

Table 21: Summary of Hydrogen Post Treatment Effect on Biocompatibility of CDC.....99

Table 22: EDS Test Result for CDC Specimens with and without Hydrogen Treatment.....101

Table 23: Summary of Vacuum Post Treatment Effect on Biocompatibility of CDC113

Table 24: EDS Test Result for CDC Specimens with and without Vacuum Treatment114

Table 25: Summary of Ammonia Post Treatment Effect on Biocompatibility of CDC.....117

Table 26: EDS Test Result for CDC Specimens with and without Ammonia Treatment.....118

LIST OF FIGURES

Figure 1: Main Components of Hip Implants ^a	1
Figure from American Academy of Orthopedic Surgeons [2]	1
Figure 2: Schematic of Typical CDC Structures [7]	4
Figure 3: SEM Images of CDC Powder, YC-TCT-1	17
Figure 4: As-fired (left) and Polished SiC Specimens	18
Figure 5 SEM Micrograph of α -SiC Layer Specimen	19
Figure 6: Schematic of CDC Synthesis Apparatus	25
Figure 7: High Temperature Furnace Equipped with Vacuum Pump	27
Figure 8: Extraction of CDC Powder	30
Figure 9: Extraction of CDC Tile Specimen	34
Figure 10: Advanced Linear Reciprocating Tribometer	37
Figure 11: Renishaw 2000 Raman Spectrometer	42
Figure 12: Raman Spectrum for Graphitic Carbon, CDC	42
Figure 13: Hitachi S-3000N Variable Pressure SEM	43
Figure 14: JEOL JSM-6490 LV SEM	44
Figure 15: Tetrazolium Salt (WST-8) and Colored Product Formazan in CCK-8 [53]	45
Figure 16: MG-63 Cells Distribution in a 96-well Plate	46
Figure 17: Cell Viability Results for 9-Scan and 25-Scan	47
Figure 18: Absorbance Reading vs.CCK-8 Incubation Time	48
Figure 19: Absorbance Readings at Day 1 and Day 3 for Different Seeding Densities	49

Figure 20: Absorbance Reading in PBS and Cell Culture Medium	50
Figure 21: Absorbance Readings vs. Viable Cells per Well at Three Different Days.....	51
Figure 22: Calibration Curve of Absorbance Reading vs Viable Cells per Well	52
Figure 23: Schematic of the Zygo New View 6300 [56].....	56
Figure 24: Fish Bone Diagram of CDC Cytotoxicity	58
Figure 25: SEM Image of Furnace Treated CDC Sample – Visible Sub-micron Particles	59
Figure 26: SEM Image of Centrifuged CDC Sample – No Sub-micron Particles.....	59
Figure 27: Cytotoxicity of CDC Powder Samples.....	60
Figure 28: Fluorescence Images of CDC Powder Samples	61
Figure 29: SEM and EDS for the Sub-Micron Particles.....	63
Figure 30: Wear Rate of CDC Specimens before and after Polishing.....	66
Figure 31: Wear rate of CDC and Standard Specimens at Different Sliding Frequencies	68
Figure 32: Wear rate of CDC and Standard Specimens at Different Sliding Time/Cycle	71
Figure 33: Wear rate of CDC Specimens at Different Processing Times.....	74
Figure 34: Wear rate of CDC Specimens at Different Chlorination Temperatures.....	76
Figure 35: SEM Images of CDC Specimens at 100x Magnification.....	76
Figure 36: SEM Images of CDC-28	80
Figure 37: Wear rate of CDC Specimens with Different Post Treatment Gas Mixutres.....	81
Figure 38: Wear rate of CDC Specimens with Different Post Treatment Times	83
Figure 39: Friction Coefficient Curves for CDC-17 and CDC-19 in BCS Solution	84
Figure 40: 100,000 Cycle Wear Rate Comparison between CDC-17 and CDC-19.....	85

Figure 41: Zygo Images of 100,000 Sliding Cycles Wear Scars	86
Figure 42: Protein Adsorption Result for CDC Specimens	88
Figure 43: Average Wear Rate vs. Adsorbed Protein for CDC Specimens.....	89
Figure 44: Summary of Protein Concentration Effect on Wear Rate	90
Figure 45: Effect of Protein Concentration on Friction Coefficient Curves.....	91
Figure 46: Summary of Protein Concentration Effect on Wear Rate (100,000 Cycles).....	92
Figure 47: Effect of Protein Concentration on Friction Coefficient Curves (100,000 Cycles)	92
Figure 48: Comparison of 100,000 Cycle Wear Test Results between CDC-17 and CoCrMo	94
Figure 49: Wear Result on the Alumina Balls	96
Figure 50: Summary of Hydrogen Post Treatment Effect on Biocompatibility	100
Figure 51: Percent Viable Cell of PE vs. Residual Chlorine for Hydrogen Treated Specimens	101
Figure 52: Fluorescence Images for Ti6Al4V at Day 2 of Cytotoxicity Test	103
Figure 53: Fluorescence Images for CDC-29 at Day 2 of Cytotoxicity Test	104
Figure 54: Fluorescence Images for CDC-30 at Day 2 of Cytotoxicity Test	105
Figure 55: Fluorescence Images for CDC-13 at Day 2 of Cytotoxicity Test	106
Figure 56: Fluorescence Images for CDC-19 at Day 2 of Cytotoxicity Test	107
Figure 57: Fluorescence Images for CDC-25 at Day 2 of Cytotoxicity Test	108
Figure 58: Fluorescence Images of Ti6Al4V at Day 7 of Cell Proliferation Test.....	109

Figure 59: Fluorescence Images of CDC-13 at Day 7 of Cell Proliferation Test.....110

Figure 60: Fluorescence Images of CDC-19 at Day 7 of Cell Proliferation Test.....111

Figure 61: Summary of Vacuum Post Treatment Effect on Biocompatibility of CDC.....113

Figure 62: Fluorescence Image for CDC-24 at Day 2 of Cytotoxicity Test.....115

Figure 63: Fluorescence Images for CDC-26 at Day 2 of Cytotoxicity Test116

Figure 64: Summary of Ammonia Post Treatment Effect on Biocompatibility of CDC117

Figure 65: Fluorescence Images for CDC-23 of Cytotoxicity Test.....119

LIST OF ABBREVIATIONS

BCA	Bicinchoninic Acid
BCS	Bovine Calf Serum
BSA	Bovine Serum Albumin
CCK-8	Cell Counting Kit-8
CNTs	Carbon Nanotubes
CDC	Carbide Derived Carbon
CoF	Friction Coefficient
CVD	Chemical Vapor Deposition
EMEM	Eagle-Minimal Essential Medium
EDS	Energy Dispersive Spectroscopy
EthD-1	Ethidium Homodimer
FBS	Fetal Bovine Serum
HRI	Hatano Research Institute
PBS	Phosphate-buffered Saline Solution

SiC	Silicon Carbide
SEM	Scanning Electron Microscopy
Ti-6Al-4V	Titanium Type-V Alloy
UHMWPE	Ultra-high Molecular Weight Polyethylene
XPS	X-Ray Photoelectron Spectroscopy
WST-8	Tetrazolium Salt

EXECUTIVE SUMMARY

Hip replacement is one of the most common orthopedic surgical procedures and is usually required due to arthritis or osteoporosis in older populations. Currently available hip implants are available in six combinations, which are based on the materials used for the femoral head and acetabular cup. These include metal-on-polymer, metal-on-metal, metal-on-ceramic, ceramic-on-ceramic, ceramic-on-metal and ceramic-on-polymer. Despite the discovery and availability of different combinations and different types of polymer, metal and ceramic materials, limited durability and lifespan due to degradation in service is still the main cause of hip implant failure. The need to find better biomaterials to address and extend the lifespan of the implants therefore continues apace.

Carbide-derived carbon (CDC) produced by processing silicon carbide (SiC) at high temperatures in the presence of a chlorine gas mixture was considered to potentially be a novel biomaterial for hip implants due to its excellent tribological properties in non-biological systems. That prompted the need for this research, which aimed to design and evaluate CDC as a biomaterial for hip implants.

The research was conducted in three parts:

Part 1: Determine the effects of residual chlorine and sub-micron CDC particles on the biocompatibility of CDC powder.

Part 2: Determine the effects of key CDC processing parameters on the tribological properties of CDC specimens under physiological simulated conditions.

Part 3: Determine the effects of post-chlorination treatments on the biocompatibility of the CDC specimens.

In Part 1, experiments were conducted to study the effect of residual chlorine and submicron particles independently on CDC cytotoxicity. High temperature (1400°C) vacuum treatment and high speed centrifugation were used to remove residual chlorine and submicron particles from the CDC samples. Subsequently, energy dispersive spectroscopy (EDS) analysis of the furnace-treated and centrifuged CDC samples confirmed the complete removal of residual chlorine and submicron CDC particles in the treated samples. Indirect cytotoxicity tests were conducted on CDC powder and furnace-treated CDC sample, both with and without centrifugation. The test results showed that both the furnace-treated (no residual chlorine) and centrifuged (no submicron particles) CDC samples were not cytotoxic, and the submicron CDC particles are cytotoxic only when residual chlorine is present.

Scanning electron microscopy (SEM) and EDS analysis results confirmed that there was no detectable chemical compositional difference between the submicron particles and the CDC layer. Additionally, the analysis results indicated that the extraction and the additional centrifugation/washing steps did not remove a significant amount of residual chlorine from the CDC samples, therefore supporting previous findings that the residual chlorine is chemically bonded to the CDC structure.

In Part 2, tribological test variables such as polishing of specimens, sliding frequencies, and sliding time were studied to determine the appropriate test parameters for this research. It was learned that CDC specimens should be lightly polished to remove loosely adhered

particles before their use in tribological testing to allow consistent evaluation of CDC microstructure effect on the wear rate. As expected, the different sliding frequencies (different dwell times) studied had negligible impact on the wear rate of CDC and on ultra-high molecular weight polyethylene (UHMWPE) specimens as these materials are non-corrosive and do not need a minimum time to form an oxide layer. In addition, higher wear rates were observed at lower sliding times for all types of specimens (UHMWPE, titanium and CDC). It is believed that this was due to the higher initial wear rate, also known as the “run-in-period”. Given this, a short sliding time of 60 minutes was used as the standard testing time in hope of observing more discriminative wear rates.

The effects of chlorination temperature (1000°C and 1100°C), chlorination time (\leq 8 hours and 19 hours) and post-chlorination treatment gas mixture (H_2 , NH_3 and vacuum) on wear rate were studied. In general, the experimental data showed no significant wear rate difference from CDC produced as the result of:

- Long vs. short processing times
- Chlorination temperature of 1000°C vs. 1100°C
- Post-chlorination treatment with H_2 and vacuum

However, SEM analysis revealed that the extensive processing conditions (long processing time and high temperature) resulted in cracks on the CDC layer which was believed to be caused by shrinkage of CDC microstructure when it was converting to the graphitic structure. Additionally, the results also indicated that the form transformation was a function of post-treatment gas mixture, with NH_3 being the most aggressive.

The effect of protein concentration in the tribological testing solution on wear rate was studied using bovine calf serum (BCS) solution (30 g/L of protein) and distilled water (0 g/L of protein). Lower wear rate and friction coefficient were obtained on the tests conducted in distilled water. The finding was confirmed by conducting 100,000 Cycle (27.8 hours) sliding tests, and further investigated with protein adsorption test using PierceTM Bicinchoninic Acid (BCA) protein assay kit. The test results showed that only a small amount of BSA protein (9-25 %) was adsorbed on the CDC surface. It is possible that the presence of protein increased the CDC surface roughness and reduced the effectiveness of the lubricant film thickness, therefore resulting in a higher wear rate.

CDC wear rates were compared to CoCrMo (the “gold standard” of existing hip implants) wear rates tested under comparable testing apparatus and conditions. This comparison showed that CDC exhibited significantly lower wear rate when compared to the wear rate of CoCrMo.

Due to the hardness difference between the test specimens and the alumina balls, and the mechanical action applied during the tribological test, some wear on the alumina balls were observed. To support the hypothesis that CDC will form a smooth layer after the run-in period, wear volumes on the alumina balls after selected tribological test were measured. As expected, sliding relatively hard SiC on the alumina balls resulted in a higher wear volume when compared to that observed for CDC specimens sliding on alumina balls. Additionally, similar wear volumes were obtained for the CDC specimens sliding for 28,800 and 100,000 cycles, which indicates further reduction of the friction coefficient and wear on the contacting

components.

In Part 3, the effect of post-chlorination hydrogen treatment on biocompatibility of CDC specimens were studied using 4 tests and 2 cell viability assays. It was learned that the CDC specimens were not very toxic, therefore more severe testing conditions were needed to produce discriminative test results. Collectively, the test results indicated that the post-chlorination hydrogen treatment improved the biocompatibility of the CDC specimens, and the treatment effect was more pronounced on the CDC specimens produced from the short processing times, which should have thinner CDC layers. Overall, it can be concluded that the CDC layers are relatively biocompatible. CDC layers with similar biocompatibility as the Ti6Al4V alloys can be produced by the selected chlorination conditions and post-chlorination hydrogen treatment.

The effect of post-chlorination vacuum treatment on the biocompatibility of CDC specimen was also studied. Study results showed that the vacuum treatment appeared to be able to remove a significant amount of residual chlorine in CDC samples, however the resultant CDC samples were still cytotoxic. It is believed that the cytotoxicity of the vacuum treated CDC samples was due to the presence of submicron CDC particles in the samples; visible cracks in the samples indicated that the integrity of the samples was compromised.

The effect of post-chlorination ammonia treatment on the biocompatibility of CDC specimen was also studied. Study results showed that the ammonia treatment appeared to be able to remove significant amount of residual chlorine in CDC samples, but the resultant CDC sample was very cytotoxic. EDS analysis of the ammonia treated sample showed that the treatment did not generate unexpected chemical composition.

Conclusion:

Biocompatible CDC layers can be produced by modulating chlorination conditions and application of a post-chlorination hydrogen treatment. Excessive processing conditions (high temperature and long processing time) are not recommended as these will affect the integrity of the resulting CDC layer.

1.0 INTRODUCTION

Hip replacement is one of the most common orthopedic surgical procedures and is usually required by older population due to Arthritis and/or Osteoporosis. Arthritis is affecting an estimated 8.6 million people in the United States as of 2005 and is projected to affect ~71 million people by 2030 [1]. Hip replacement is a cost effective option for the arthritis patients to live a normal life and resume normal activity without too much risk since hip replacement treatment has a very high success rate. A total hip replacement consists of 3 main parts as shown in Figure 1: (1) Femoral stem, (2) Femoral head, and (3) Acetabular components.

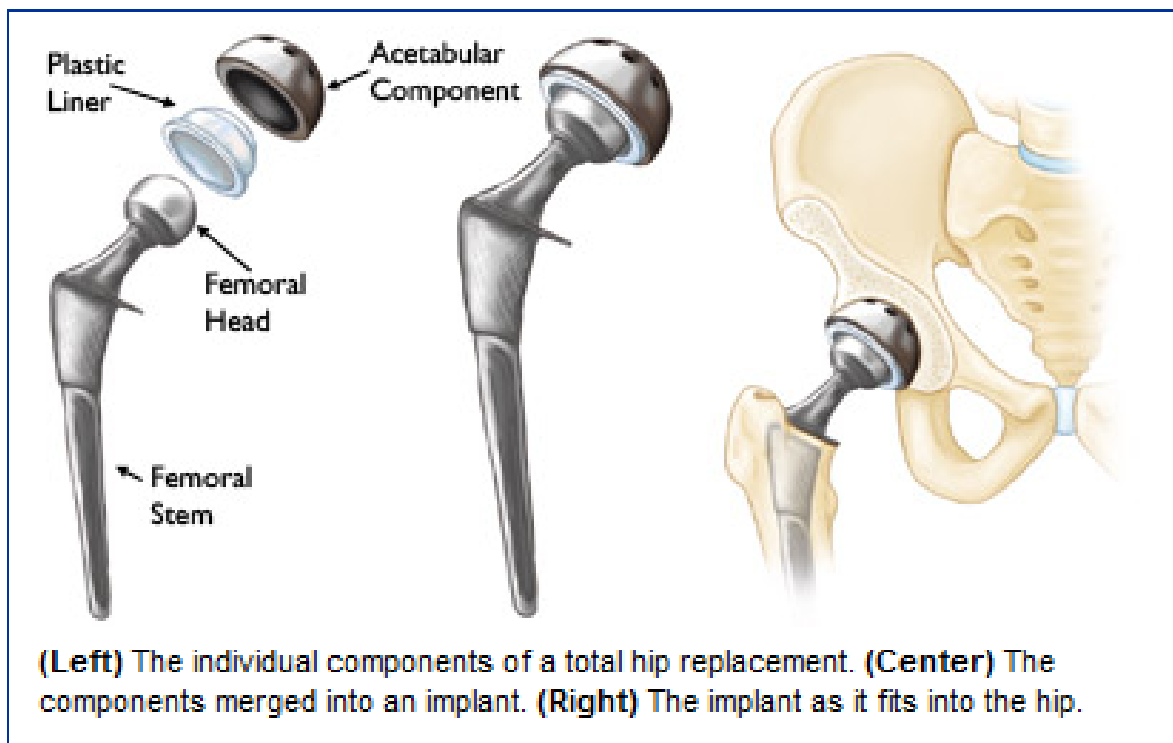


Figure 1: Main Components of Hip Implants^a

^aFigure from American Academy of Orthopedic Surgeons [2]

Currently commercially available hip implants are available in six combinations based on the materials used for the femoral head and acetabular cup: metal-on-polymer, metal-on-metal, metal-on-ceramic, ceramic-on-ceramic, ceramic-on-metal and ceramic-on-polymer. The metals used include stainless steel, cobalt chromium molybdenum alloy and titanium aluminum vanadium alloy. The polymer used is mainly ultra-high molecular weight polyethylene (UHMWPE). Ceramic implants are mainly made out of alumina and zirconia.

In hip replacement, the acetabular cup is inserted into the hip socket and replaces the worn cartilage. It is constantly in contact with the femoral head therefore is prone to friction and wear. **One of the main challenges with hip implants is its limited durability and lifespan due to degradation in service. The main causes of failure of hip implants are loosening of the implant due to wear, corrosion, and inflammation due to micro debris that are bioreactive [3] [4].**

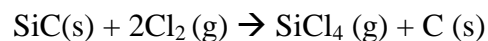
Metal-on-polymer implant is the most popular implant choice as it has a long standing proven track record. However, it suffers from wear degradation resulting in polyethylene wear debris that contributes to osteolysis and results in implant loosening and failure.

Metal-on-metal implants have less wear than metal-on-polymer and gave lower friction coefficient in bovine serum but still could not escape from the failure due to wear debris [1]. Tribological issues severely affect the performance of metal-on-metal implants and FDA issued a recall on metal-on-metal hip implant in February 2011. In fact, the recall caused a surge in research to better understand the failure mechanisms of metal-on-metal, which has less wear than metal-on-polymer [1]. One study reported that graphitic materials were observed on metal-on-metal hip implants retrieved from patients [1]. **Even though the exact mechanism for how the graphitic material is formed has not been determined, the**

observation supports the hypothesis that the presence of graphitic materials lowers the friction and/or wear in the implant.

Ceramic-on-ceramic hip components have superior wear resistance and lower wear rates than both metal-on-metal and metal-on-polymer implants but it has no long term data available and the early generation of ceramic-on-ceramic implants was susceptible to fracture. The wear debris problems with the metal-on-polymer and metal-on-metal implants inspire the need to find better biomaterial for hip implant.

It is known that silicon carbide (SiC) is widely used in applications requiring high endurance due to its superior mechanical and chemical properties. However, it is not lubricious and suffers from high frictional losses when used in sliding contact applications, and therefore presents the need for more lubricious and durable material for contact applications. That led to the invention of CDC produced by a novel high temperature chlorination process [5] over a decade ago.



In the process, SiC is exposed to chlorine gas at high temperature. Chlorine reacts with silicon to form volatile compounds, leaving carbon behind. Previous studies concluded that a wide variety of carbon structures were observed in CDC samples depending on the chlorination conditions [6]. A schematic of the carbon structures in a typical CDC sample is shown in Figure 2 [6]. In general, nano-crystalline hexagonal diamond and cubic diamond were observed at the SiC and CDC interface while graphitic structure was observed near the top surface of the CDC layer [6].

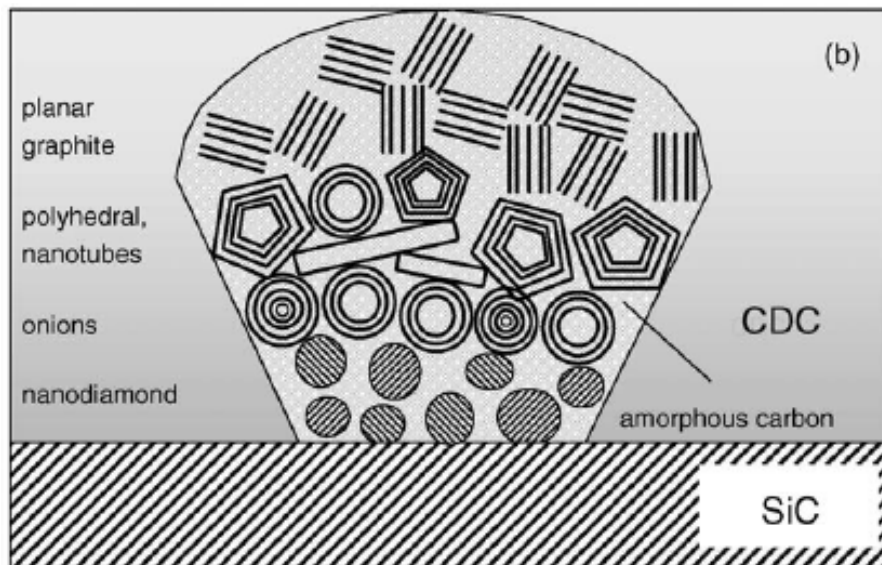


Figure 2: Schematic of Typical CDC Structures [7]

The structural variation over the CDC layer depth resulted in a graded hardness; high hardness at the SiC and CDC interface and a gradual reduction to lower hardness at the CDC interface [7]. The graded hardness and specifically the nanodiamond CDC hardness closely matches the hardness of SiC gave CDC excellent resistant to spallation and delamination [7].

CDC was reported to possess excellent mechanical properties and excellent tribological properties (friction coefficient ~ 0.03) depending on the synthesis conditions and tribological testing apparatus/setup and environmental conditions [7] [8] [9]. Extensive research has been conducted to understand the factors that could affect the tribological properties of a CDC layer in non-biological systems using a pin-on-disc apparatus. It was determined that the tribological properties are affected by the CDC structure, surface chemistry and residual chlorine [5] [8] [9] [10] [11] [12] [13] [14] [15] [16] [17] which are directly affected by the chlorination conditions and post chlorination treatment.

A chlorination temperature of 1000°C was deemed to allow higher CDC growth rate as compared to 700-800 °C [5]. Graphite is the thermodynamically stable phase of carbon therefore higher chlorination temperatures tend to produce more graphitic carbon by driving the process rapidly toward equilibrium. A mixture of amorphous carbon and rhombohedral crystalline graphite were observed in CDC produced at chlorination temperature of 1200 °C (10 hours with gas mixture of Cl₂:H₂ = 5.0:2.5) and it was concluded that the higher temperature improved the tribological properties of CDC due to the self-lubricating properties of the rhombohedral crystalline graphite [13]. Higher chlorination temperature (1000°C vs. 900°C at 3.5% Cl₂-Ar for 8 hours) produced more graphitic CDC was confirmed by another study [17].

Graphitic CDC was observed from chlorination at 1000 °C using gas mixtures without hydrogen. Inclusion of hydrogen in the chlorination gas mixture allows formation of nanocrystalline diamond CDC with mechanical properties close to that of a SiC [5]. It was reported that higher hydrogen content in the chlorination gas mixture improved the tribological performance of the resulting CDC layer [11]. Another study found that the diamond-to-graphite ratio decreased with increasing hydrogen content in the gas mixture and the CDC pore size increased up to 2.5nm as a function of the hydrogen content [14]. As a result, the hardness and elastic modulus of the CDC decreased with increasing hydrogen content. This could be an artifact of slower reaction rate and longer chlorination time (led to more graphitic CDC) when higher hydrogen content was used in the gas mixture. It was reported that increasing the hydrogen content over 2:1 Cl₂:H₂ in the gas mixture had a dramatic effect on the kinetics of the reaction [5] [14]. Furthermore, it was reported that

inclusion of hydrogen in the chlorination gas mixture resulted in residual chlorine molecules that were chemically bonded to the CDC and cannot be removed at the post-chlorination hydrogenation step [17].

Due to the reactive (dangling/unsatisfied bonds) CDC surface a lower CDC friction coefficient was obtained with post chlorination-hydrogen treatment and decreasing humidity in the tribological test environment [9] [10] [12] [17]. Previous data support the hypothesis that the post chlorination-hydrogen treatment eliminated the dangling bonds with the highly reactive hydrogen atom and therefore reduced CDC friction coefficient.

Additionally, previous study shows that nanoporous CDC layer can retain a significant amount of chemical bonded residual chlorine that is hard to remove [17] [18]. Also, several methods such as incubating in cell culture media, immersing in water, boiling in deionized water, and sterilization in an autoclave were tested to remove the chlorine however none of the methods were successful in eliminating the biocidal activity of the CDC layer produced from the chlorination process. It was reported that CDC containing 2 wt% of chlorine killed all the bacterial spores in 120 minutes [18]. The same study reported observation of a higher chlorine level in larger CDC pores. Furthermore, another study demonstrated that the porosity of CDC can be customized by optimizing the chlorination temperature, particle size of carbide precursor, and post chlorination treatment [19].

To summarize the previous work, tribological and mechanical properties of a CDC layer are affected by the CDC structure, surface chemistry and residual chlorine which are directly affected by the chlorination process and post chlorination treatment. There is no doubt that pure carbon has excellent biocompatibility [19], however the residual chlorine in the CDC layer could be detrimental to biocompatibility of the CDC layer. The amount of residual

chlorine retained in the CDC may be affected by the CDC structure and porosity. Significant research has been conducted to determine the factors that could affect the tribological and mechanical properties of CDC. However, none of the studies was conducted in the context of a biomaterial where specific ASTM or ISO tests, mimicking biological systems specifically hip joint, should be used for the evaluation. It is well known that the protein concentration in biological fluids such as bovine serum is important to determine friction and wear [20] as the adherence of proteins to the surface could effectively increase surface roughness and reduce the effectiveness of lubricant film thickness. CDC surface characterization to better understand protein adsorption ability could be critical in biotribology. Additionally, the effect of physio-chemical properties of CDC such as retained chlorine and submicron particle size on biocompatibility has not been studied. There was a need to conduct a comprehensive study in the context of a biological and/ or hip joint system, specifically to design and develop a CDC layer for use as a novel biomaterial for hip implant.

This thesis work can be divided into 3 parts:

Part 1: Determine the effect of residual chlorine and sub-micron CDC particles on the biocompatibility of CDC powder.

Part 2: Determine the effects of key CDC processing parameters on tribological properties (Coefficient of friction and wear rate) of CDC specimens under physiological simulated conditions (linear reciprocating tribometer and protein solution).

Part 3: Determine the effect of post chlorination treatments on the biocompatibility of the

CDC specimens.

Successful completion of this project will serve as a promising first step toward alleviating the main cause of hip implants failure: implant loosening due to wear, corrosion, and inflammation caused by micro debris.

2.0 LITERATURE REVIEW

2.1 Carbon

Carbon, C, atomic number 6 is a member of group 4 on the periodic table. It has four electrons in its valence shell that can hold eight electrons therefore each carbon atom can form covalent chemical bonds with up to four different atoms. This allows carbon to bond with other elements as well as with itself. Carbon is the fourth most ample element in the universe by mass after oxygen, hydrogen and helium [21]. It is the second most abundant element in the human body by mass after oxygen [21].

Carbon has a very high melting point and remains unreactive at normal conditions. At high temperature, carbon reacts with oxygen and some metals to form carbon oxides and metal carbides, respectively. Carbon has three naturally occurring isotopes (same number of protons for each atom, they differ in neutron numbers; the neutron number has drastic effects on nuclear properties) namely ^{12}C , ^{13}C , and ^{14}C where the former two are stable and the third one is radioactive [21].

Carbon has many allotropes and the properties of carbon vary widely with the allotropic form. The most well-known allotropes include graphite, diamond, amorphous carbon and fullerenes such as buckyballs, carbon nanotubes, carbon nanobuds and nanofibers [21]. Diamond is highly transparent, hard, high thermal conductivity and low electrical conductivity. In contrast, graphite is opaque, soft and a good conductor. Graphite is the most thermodynamically stable form under terrestrial conditions. Fullerenes have a graphite-like structure and contain pentagons (or even heptagons) of carbon atoms, which bend the sheet into cylinders, spheres or ellipses [21]. Fullerenes do not have high melting points and are

the only carbon allotropes soluble in organic solvents. The cage like fullerene molecules can be used as a vehicle to carry drug and pass through cell wall.

Carbon nanotubes (CNTs) are one of the most intensively studied and characterized nanomaterials [22]. Carbon nanotubes consist of tiny cylinders of carbon differing in size and atomic arrangement that have very different properties. Single or multiple-walled carbon tubes, made from concentric nanotubes (one tube inside a larger nanotube) can be formed. It has many potential applications due to its outstanding mechanical, thermal electronic, electrical, chemical and physical properties [23]. Some nanotubes are excellent insulators, semiconductors or conduct electricity and can be stronger than steel [23]. In addition, its large surface area can be used a component of industrial catalyst. CNTs are hydrophobic hence insoluble in water which limit their application in biomedical systems. Various functionalization methods have been utilized to convert CNTs to be hydrophilic [23].

2.2 Silicon Carbide

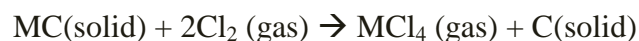
SiC is the chemical formulation for silicon carbide. It is a compound of silicon and carbon. It occurs naturally as an extremely rare mineral, therefore vast majority of commercially available SiC are produced synthetically [24]. The type of manufacturing process determines its density, grain size and hardness. Silicon carbide manufactured by different processes can be polished into difference surface finishes (CVD: a few Angstroms, reaction bonded: 20 - 50 Angstrom, hot pressed: 50 - 100 Angstrom, and sintered: 100 Angstroms and often much higher) [24]. Large crystals of silicon carbide are grown synthetically as the diamond imitation jewel moissanite [24]. There are about 250 polymorphs of SiC with alpha silicon carbide (α -SiC) as the most common one, follows by beta silicon carbide (β -SiC) [25]. α -SiC

is formed at temperatures greater than 1700°C and exhibits a hexagonal crystal structure. On the other hand, β -SiC is formed at temperatures below 1700°C and has a zincblende crystal structure similar to diamond [26]. SiC is an extremely hard, durable substance that is used in sliding applications like car brakes, turbine mechanics, and certain types of seals and bearings.

2.3 Carbide Derived Carbon (CDC)

CDC refers to carbon materials derived from binary or ternary carbide precursors. A number of carbides have been used to produce CDC which include SiC, TiC, Ti_3SiC_2 , WC, Al_4C_3 , Fe_3C and etc [5] [27] [28]. A wide variety of carbon structures have been reported in CDC samples depending on the carbide precursor and processing conditions: micro-porous carbon, meso-porous carbon, amorphous carbon, carbon nanotubes, onion-like carbon, nano-crystalline diamond, graphene and graphite [29].

CDC can be produced from several chemical and physical synthesis methods [30]. The most common chemical synthesis method is chlorine treatment of metal carbide in the presence of chlorine (or other halogen) gas at moderate to high temperature. In the process, chlorine reacts with the metal to form a volatile compound and leaving carbon behind.

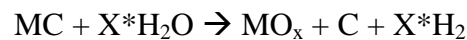


Chlorination temperatures ranging from 200° to 1200°C have been used to produce CDC. More graphitic CDC was observed at higher chlorination temperatures as graphite is the most thermodynamically stable form. It was reported that chlorination temperatures beyond

1000°C result in CDC with predominantly graphitic structures and therefore shrinkage of the material during conversion is expected [30].

In addition to the chlorine treatment, CDC can also be produced from vacuum decomposition where metal atoms in the carbides are extracted at temperature above 1200°C under vacuum. This method utilizes the high melting and boiling point of carbon as compared to the metals in the carbide, which melt and evaporate, leaving the carbon behind [31]. It was reported that this method produces CDC with higher degree of order, and carbon nanotubes and graphene can be produced [32].

Hydrothermal decomposition is another physical synthesis method for CDC production. In this process, metal carbides are reacted with water at temperature between 300°C and 1000°C under pressure of 2- 200 MPa [30].



Higher pressure and lower temperature result in higher carbon-containing gases and therefore lower solid carbon [30].

CDC's unique physical, chemical, mechanical and tribological properties offer a lot of potential applications such as energy storage, gas storage, carbon dioxide capturing, tribological coatings, protein adsorption, catalyst support and capacitive deionization [30].

2.4 Carbons Used in Biomedical Application

Carbon in activated charcoal is by far the most commonly used carbon in biomedical application. These very fine and highly porous carbon particles are very reactive and can bind to many harmful substances. In fact, this type of carbon is typically used in the hospital to treat drug overdoses and chemical poisoning. Upon oral or enteral (via tracheal tube) administration, the carbon will travel through the gastrointestinal tract. Since it is not digested so it will stay in the gastrointestinal tract until it is discharged via bowel movement.

Carbon nanotubes (CNTs) are the most widely studied materials among the type of carbon that are being investigated. The well-ordered molecular structure, high aspect ratio, unique size and shape of carbon nanotubes (CNTs) offer many excellent physical, mechanical, electrical and optical properties. It is also the most widely studied nanotube for biomedical application. Currently some of the more prominent biomedical applications of CNTs include drug delivery, tissue engineering, gene delivery, stem cell therapy, thermal therapy, biological detection and imaging [22].

2.5 Definition of Biocompatibility and Toxicity in Biomedical Engineering

The widely recognized definition for biocompatibility is the one written by D.F. Williams, “Biocompatibility refers to the ability of a biomaterial to perform its desired function with respect to a medical therapy, without eliciting any undesirable local or systemic effects in the recipient or beneficiary of that therapy, but generating the most appropriate beneficial cellular or tissue response in that specific situation, and optimizing the clinically relevant performance of that therapy” [33]. What is toxicity and how does it differ from cytotoxicity? “Nanoparticles toxicity refers to the ability of the particles to adversely affect the normal physiology as well as to directly interrupt the normal physiology organs and tissues of humans and animals” [33]. Cytotoxicity is the degree of toxicity on a substructure of an organism such as a cell.

2.6 Biocompatibility and Toxicity of CNTs

A lot of research has been conducted to study the toxicity of CNTs. Collectively, the data suggest that physicochemical properties of CNTs, such as dimensions, surface properties, functionalization, concentration and residual metal catalyst, are likely to impact the toxicity of the CNTs [34] [35] [36] [37] [38] [39] [40] [41] [42] [43]. However, the findings are inconsistent and there is no definitive conclusion on how these physicochemical properties affect the toxicity of CNTs. From this literature review, it was noted that CNTs from different sources were used in the studies. CNTs from different sources could be produced from different methods and may possess different physicochemical properties such as metal impurities. Additionally, different material characterization methods are used to characterize the CNTs, and different cell lines, cell viability and analysis methods were used to carry out

the studies. These differences make it impossible to compare the toxicity data across the different studies. Despite the inconsistent findings, there is a broad agreement that:

- Frustrated phagocytosis is uncommon in a CNT dimension threshold of less than 5 μ m,
- Well dispersed CNTs are found to be less toxic,
- Surface properties and functionalization of CNTs are key factors to reduce or modulate toxicity of CNTs,
- Dose or concentration dependent cytotoxicity is more pronounced when lower purity CNTs are used, and
- Metal residue can cause oxidative stress and cytotoxicity. Purity of CNTs is greatly depended on the method of manufacture and the method of purification. Post synthesis purification process and residual metal catalyst in CNTs should be considered when assessing cytotoxicity of CNT.

2.7 Bio-tribology with a Focus of Artificial Joints

According to the Oxford dictionary, tribology means “the study of friction, wear and lubrication, and design of bearings, science of interacting surfaces in relative motion”. Bio-tribology is the tribology of biological systems such as wear of denture, tribology of contact lenses, the wear of replacement heart valves, the lubrication of the pump in the total artificial hearts, and tribology of natural synovial joints and artificial replacements [44]. Bio-tribology study of artificial joints should be studied in conjunction with cytotoxicity study of wear debris since wear debris is one of main causes of hip implant loosening and failure.

As known that all surfaces are rough when viewed under microscopic scales. Surface roughness is typically characterized by the arithmetical mean deviation which is denoted as R_a . Surface roughness can be measured by contacting Talysurf profilometer or non-contacting white light interferometer. Typical surface roughness values for orthopaedic implants are 0.005-0.01 μm , 0.005-0.025 μm , and 0.1-2.5 μm for ceramic (alumina), metal (cobalt chrome), and plastic (UHMWPE) implants, respectively [45].

Friction is known as resistance to movement. First law of dry friction defines that the force of friction (F) is directly proportional to the applied load (W). Friction is typically expressed in a dimensionless term, coefficient of friction and is calculated by F/W . It is well accepted that coefficient of friction is greatly affected by nature of the contact surfaces and the presence of biological lubricants. Low friction is desired to reduce the stress transmitted to the fixation interface. However, low friction does not always equal to low wear volume. It was reported that the early Teflon hip joint exhibited optimal coefficient of friction but failed quickly due to wear [45].

“Wear is defined as progressive loss of substance from the operating surface of a body occurring as a result of relative motion at the surface [44]”. There are at least 5 types of wear: abrasive, adhesive, fatigue, erosive and corrosive. The former 4 wear types are mainly contributed by mechanical actions while corrosive is a result of chemical action.

3.0 EXPERIMENTAL MATERIALS

3.1 CDC Powder

CDC powders (lot number YC-TCT-1) supplied by Y-Carbon were used in the experiments to determine the effect of residual chlorine and submicron CDC particles on the biocompatibility or cytotoxicity of CDC powder. The CDC powders were produced from chlorination with pure chlorine gas at 1000°C for 6 hours and post chlorination hydrogen treatment at 600°C for 2 hours. SEM images of the CDC powder, YC-TCT-1, is shown in Figure 3.

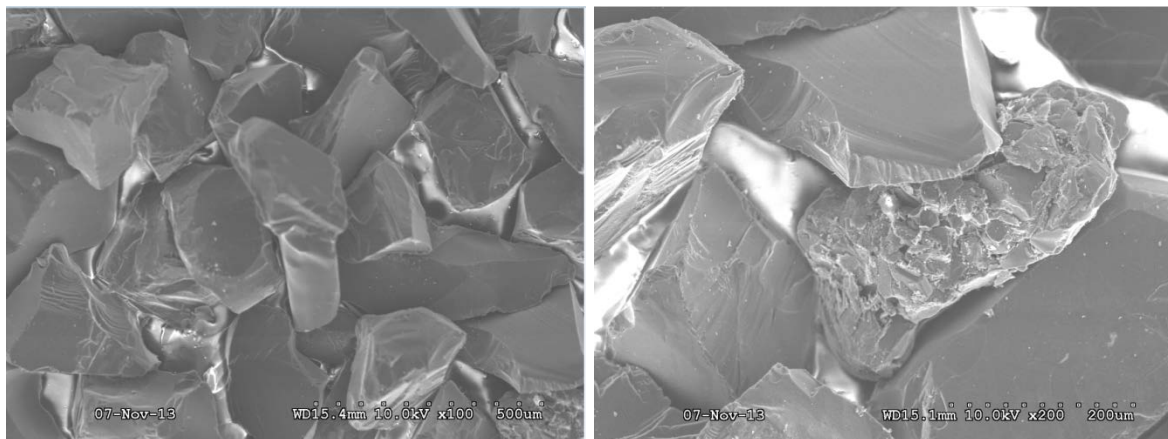


Figure 3: SEM Images of CDC Powder, YC-TCT-1

3.2 Polycrystalline Silicon Carbide

Polycrystalline α -SiC specimens supplied by Saint Gobain Ceramics (Hexoloy® SA Silicon Carbide) were used to synthesize CDC. The SiC specimens were supplied in 2 finishing conditions: as-fired and polished, as shown in Figure 4. The as-fired SiC has a surface roughness (Ra) of ~ 352 nm while the polished SiC has a surface roughness of ~ 15 nm. All the SiC layer specimens used in this research (Hexoloy® SA Silicon Carbide) are produced by pressureless sintering of submicron SiC powder. The process yields self-bonded, fine grain (less than $10\mu\text{m}$) SiC material with a theoretical density greater than 98%.



Figure 4: As-fired (left) and Polished SiC Specimens

The SEM micrograph of the α -SiC layer specimen is shown in Figure 5.

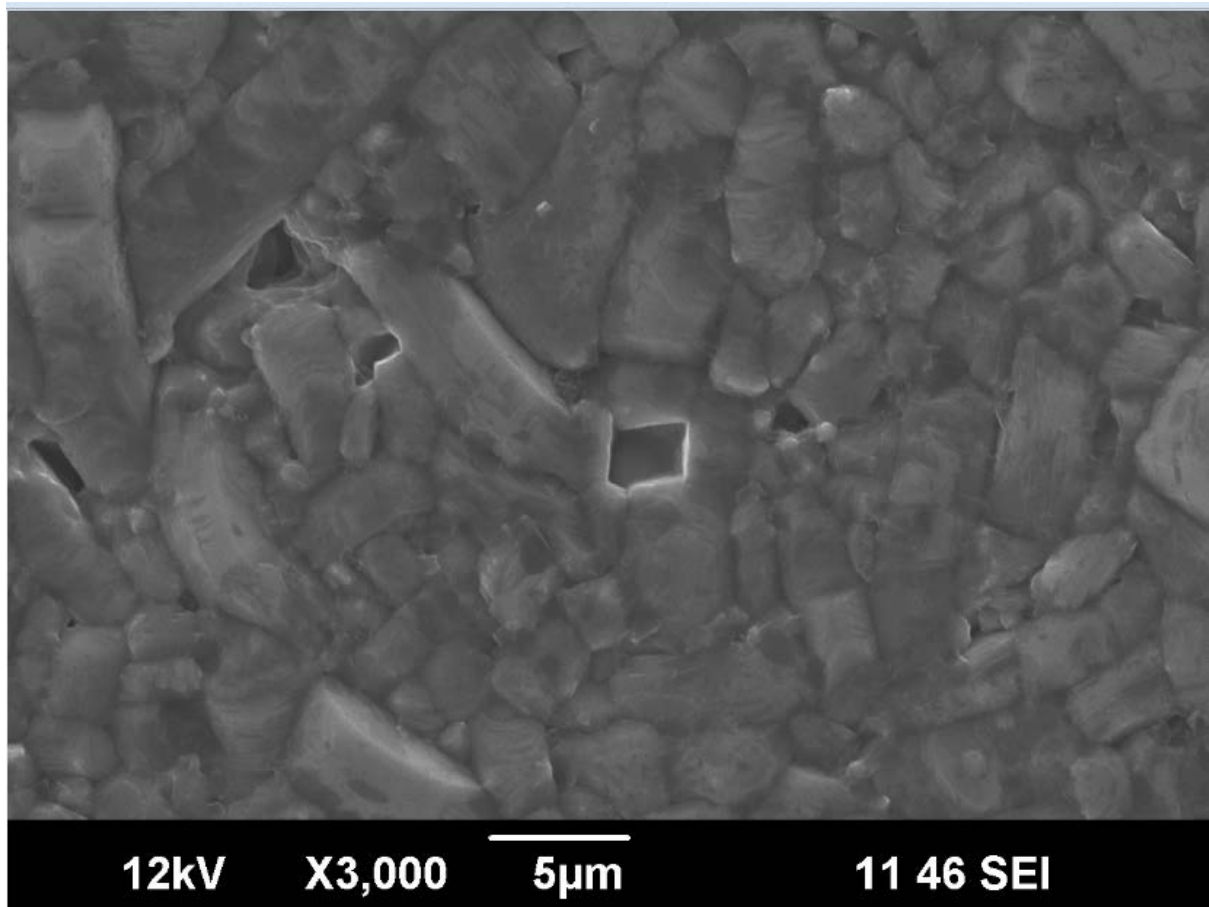


Figure 5 SEM Micrograph of α -SiC Layer Specimen

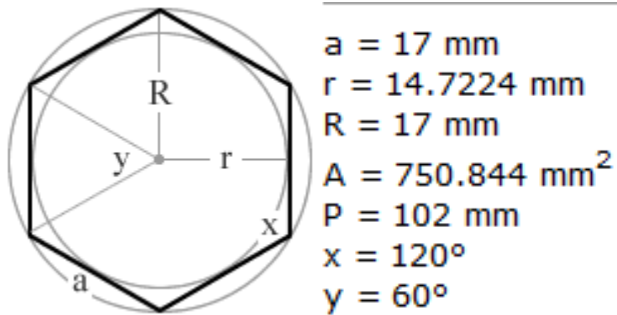
Some of the typical physical properties of the α -SiC layer specimen is tabulated in Table 1.

Table 1: Typical Physical Properties of α -SiC Layer Specimen [17] [46]

Property	Units	Typical Value
Grain Size	μm	4-10
Density	g/cm^3	3.1
Hardness (Knoop 0.1 Kg load)	kg/mm^2	2800
Modulus of Elasticity @ RT	GPa	430
Poisson Ratio	N/A	0.14
Additives	N/A	B, C

The area for one side of the specimen was calculated as following:

$$Area = \frac{3}{2} * a^2 * \sqrt{3} = \frac{3}{2} * 17 \text{ mm}^2 * \sqrt{3} = 750.8 \text{ mm}^2 = 7.5 \text{ cm}^2$$



3.3 Reference Materials for Biocompatibility

ZDBC polyurethane film (RM-B) and high density polyethylene film (RM-C) were used as the primary positive and negative controls, respectively, for the cytotoxicity tests in this research. These materials are the recommended standard materials by the Japanese guidelines for basic biological tests of medical devices (MHLW Japan, 2003) and ISO10993/TC194 for verifying sensitivity and accuracy of cytotoxicity and implantation tests. Each batch of the materials is certified for the specific biological activity and stability by bioassay in Hatano Research Institute (HRI), Food and Drug Safety Center (FDSC).

3.4 Bovine Calf Serum Solution for Tribological Test

The protein concentration of the bovine calf serum (BCS) solution used in this research is 30g/L and a pH value of 7.6. The BCS solution is prepared in 2 steps: (1) Preparation of a basic solution, and (2) Preparation of the BCS solution. Procedures for preparing the basic solution are listed as following:

- Dilute 18g of sodium chloride with 1300 mL of deionized water ,
- Mix with a magnetic stirrer for about 5 minutes,
- Add 54 g of Tris (27 g/L),
- Add 400mg of EDTA (200 mg/L),
- Mix with a magnetic stirrer for about 15 minutes,
- Calibrate pH electrode,
- Adjust solution pH to a value of 7.6 by adding a 5 N hydrochloric acid solution carefully, and
- Fill up beaker with deionized water to 2000 mL

The basic solution should be stored in a refrigerator and can be used up to 2 months. The BCS solution is prepared by:

- Defrost frozen bovine calf serum in a water bath set at 37-39°C. The protein concentration in the BCS is about 65 g/L,
- Add 272.7 mL of the BCS to a beaker,
- Add 327.3 mL of the basic solution to the beaker, and
- Mix with a magnetic stirrer for about 5 minutes.

This procedure yielded a BCS solution with 30 g/L of protein and a pH value of 7.6. The BCS solution should be stored in a refrigerator and can be used up to 1 month.

3.5 Reference Materials for Tribological Test

UHMWPE and titanium type-V alloy (Ti-6Al-4V) were used as the reference materials for the tribological test in this research as these materials are being used in the commercial hip implants. An impact-resistant slippery UHMWPE rod was purchased from McMaster-CARR. The rod was then machined into individual disc with a diameter of 15 mm and a thickness of 3 mm. Each disc was manually polished using 800 grit sand papers to get rid of the machining lines, to smooth out the surface prior to use in the tribological test.

A Ti-6Al-4V bar was purchased from Vulcanium, a division of United Performance Metals. It was manufactured per ASTM F-1472, Standard Specification for Wrought Titanium-6Aluminium-4Vanadium Alloy for Surgical Implant application. Subsequently, the titanium bar was machined into individual disc with a diameter of 15mm and a thickness of 2 mm. Each disc was manually polished prior to use. The polishing procedures include a preliminary polishing using 240, 320, 400, 600 and 800 grit sand papers, and then a final polishing to mirror finish using Texmet polishing cloth with diamond paste mixed with lubricant fluid followed by chemomet polishing cloth with colloidal silica polishing suspension.

In addition to UHMWPE and Ti-6Al-4V, wear rates of selected CDC specimens were also compared to the wear rates of CoCrMo that was tested under similar testing conditions. A CoCrMo bar was obtained from ATI Allvac (TJA-1537, UNS Number: R31537). Chemical composition of the CoCrMo bar is tabulated in Table 2. It was manufactured per ASTM F-1537, Standard Specification for Wrought Cobalt-28Chromium-6Molybdenum Alloys for

Surgical Implants, and has a density of 8.30 g/cm³ [47]. The bar was then machined into the desired dimension and manually polished prior to use [48].

Table 2: Chemical Composition of CoCrMo (Allvac TJA-1537, UNS # R31537) [47]

Chemical	Weight %
Molybdenum	5.0-7.0
Chromium	26.0-30.0
Silicon	< 1.0
Nickel	< 1.0
Manganese	< 1.0
Iron	< 0.75
Carbon	< 0.35
Nitrogen	< 0.25
Cobalt	Balance

4.0 EXPERIMENTAL SETUP AND APPROACHES

4.1 CDC Synthesis

CDC specimens were produced by heating SiC specimens with 3.5% Cl₂-Ar gas in a fused silica reaction tube inside a resistance-heated electric furnace under ambient pressure. A schematic of the CDC synthesis apparatus is depicted in Figure 6. It was learned that oxygen contamination is detrimental to the chlorination process where significant leaks in the system will impede the CDC production. Silicone sealer was used to seal all the plastic tubing connections to minimize leaks in the system. It should be pointed out that heating and cooling should be carried out in an argon gas, and the chlorine gas mixture should only be applied when the desired furnace temperature is reached. This will allow production of the desired CDC microstructure. Following are the procedures used in this research to produce CDC:

- Purge the entire system with argon gas flow at 40cm³/s (furnace tube's internal diameter= 7 cm, linear velocity = 1.04 cm/s)
- Turn on the furnace and heat to the desired temperature with argon gas flow at 25 cm³/s (linear velocity 0.65 cm/s)
- Start chlorine-argon gas mixture flow at 25 cm³/s for the desired length of time
- Turn off furnace and start argon gas flow at 25 cm³/s for the entire cool down period (8-9 hours).

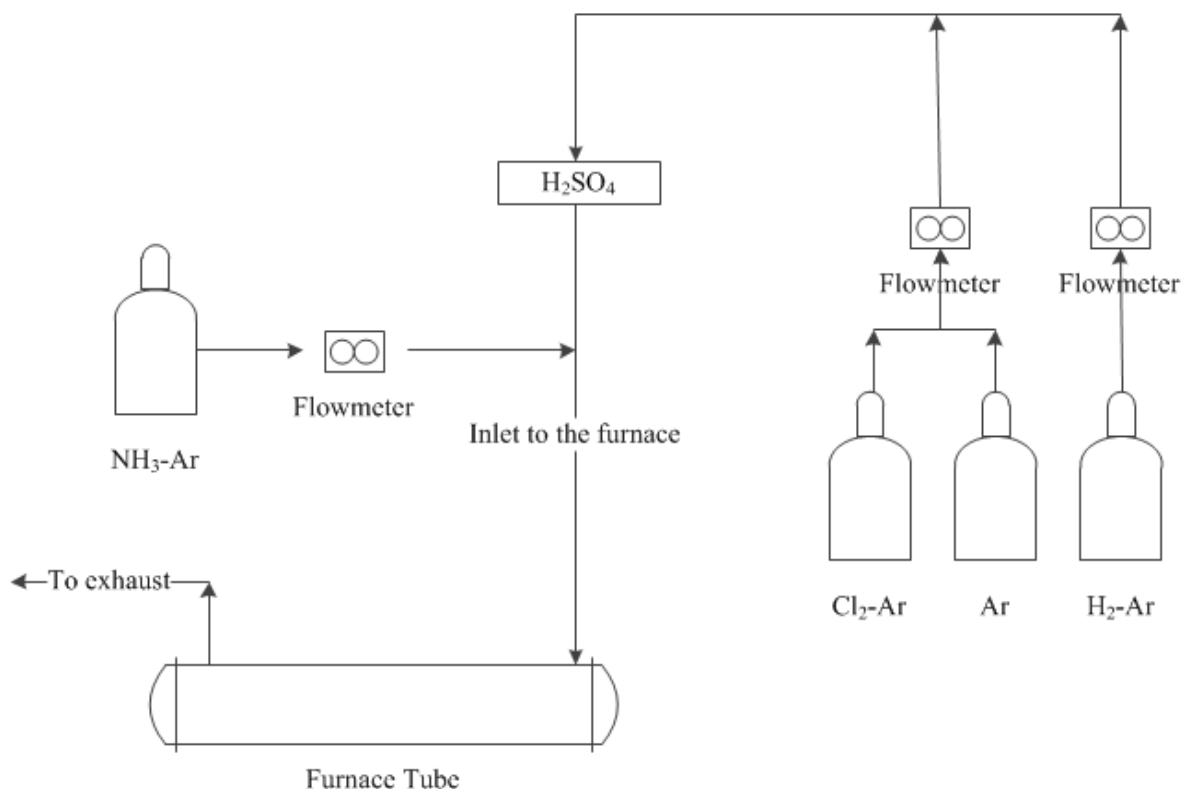


Figure 6: Schematic of CDC Synthesis Apparatus

4.2 Post Synthesis Treatment

Three post synthesis treatments were studied in this research. The treatments include:

- 5 % Hydrogen-argon treatment
- 5 % Ammonia-argon treatment
- Vacuum treatment

The post synthesis hydrogen and ammonia treatments were carried out in the same apparatus as the CDC synthesis where two procedures were used in this research, depending on the chlorination time.

Procedure for 8 hours chlorination time:

- Purge the entire system with argon gas flow at $40\text{cm}^3/\text{s}$
- Turn on the furnace and heat to the desired temperature with argon gas flow at $25\text{cm}^3/\text{s}$
- Start chlorine-argon gas mixture flow at $25\text{cm}^3/\text{s}$ for the desired length of time
- Turn off furnace and start argon gas flow at $25\text{cm}^3/\text{s}$ for the entire cool down period (overnight).
- Turn on the furnace (the next day) and heat to the desired post treatment temperature with argon gas flow at $25\text{cm}^3/\text{s}$
- Start hydrogen or ammonia gas mixture flow at $25\text{cm}^3/\text{s}$ for the desired length of time.
- Turn off furnace and start argon gas flow at $25\text{cm}^3/\text{s}$ for the entire cool down period (8-9 hours).

Procedure for 19 hours chlorination time:

- Purge the entire system with argon gas flow at $40\text{cm}^3/\text{s}$
- Turn on the furnace and heat to the desired temperature with argon gas flow at $25\text{cm}^3/\text{s}$
- Start chlorine-argon gas mixture flow at $25\text{cm}^3/\text{s}$ for the desired length of time
- Set furnace temperature to the desired post treatment temperature
- Start hydrogen or ammonia gas mixture flow at $25\text{cm}^3/\text{s}$ for the desired length of time
- Turn off furnace and start argon gas flow at $25\text{cm}^3/\text{s}$ for the entire cool down period (8-9 hours or overnight).

The post synthesis vacuum treatment was conducted in a brazing vacuum furnace equipped with vacuum pump as shown in Figure 7.



Figure 7: High Temperature Furnace Equipped with Vacuum Pump

The procedures used are summarized as following:

- Place specimen in the furnace (as shown in Figure 7 – right picture)
- Start the pump vacuum to achieve a vacuum of at least 1×10^{-5} Torr
- Set furnace temperature to 150 °C and wait for the temperature to reach the set point
- Increase the furnace temperature set point to 790 °C and wait for the system to stabilize
- Hold at the temperature and vacuum setting for the desired duration of time
- Turn off furnace and wait for the internal temperature to reach 100°C or lower before turning of the vacuum pump

4.3 In-vitro Cytotoxicity Tests and Cell Culture

The In-vitro cytotoxicity tests in this research were conducted using MG-63 human osteoblast-like cells per the requirements listed in ISO 10993-5:2009 (Biological evaluation of medical devices- Part 5: Tests for in vitro cytotoxicity. ISO (the International Organization for Standardization) is a worldwide federation of national standards setting bodies. Three categories of test are listed in this ISO standard: extract test, direct contact test, indirect contact test. ISO specified that the selection of test or tests is depending on the nature of the sample and the potential site of use for the biomaterial. To be comprehensive, all three tests listed in the ISO were used in the in-vitro cytotoxicity evaluation of the CDC specimens. All the tests were conducted with positive and negative controls to ensure an appropriate test system response and to identify background response of the cells. At the end of the exposure time, the extent of the cytotoxic effect was evaluated by cell viability and/or cell growth using Cell Counting Kit-8 (CCK-8) and/or LIVE/DEAD[®] Viability/Cytotoxicity Kit for mammalian cells.

MG-63 human osteoblast-like cells were cultured in Eagle-Minimal Essential Medium (EMEM) supplemented with 10 v/v% of fetal bovine serum (FBS), and 1v/v % of penicillin streptomycin. Cells were incubated at 37 °C in a humidified atmosphere of 5% CO₂ in air where cell culture medium was changed/ replenished every other day. These cells were routinely sub-cultured every seventh day in 75 cm² flasks at a seeding density of 500,000 cells and a passage density of ~ 5,000,000 cells (80% confluency). Cell passage beyond 10 was not used in this research to avoid undesired mutation effect.

PBS with calcium and magnesium was used in this research to wash and/ or immerse cells. The metal ions help with cell attachment therefore should minimize any undesired cell morphology changes during the procedure.

4.4 Indirect Contact Cytotoxicity for CDC Powder

Cell culture medium with serum (EMEM+ 10 v/v% FBS + 1v/v% penicillin) was used as an extract solvent in this part of the research. It is the recommended extraction solvent per the ISO as it can extract both the polar and non-polar (due to the serum) compounds in the samples and it can support cellular growth subsequently [49].

First of all, CDC powders were sterilized by autoclaving at 121°C for 15 minutes. Then, extraction was carried out by adding 1 mL of cell culture medium to 0.1g of sterilized CDC powder (see Figure 8) per the ISO requirements for extraction solid-to-solvent ratio as summarized in Table 3. Then, the specimens in glass vials with Teflon caps were stored in an incubator at 37°C for 3-5 days. It should be noted that this extraction duration is more aggressive than the requirement listed in the ISO; 24 hours for extraction at 37°C. At the end of the extraction time, the specimen extracts were filtered using sterilized 0.45µm nominal filters and then added to a monolayer of cells in 4 wells (n=4) of a 96-well plate. Subsequently, the extent of the cytotoxic effect was evaluated by cell viability using cell counting kit-8 (CCK-8).

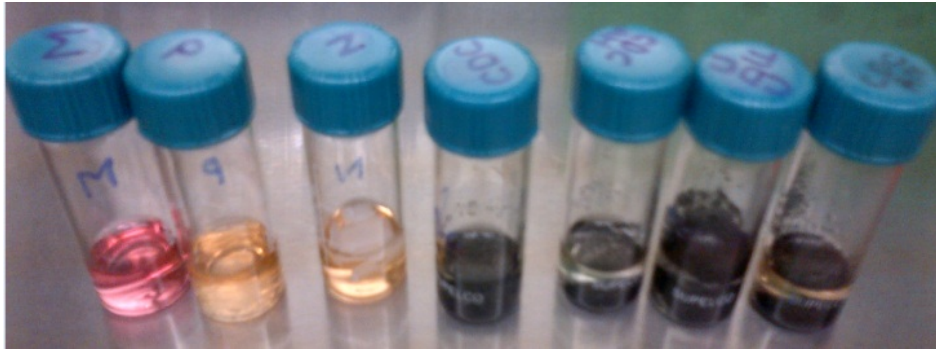


Figure 8: Extraction of CDC Powder

Table 3: ISO Requirements for Extraction (Solid-to-solvent) Ratio [49]

Thickness mm	Extraction ratio (surface area or mass/volume) ±10%	Examples of forms of materials
<0.5	6 cm ² /ml	Film, sheet, tubing wall
0.5 to 1.0	3 cm ² /ml	Tubing wall, slab, small moulded items
>1.0	3 cm ² /ml	Larger moulded items
>1.0	1.25 cm ² /ml	Elastomeric closures
Irregularly shaped solid devices	0.2 g/ml	Powder, pellets, foam, non-absorbent moulded items
Irregularly shaped porous devices (low-density materials)	0.1 g/ml	Membranes, textiles

In addition to the procedures described, CDC powder samples were also tested without the presence of sub-micron particles. As known that most particles are so small that gravitational force is insufficient to overcome the random molecular forces of particles and other forces to influence separation. Centrifugation is a commonly used method to increase the magnitude of the gravitational field. A Thermo Scientific CL10 Centrifuge was used to remove sub-micron CDC particles in this research. After the centrifugation, sub-micron particles remained in the supernatant were discarded. Following are the centrifugation equations and Stoke’s law used to calculate the required centrifugation speed and time to remove sub-micron particles [50] [51]:

$$\text{Gravitational force, } \mathbf{G} = (\mathbf{r}\omega^2)/\mathbf{g} \text{ ----- (1)}$$

$$\omega = 2\pi n \text{ ----- (2)}$$

Substituting (2) into (1)

$$G = [r (2\pi n)^2]/g$$

$$G = r (2*3.14*[n/60])^2/9.81$$

$$G = 1.12*10^{-3} r n^2$$

$$G = 1.12*10^{-3} r (\text{RPM})^2 = 197 (\text{m/s}^2)$$

Where:

r = distance from the axis of rotation (m) = 0.078 m

ω = angular velocity (radians/s)

g = acceleration due to gravity = 9.81 m/s²

n = rotation speed = 1500 rpm

$$\text{Stoke's Law: Terminal velocity: } V = \frac{d^2 (\rho_s - \rho_L) G}{18 \mu}$$

Where:

V = velocity of the sphere = 0.0000167 m/s (assumed the smallest particles that is larger than 1 μm travels extremely slow, at 0.01 m per 10 minutes)

d = diameter of the sphere = 1 μm

ρ_s = density of solid = density of graphite ~ 2.1 g/cm³ = 2100 Kg/m³

ρ_L = density of liquid = density of PBS ~ 1.0 g/cm³ = 1000 Kg/m³

μ = viscosity of liquid = viscosity of water ~ 8.9 x 10⁻⁴ Kg/m-s

G = gravitational force (m/s²)

Following are steps to remove sub-micron particles and to determine cytotoxicity of CDC powder samples without the presence of submicron particles:

Step 1: Add 0.1 g of sterile CDC powder to a sterile centrifuge tube.

Step 2: Add 10 mL of PBS to the centrifuge tube.

Step 3: Use a 1mL sterile disposable pipet to wet the surface of the CDC by pipetting in and out.

Step 4: Centrifuge at 1500 rpm for 10 minutes.

Step 5: Decant off the PBS supernatant and repeat steps 2-4 twice with PBS

Step 6: Repeat step 2-4 with cell culture medium to exchange the fluid from PBS to media.

Step 7: Decant off the supernatant cell culture medium and add 1 mL of fresh cell culture medium for extraction in the incubator (37⁰C for 3 days).

Step 8: After 3 days, centrifuge the tube at 1500rpm for 10 minutes and filter the filtrate solution through a 0.45um nominal sterile filter.

Step 9: Use the filtrate for biocompatibility test. Add 100μL of the filtrate to a monolayer of cells in 4 wells (n=4) of a 96-well plate where the extent of the cytotoxic effect was evaluated by cell viability using cell counting kit-8 (CCK-8).

4.5 Indirect Contact Cytotoxicity for CDC layer

Cell culture medium with serum (EMEM+ 10 v/v% FBS + 1v/v% penicillin) was used as an extract solvent in this part of the research. A different procedure was used to sterilize the specimens because titanium type V alloys cannot be sterilized using autoclave as the procedure will produce toxic oxide layer. Sterilization was conducted by soaking specimens in 70 v/v% ethanol/water for 30 minutes followed by washing the specimens 3 times in PBS, and one time in cell culture medium.

Extraction was conducted by placing individual specimen in 6-well plates as shown in Figure 9. FALCON's polystyrene six-well tissue culture plate, treated by vacuum gas plasma with low evaporation lid was chosen for this step because the size of the individual well is just slightly larger than the size of a CDC specimen, therefore allow total immersion of the specimen with just 1 mL of solution.

An extraction solid-to-solvent ratio of 1 CDC specimen (7.5-15 cm²) per mL was used for the extraction. Note that, this ratio is far more stringent than the ISO requirement. It was determined that the ISO requirement is not appropriate for the evaluation of CDC specimens because the CDC specimens are not very toxic therefore more stringent extraction conditions were needed to give a discriminative test. The 6-well plates were placed in an incubator at 37°C for 3-5 days for the extraction to take place. Again, the extraction duration is longer than the ISO requirement of 1 day.

At the end of the extraction time, the specimen extracts were added to a monolayer of cells in 4 wells of a 96-well plate where the extent of the cytotoxic effect was evaluated by cell viability using cell counting kit-8 (CCK-8).



Figure 9: Extraction of CDC Tile Specimen

4.6 Indirect Contact Cell Proliferation for CDC layer

Cell culture medium with serum (EMEM+ 10 v/v% FBS + 1v/v% penicillin) was used as an extract solvent in this part of the research. Sterilization was conducted by soaking the specimens in 70 v/v% ethanol/water for 30 minutes, followed by washing the specimens 3 times in PBS, and one time in cell culture medium.

Extraction was conducted by placing individual specimen in 6-well plates. An extraction solid-to-solvent ratio of 1 CDC specimen (7.5-15 cm²) per mL was used for the extraction. The specimens immersed in cell culture medium were placed in an incubator at 37°C for 7 days, beyond the ISO requirement of 1 day.

At the end of the extraction time, each of the specimen extracts was added to three or four wells ($n = 3$ or 4) in two 96-well plates (total of 6 or 8 wells) that were pre-seeded with 2200 cells per well. This low cell seeding density is a direct scale-down from cell culture of MG-63 in T-75 cell culture flasks.

To see the cells on 96-well plates, a predetermined amount of cells (2,200 cells per well) were suspended in $(100 \times \text{number of well}) \mu\text{L}$ of cell culture medium and then added to the wells. Subsequently, the cells were incubated at 37°C with humidified air containing 5% CO_2 for at least 5 hours to allow the cells to adhere to the bottom of the wells. Then, the cell culture medium in the wells was replaced by the sample extracts and returned to the incubator for the predefined exposure time periods. At the end of each of the exposure times, the extent of the cytotoxic effect was evaluated by cell viability using cell counting kit-8 (CCK-8) where a 96-well plate was processed and analyzed per the predefined procedure.

4.7 Direct Contact Cytotoxicity for CDC layer

This test was started by sterilizing the specimens by soaking the specimens in 70 v/v% ethanol/water for 30 minutes followed by washing the specimens 3 times in PBS, and one time in cell culture medium. Then, the specimens were placed in 6-well plates. Each specimen was seeded with 500,000 cells in 500 μL of cell culture medium. The plates were placed in the incubator at 37°C with humidified air containing 5% CO_2 for at least 5 hours to allow the cells to adhere to the specimen surface. After the 5 hours incubation time, 5 mL of additional cell culture medium was added to each well to support cell growth.

After that, the plates were returned to the incubator and incubated for another 2 days. At the end of the incubation time, each of the specimens were washed three times with PBS to remove or dilute serum esterase activity prior to adding the LIVE/DEAD[®] Viability/Cytotoxicity staining solution for cell viability determination.

4.8 Direct Contact Cell Proliferation for CDC layer

This test was started by sterilizing the specimens by soaking the specimens in 70 v/v% ethanol/water for 30 minutes followed by washing the specimens 3 times in PBS, and one time in cell culture medium. Then, the specimens were placed in 6-well plates. Each specimen was seeded with 60,000 cells in 500 μ L of cell culture medium. The low seeding density is corresponding to the seeding density for cell culture of MG-63 in T-75 cell culture flasks. The plates were placed in the incubator at 37°C with humidified air containing 5% CO₂ for at least 5 hours to allow the cells to adhere to the specimen surface. After the 5 hours incubation time, 5 mL of additional cell culture medium was added to each well to support cell growth.

The 6-well plates were returned to the incubator and incubated for another 7 days. Cell culture medium was changed and replenished every other day throughout the 7-day period. At the end of the incubation time, the specimens were washed three times with PBS to remove or dilute serum esterase activity prior to adding the LIVE/DEAD[®] Viability/Cytotoxicity staining solution for cell viability determination.

4.9 Bio-tribological Test

Ducom's the advanced linear reciprocating tribometer was used for all the tribological testing in this research. It has a ball-on-disc configuration as shown in Figure 10. The reciprocating movement is a better simulation of the kinematics of a hip joint as compared to a pin-on-disc apparatus.

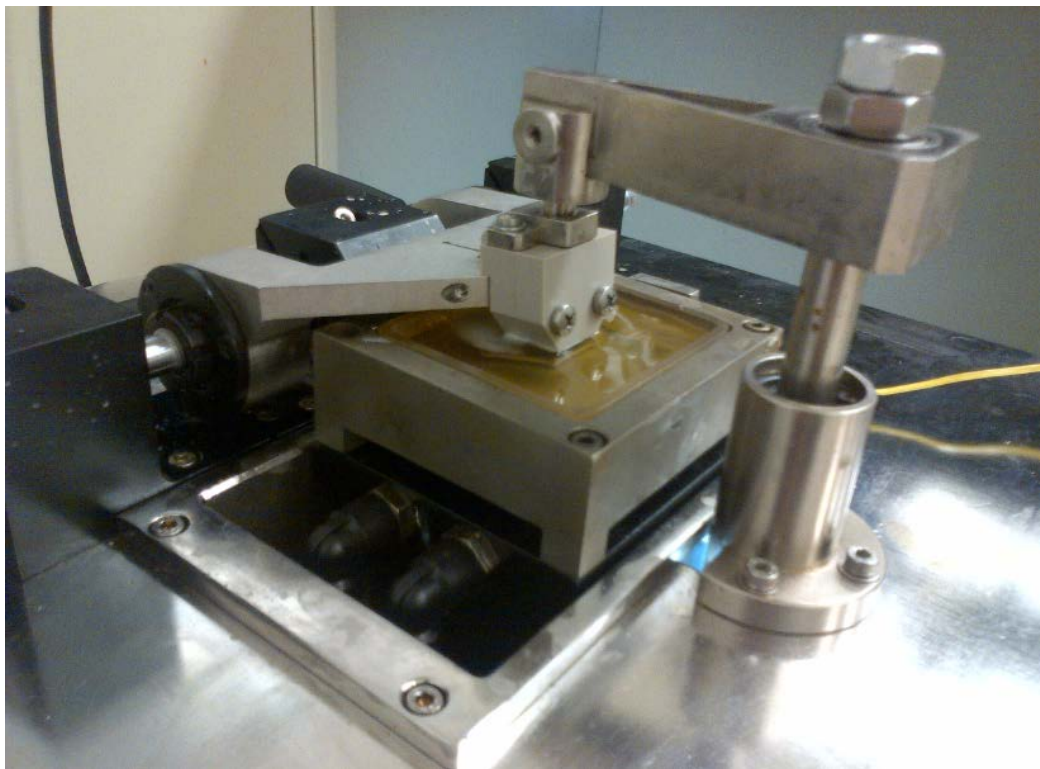


Figure 10: Advanced Linear Reciprocating Tribometer

The test variables include sliding counterpart, lubricant, lubricant temperature, sliding frequency, sliding distance, sliding time and normal load. Alumina balls with a diameter of 9 mm were used as the sliding counterpart for all the experiments. These balls were procured from McMaster Carr (Part number: 9599k15, Very High Temperature Nonporous High Alumina Ceramic balls). It has a polished surface with roughness, Ra value of 38-51 nm (3

measurements). The Young's modulus and Poisson's ratio for the alumina ball are 350 GPa and 0.3, respectively.

Bovine Calf Serum (BCS) solution with protein concentration of 30g/L and a pH value of 7.6 was used as the lubricant in this research. Due to the design of the sample holder (made up of PEEK, a non-conductive material) the solution temperature was not controlled in all the tests.

The effects of sliding frequency, sliding distance (displacement), and sliding time on wear rate were studied. However, a more generally accepted testing conditions for hip joints were used as the standard conditions in this research. The conditions are summarized as following:

- Sliding frequency = 1 Hz
- Sliding distance = 3 mm
- Sliding time = 1 hour
- Normal load = 12.5 N

The normal load of 12.5 N was chosen based on stability of the friction coefficient readings during sliding and the fact that this is equivalent to a normal pressure for hip joint calculated using the Hertzian Contact Stress equation. According to Hertzian's theory, an elastic contact is established upon contact of a sphere and a plane material. The area of contact, a , is calculated by:

$$a = \left(\frac{3 \times F_n \times r}{4 \times E} \right)^{1/3}$$

,where F_n is the normal load, r is the radius of the sphere, E the elastic modulus which depends on Young's modulus, and on the Poisson's ratios for the materials of the plane (E_1 and ν_1 , respectively) and of sphere (E_2 and ν_2 , respectively) as follow:

$$\frac{1}{E} = \frac{(1 - \nu_1^2)}{E_1} + \frac{(1 - \nu_2^2)}{E_2}$$

The resultant mean and maximum pressures are calculated by the following equations:

$$p_{mean} = \frac{F_n}{\pi \times a^2}$$

$$p_{max} = \frac{3 \times F_n}{2\pi \times a^2}$$

Table 4 summarizes the mechanical properties and the corresponding initial Hertzian contact stresses for the materials used in this research. The calculation was done using the standard tribological conditions. Note that, a wide range of mean and maximum pressures were exerted on the materials, predominantly depending on the Young's modulus value of the material.

Table 4: Mechanical Properties and Initial Hertzian Contact Stress Values

Material	Sphere Counterpart (2)	Flat Sample (1)			
	Alumina ball	CDC	UHMWPE	Ti6Al4V	CoCrMo
Radius, r (mm)	4.5	0	0	0	0
Young's modulus, E (GPa)	350	25	0.83	114	241
Poisson ratio, ν	0.3	0.3	0.4	0.342	0.3
Mean Pressure (GPa)	-	285	33	687	947
Maximum Pressure (GPa)	-	428	49	1031	1420

4.10 CDC Sample Polishing

CDC is very soft so the typical material polishing procedure is too harsh for it. This also means that CDC is a lot easier to polish as compared to SiC and other metals, which should be an advantage for commercializing the material. The CDC specimens used in this research has a thickness of 3mm. Therefore, a sample holder made out of aluminum was used to hold the sample during polishing. The first step in the polishing is to create some shallow lines on the specimen surface using a 1200 grit sand paper. This was done by sliding the specimen gently over the sand paper, in a horizontal direction, 3-5 times. The next step is to remove the lines by sliding the specimen on a polishing cloth that was sprayed with a Gamma Alumina power (0.05 μm) solution. The sliding on the cloth was done in a circular motion. The polishing was considered done when all the visible lines are gone. The last step in the procedure is to wash the specimen with an ethanol solution and dry the specimen using compressed air.

5.0 CHARACTERIZATION TECHNIQUES

5.1 Raman Spectroscopy

Raman spectroscopy has been widely used to observe vibrational, rotational, and other low-frequency modes in materials and therefore indirect structural characterization. It utilizes inelastic scattering (or Raman scattering) of monochromatic light in the visible, near infrared and near ultraviolet range [52]. The Raman scattering occurs when an incident light strikes a material where the scattered light has mostly the same wavelength as the incident light except for a very small fraction of light which scattered at a different wavelength, also called as the Raman Effect. The energy difference is proportional to the difference between two energy levels of a molecular vibration, and therefore a direct measure of the vibrational energies of the molecule [17].

For graphite and graphitic carbon, the observed Raman spectrum is characterized by a G band located at 1580-1600 cm^{-1} and a D band located around 1360 cm^{-1} . The G band is associated with the in-plane vibrations of carbon atoms in graphite structure, while the D band corresponds to disordered graphite phase.

In this research, a Renishaw 2000 Raman spectrometer (See Figure 11) was used for the characterization of CDC samples. The system has a depth resolution of 2 μm and a spatial resolution of 1 μm . The Raman analyses were run at an output of 30 mW using an Argon ion green laser. A typical Raman spectrum for a CDC sample is shown in Figure 12.



Figure 11: Renishaw 2000 Raman Spectrometer

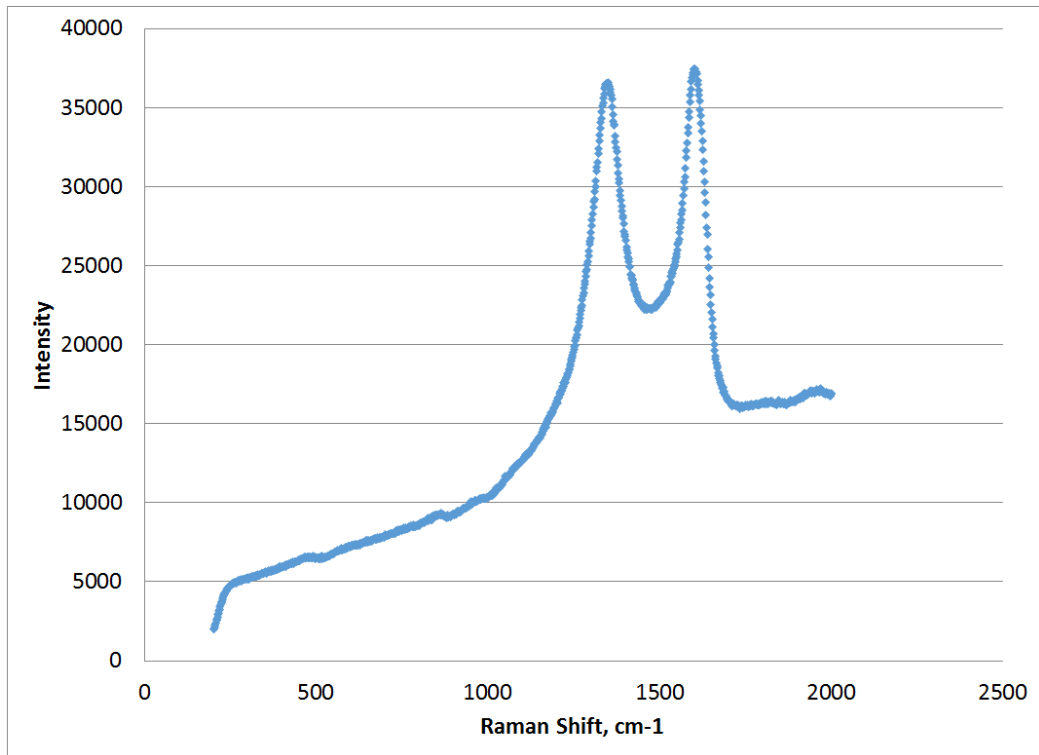


Figure 12: Raman Spectrum for Graphitic Carbon, CDC

5.2 Scanning Electron Microscopy

SEM images in this research were taken with a Hitachi S-3000N and a JEOL JSM-6490LV scanning electron microscopes. Both microscopes are a Variable Pressure SEM with a tungsten electron source, which allows non-conducting specimens to be observed without coating with a conductive film in a variable pressure mode. The operating ranges for the instruments are voltages between 0.3-30 kV, with a resolution of 2.5-3 nm at 30 kV, maximum magnification of 300,000x and 100,000x for the Hitachi and the JEOL, respectively. Both instruments have an Oxford Inca EDX system with a light element X-ray detector therefore allow chemical analysis in addition to the morphology analysis.

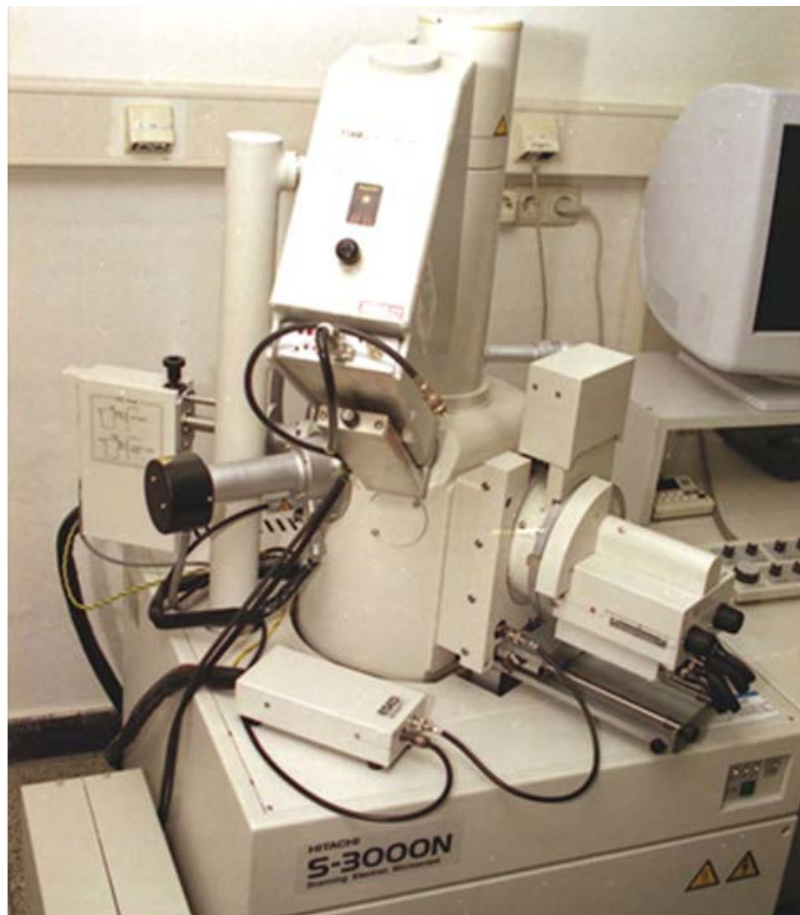


Figure 13: Hitachi S-3000N Variable Pressure SEM



Figure 14: JEOL JSM-6490 LV SEM

5.3 Energy Dispersive X-ray Spectroscopy

Chemical compositional analysis in this research was conducted with energy dispersive spectroscopy (EDS) which is equipped with the SEM microscopes. EDS utilizes the fact that energy levels of electrons in all elements are different and the energy of each X-ray photon is characteristic of the element from which it was emitted. Therefore, by analyzing the emitted X-rays from the specimen EDS can predict the composition for the specimen.

5.4 Quantitative Cell Viability using CCK-8

CCK-8 is a commercially available cell proliferation and cell cytotoxicity assay. It uses WST-8, a highly water-soluble tetrazolium salt, which can be reduced by enzyme activity in cells to give a yellow colored product, formazan (absorbance at 450nm) [53]. Molecular structure of WST-8 and formazan are depicted in Figure 15. The amount of the formazan dye produced by the activity in cells is closely proportional to the number of living cells [53]. This allows quantification of living cells based on the intensity of the absorbance reading upon establishment of a calibration curve (number of living cells vs. absorbance intensity). Synergy HT Multi-Mode Microplate Reader was used in this research to obtain the absorbance reading from a 96-well plate.

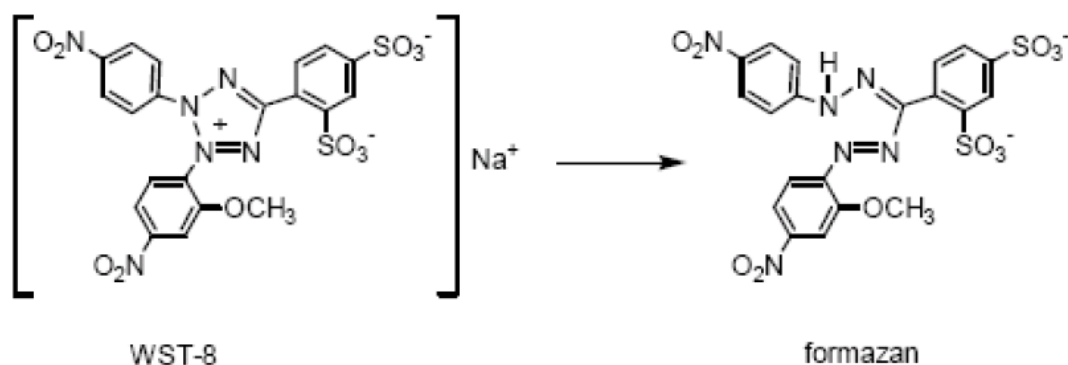


Figure 15: Tetrazolium Salt (WST-8) and Colored Product Formazan in CCK-8 [53]

CCK-8 assay was evaluated and optimized for use in this research. Test method variables evaluated include:

- Plate Reading Mode – End point, area scanning
- CCK-8 Incubation time – 1, 2, 3, 4 hours

- Cell seeding density (cells/well) – 5000, 7500, 10,000 cells/well
- CCK-8 buffer solution – Phosphate-buffered saline solution (PBS), media

A screen print of the plate reader's local display is shown in Figure 16. As can be seen that MG-63 cells have a higher affinity to adhere and grow on the edges of the wells and exhibited a non-uniform cell distribution in the wells. Given this, it was clear that area scanning mode is more appropriate and can give more representative absorbance readings.

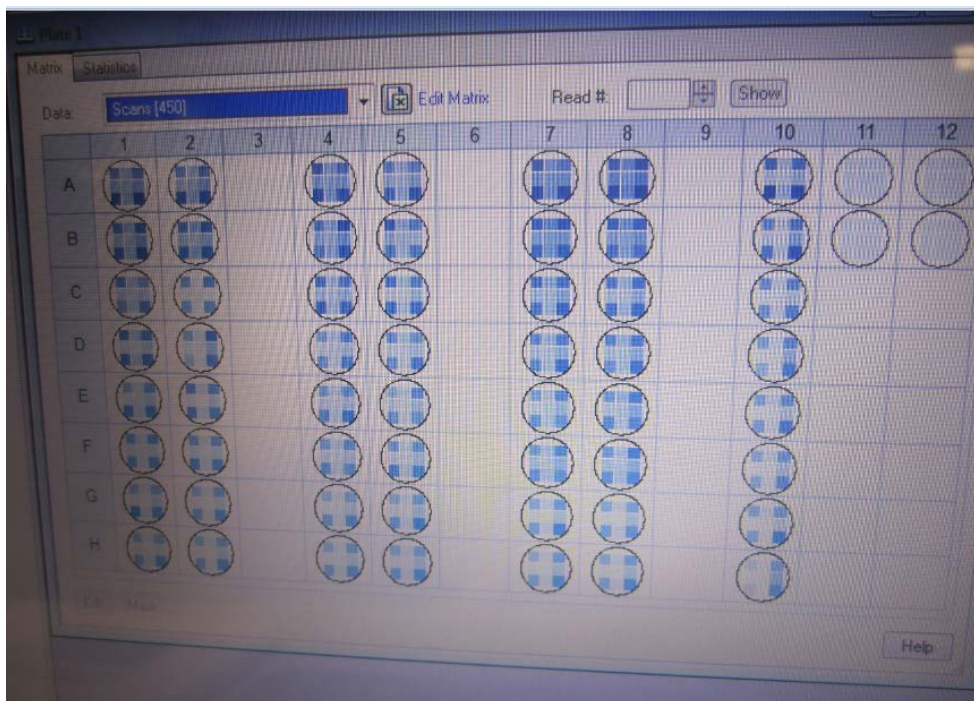


Figure 16: MG-63 Cells Distribution in a 96-well Plate

Area scanning can be carried out with different numbers of scan (3x3, 5x5, 6x6, and etc) to obtain the desired representative result. 9-scan and 25-scan were evaluated using a same set of samples. The samples were processed per the predefined procedures and added to a monolayer of cells in a 96-well plate. Each sample extract was added to 4 wells ($n = 4$). After the predefined CCK-8 incubation time had elapsed, the absorbance reading of the plate was taken with 9-scan followed by 25-scan. Figure 17 shows a comparison of the test results between the 9-scan and the 25-scan. Standard deviation of the test results are shown by the

error bars. As shown that comparable results were obtained from both scans. The results show that the 25-scan did not result in lower standard deviation as compared to the test results obtained from the 9-scan. It was noted that the 25-scan gave slightly higher absorbance readings as compared to the absorbance readings from the 9-scan. This could be due to the fact that 25-scan allows better coverage on the edges of wells where there are more cells and therefore higher intensity of the formazan color. It was concluded that both scans gave representative result and 9-scan is more efficient.

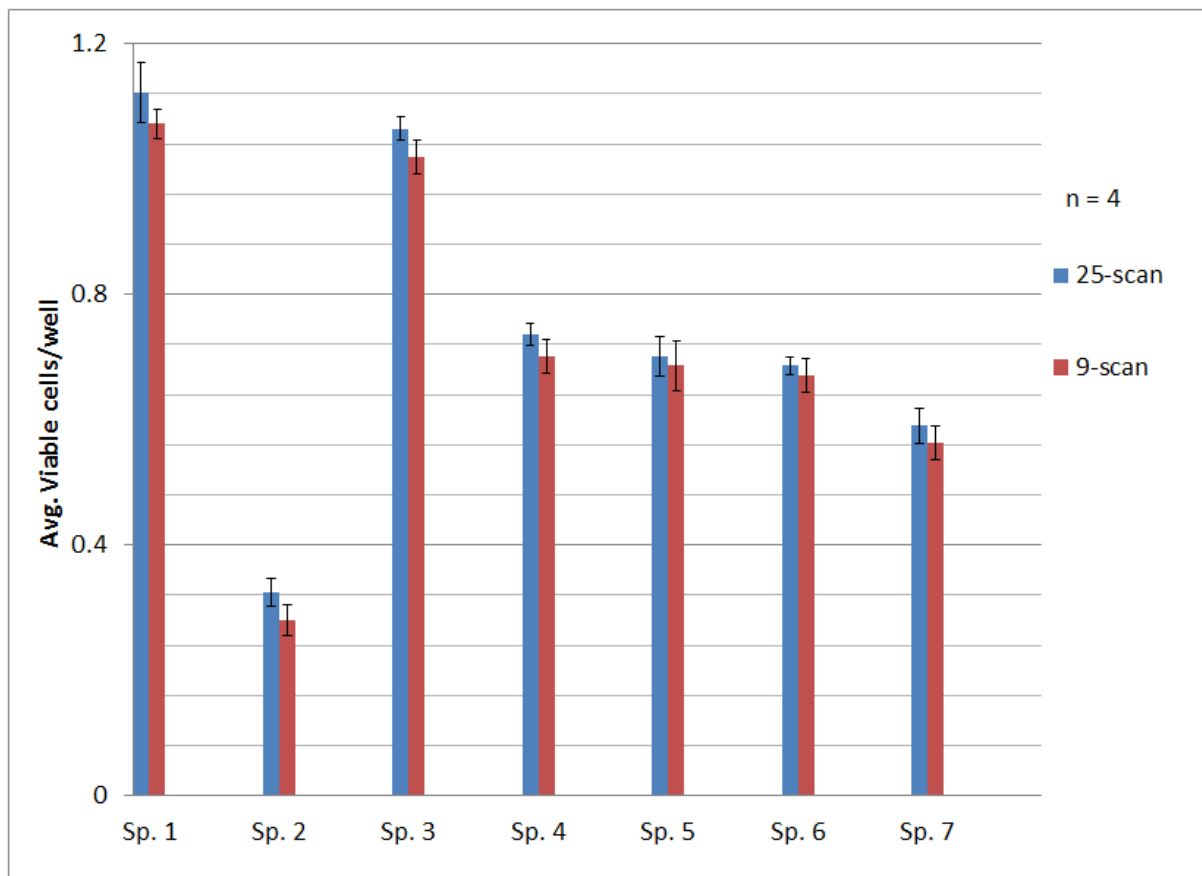


Figure 17: Cell Viability Results for 9-Scan and 25-Scan

CCK-8 incubation times of 1, 2, 3, and 4 hours were studied to ensure that the reduction process is linear with time. Figure 18 shows the absorbance readings of 3 seeding densities

after each of the incubation times. The test results confirmed that the reduction process is linear from 1 to 4 hours, with 4 hours gave the highest absorbance readings.

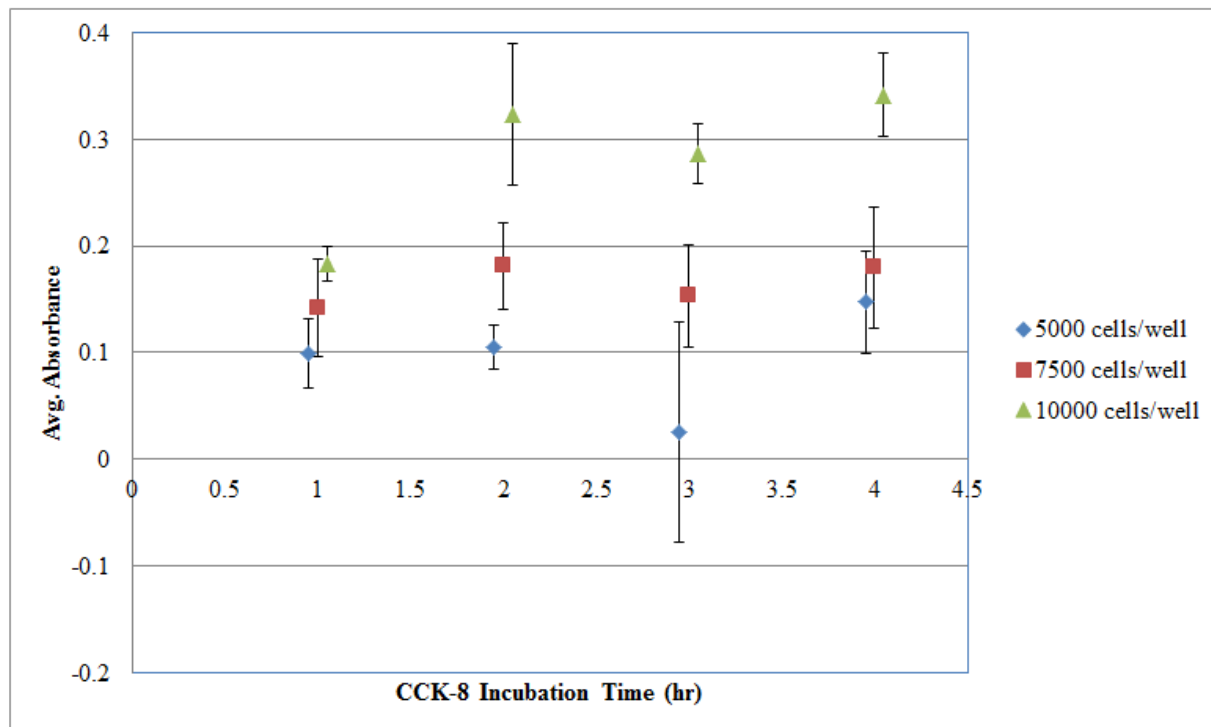


Figure 18: Absorbance Reading vs.CCK-8 Incubation Time

Seeding density is one of the key variables in the test method as it is critical to achieve a monolayer of cells in the wells prior to exposure to the sample extract. Three seeding densities were evaluated (5000, 7500 and 10,000 cells/well) at 2 time intervals (1 and 3 days). After the desired amount of cells were seeded per well, the 96-well plates were incubated for one and three days. CCK-8 was added to each well with PBS as buffer solution and incubated for 4 hours prior to taking the absorbance reading. Figure 19 shows the absorbance readings at day 1 and day 3. As expected that higher seeding densities gave higher absorbance readings. At day 3, 7500 cells/well was ~80% confluent and 10000 cells/well was ~100% confluent based on visual observation using an optical microscope. The results support that seeding densities of 8000-10,000 cells/well are appropriate

depending on the cells exposure time (the length of the experiment). It was determined that 8000 cells/well is suitable for a 4-day experiment and 10,000 cells/well is appropriate for a 2 days experiment.

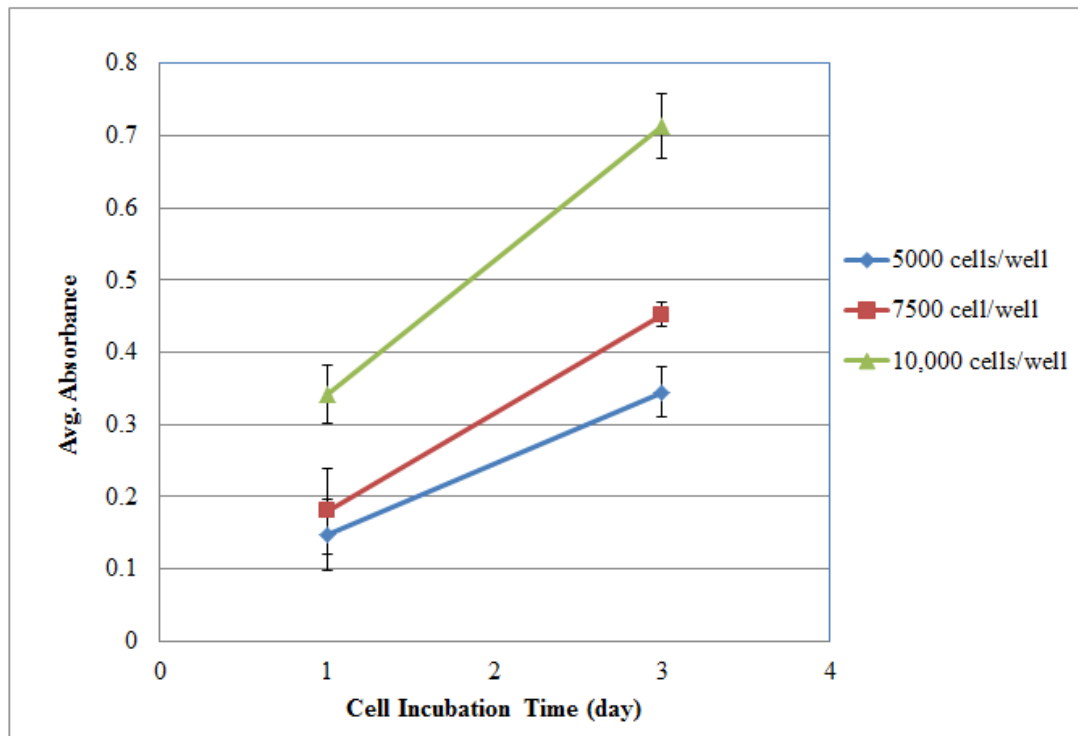


Figure 19: Absorbance Readings at Day 1 and Day 3 for Different Seeding Densities

Phosphate-buffered saline solution (PBS) and cell culture medium were evaluated as the buffer solution of the CCK-8 assay. Figure 20 shows the absorbance readings for 3 seeding densities in PBS and cell culture medium as the buffer solution. As shown that, the cell culture medium gave significant higher absorbance readings as compared to the PBS. Both 7500 cells/well and 10000 cells/well in cell culture medium gave the desired level of absorbance readings (over 1.00).

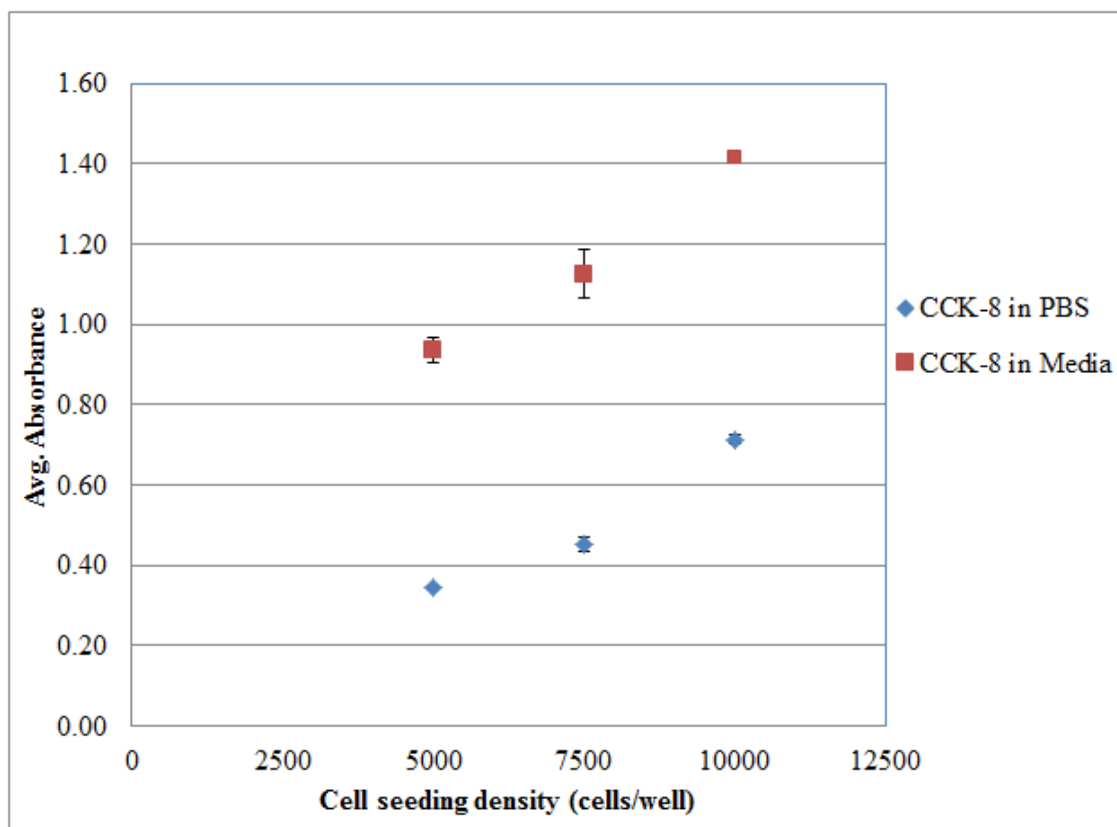


Figure 20: Absorbance Reading in PBS and Cell Culture Medium

To summarize the CCK-8 assay optimization work, it was determined that area scanning with 9-scan, CCK-8 incubation time of 4 hours, cell seeding density in 96-well of 8,000-10,000 cells/well, and using cell culture medium as buffer are the optimized conditions for the cell, MG-63. These were the conditions used for the assay throughout this research.

The optimized assay was used to generate a calibration curve of absorbance reading vs. viable cells per well. Three calibration curves were obtained in three different days using three different passages of cells. Each curve was obtained by seeding a known amount of cells to 4 wells ($n = 4$), incubated in 37°C with 5% CO_2 air overnight, and determined the amount of viable cells per well using the optimized CCK-8 assay. Figure 21 shows the average absorbance reading vs. number of viable cells per well for the three different days. In general, a linear relationship was observed up to $\sim 10,000$ cells per well for all three curves. A significant variability can be seen from the measurements taken among the

different days which was mainly attributed by the cell hemocytometer measurement. Figure 22 shows the linear range of the curves with a relationship of:

$$\text{Viable cell per well} = \frac{\text{Absorbance}}{0.00007}$$

This relationship was used to quantify the number of viable cells per well throughout this research.

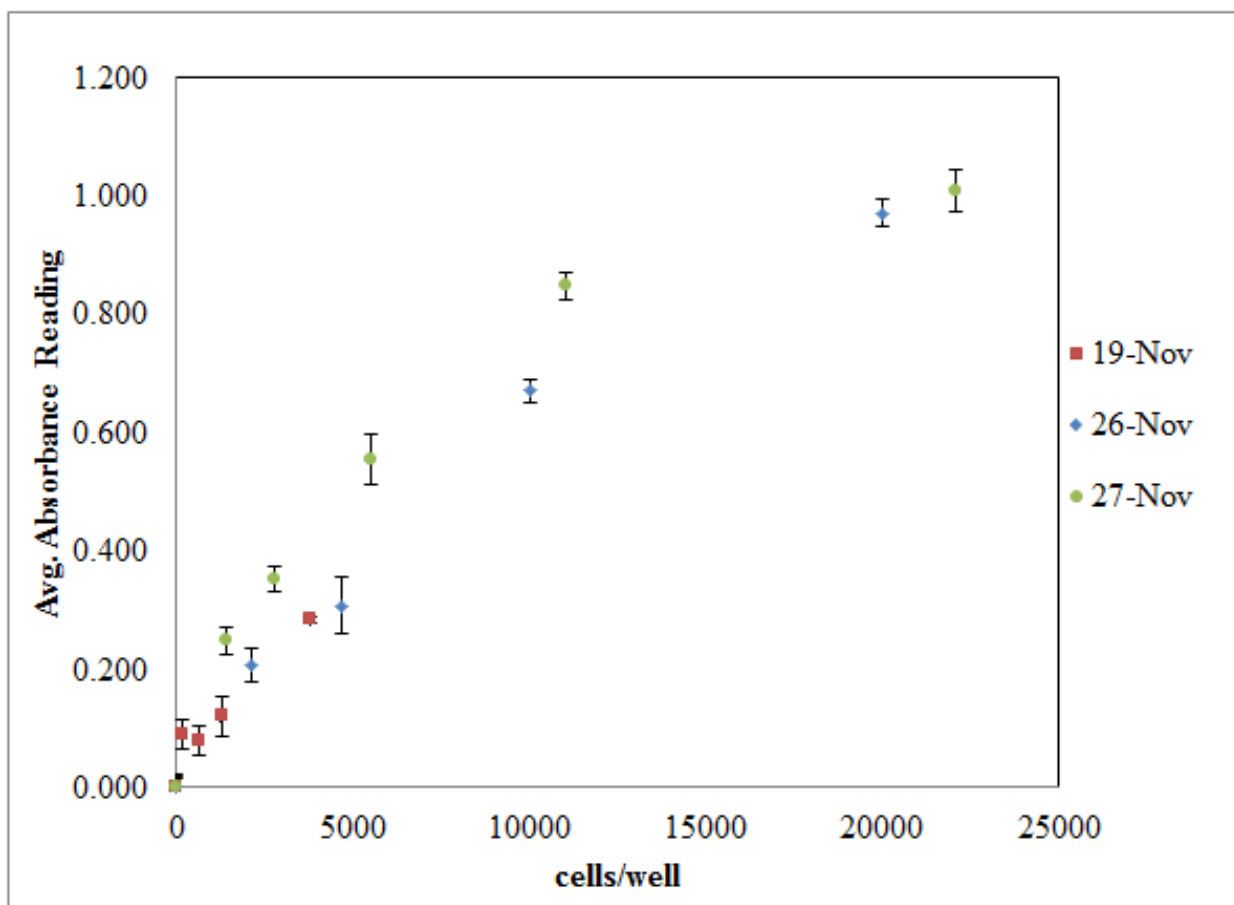
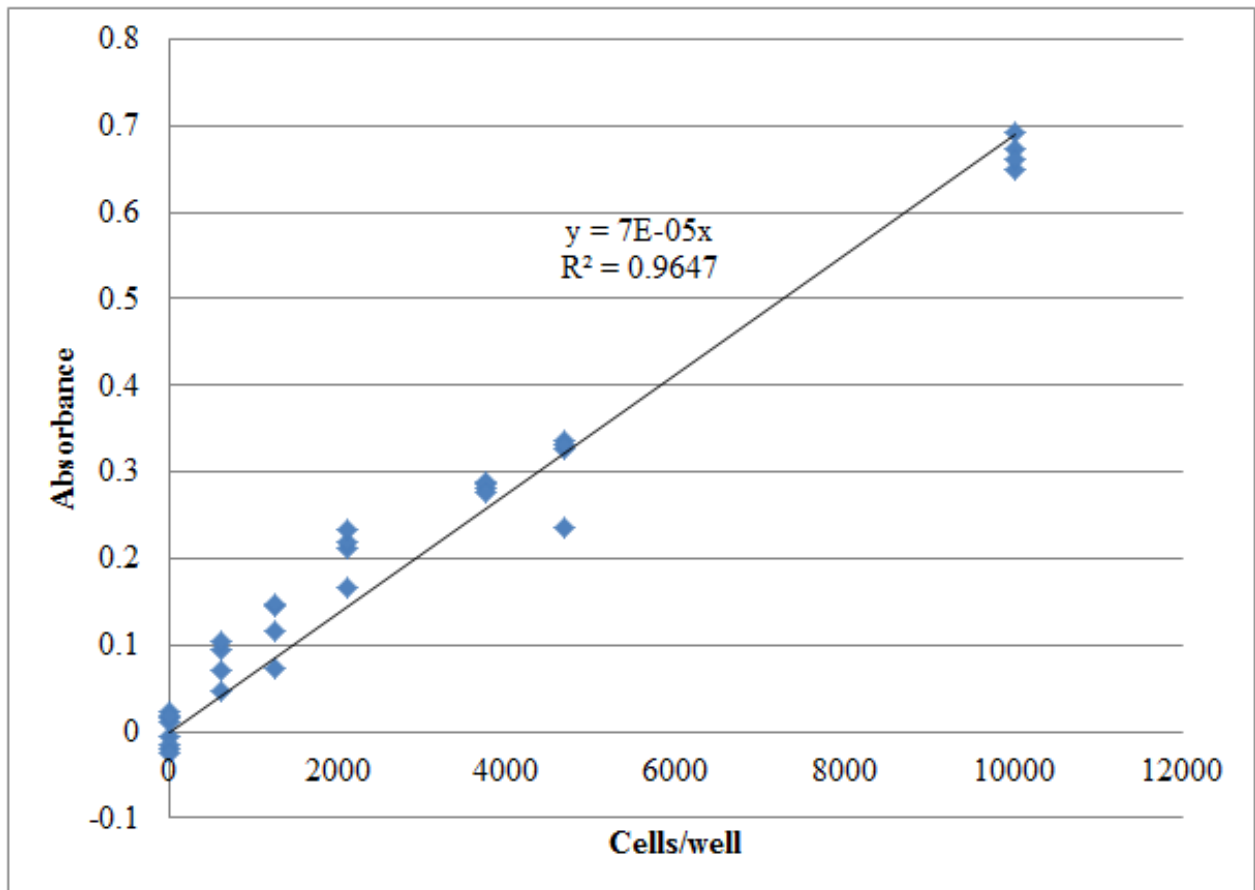


Figure 21: Absorbance Readings vs. Viable Cells per Well at Three Different Days



MG-63 cells are adherent cells. To determine the viability of MG-63 cells, first of all a known quantity of MG-63 cells are seeded on the surfaces of sterilized specimens. The specimens were incubated at 37°C in a humidified environment with 5% CO₂ air for a predefined period of time. At the end of the incubation time, the cells were washed twice with PBS to remove or dilute serum esterase activity prior to adding the LIVE/DEAD[®] Viability/Cytotoxicity staining solution. The staining solution was prepared by adding 20 µL of 2 mM EthD-1 to 10 mL of PBS and mixed. Then, followed by adding 5 µL of 4 mM Calcein AM to the same 10 mL of PBS and applied thorough mixing after the addition.

A sufficient quantity of the staining solution was added to each specimen to thoroughly cover the cells with the solution. The specimens were incubated in an incubator at 37°C for 30 minutes. Following the incubation time, each specimen was washed with PBS three times to remove any excess staining solution. It should be mentioned that extra caution should be practiced when washing the cells to avoid cell detachment and to minimize the time duration where cells are not immersed in the PBS, also called the “dry” time. Extended period of the “dry” time will result in unintentional cell death and/or unintentional change of cell morphology due to procedural errors. Specimens should be immersed in the PBS at all time until they are ready to be analyzed. Finally the cell morphology and optical density were viewed and recorded by a fluorescent microscope (Nikon Eclipse 80i, Nikon Instrument Inc, NY).

5.6 Protein Adsorption using Pierce™ Bicinchoninic Acid (BCA) Protein Assay Kit

Pierce™ BCA Protein Assay Kit was used to measure the amount of protein adsorbs onto the CDC surface upon a predefined period of exposure time. The BCA Protein Assay consists of two reagents, A and B [55]. Reagent A contains sodium bicarbonate, sodium carbonate, bicinchoninic acid and sodium tartrate in 0.1M sodium hydroxide. Reagent B contains 4% of cupric sulfate. The presence of protein will reduce Cu^{2+} to Cu^{1+} in the alkaline medium. Subsequently, BCA reacts with the reduced cuprous cation to form an intense purple-colored product. “The BCA/copper complex is water-soluble and exhibits a strong linear absorbance at 562 nm with increasing protein concentrations” [55]. This allows quantification of the absorbed protein based on the intensity of the absorbance reading upon establishment of a calibration curve (known protein concentration vs. absorbance intensity). Synergy HT Multi-Mode Microplate Reader was used in this research to obtain the absorbance reading from a 96-well plate.

The test was started by cleaning each of the CDC specimens with sonication in 200-proof ethanol for 5 minutes, followed by rinsing the specimens with copious amount of distilled water. Then, the specimens were placed in 6-well plates where 2 mL of BCS solution (the same solution used in tribology testing) was added to each well. After that, the specimens were stored at 37°C for 90 minutes to allow the protein to adsorb onto the specimens’ surface. After the exposure time, each specimen was washed PBS 5 times to remove any excess and non-absorbed protein. Subsequently, 1 mL of SDS (surfactant) was added to each well and then the 6-well plates were shook at 50 rpm for 60 minutes to detach any absorbed protein. Then, the amount of protein in SDS was analyzed with the BCA protein assay.

5.7 Volumetric Wear Rate Determination with Zygo

Wear rates in this research were determined using a 3-D non-contacting optical surface profiler that uses a white light interferometer system, Zygo New View 6300. It offers high precision and accuracy on topography measurement, which can measure worn volume directly without any calculations or conversions. Furthermore, sample preparation is not required for the use of this microscope, providing that the sample is free of loose wear debris. Zygo offers a field stitching feature which allow scan and display areas up to 203 x 203 mm [56]. A zoom lens of 2.0X was used in all the measurement in this research. A schematic of the microscope is shown in Figure 23.

The system is based on scanning white light interferometry which can be described as a pattern of dark and bright lines results from an optical path difference between a sample beam and a reference. First of all, incoming light is split into two: one goes to an internal reference surface and the other goes to the sample surface. The beams reflect and then undergo constructive and destructive interferences which produce the bright and dark lines or patterns. These patterns are then processed by vertical scanning transducer and camera to generate 3-D interferogram of the surface. Subsequently, it is transformed to 3-D images by frequency domain analysis in the computer.

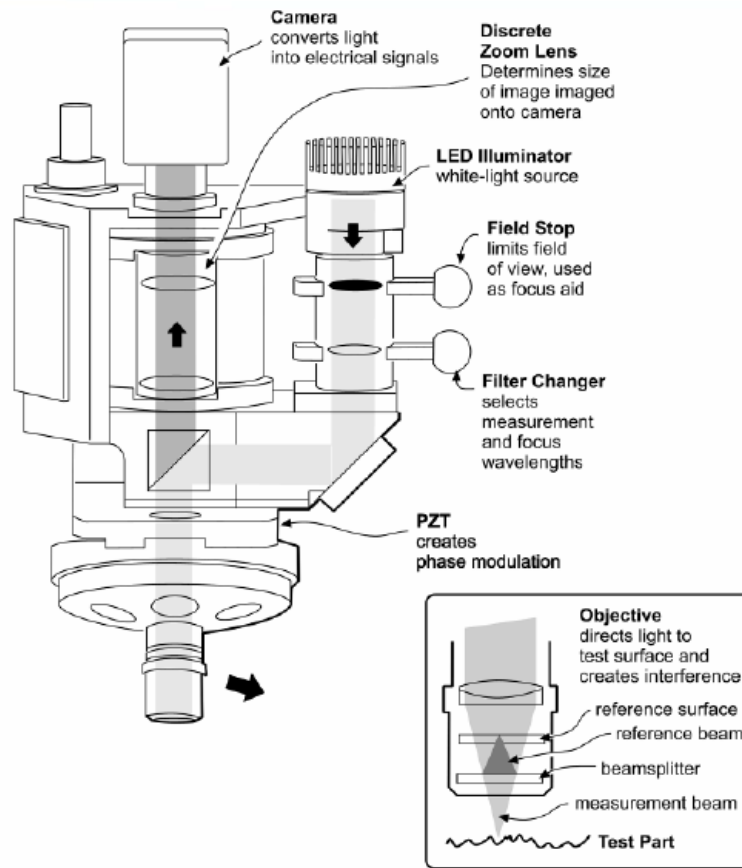


Figure 23: Schematic of the Zygo New View 6300 [56]

6.0 RESULTS AND DISCUSSIONS

6.1 Determine the Effect of Residual Chlorine and Submicron CDC Particles on the Biocompatibility of CDC Powder

Despite the fact that cytotoxicity of CDC has not been studied, a lot of studies have been conducted to study the cytotoxicity of CNTs, another carbon material. Undoubtedly, cytotoxicity of CNTs is a very complex manner. Even though there are no definitive findings from these studies, collectively the data suggest that the physiochemical properties of CNTs are likely to impact the cytotoxicity of CNTs (see Section 2.6, Biocompatibility and Toxicity of CNTs). EDS analysis on CDC powder produced from a standard chlorination conditions (1000 °C and 6 hours) show that the CDC powder contains Si, O, C and Cl atoms as summarized in Table 5. Based on this, it was hypothesized that the physiochemical properties that could impact the cytotoxicity of CDC include functionalized or non-functionalized residual chlorine in CDC, CDC particle size, CDC particle shape, CDC concentration (amount of CDC), and CDC surface properties, as shown in Figure 24.

Table 5: Chemical Composition of CDC Powder

CDC Sample:	C	O	Si	Cl
YC-TCT-1	Weight Percentage			
Spectrum 1	98.66			1.34
Spectrum 2	95.53	2.10	0.97	1.40
Spectrum 3	98.25			1.75
Spectrum 4	98.67			1.33
Spectrum 5	99.04			0.96
Spectrum 6	98.16		0.53	1.31
Spectrum 7	98.33			1.67
Spectrum 8	97.96			2.04
Max.	99.04	0.00	0.97	2.04
Min.	88.21	2.10	0.53	0.96

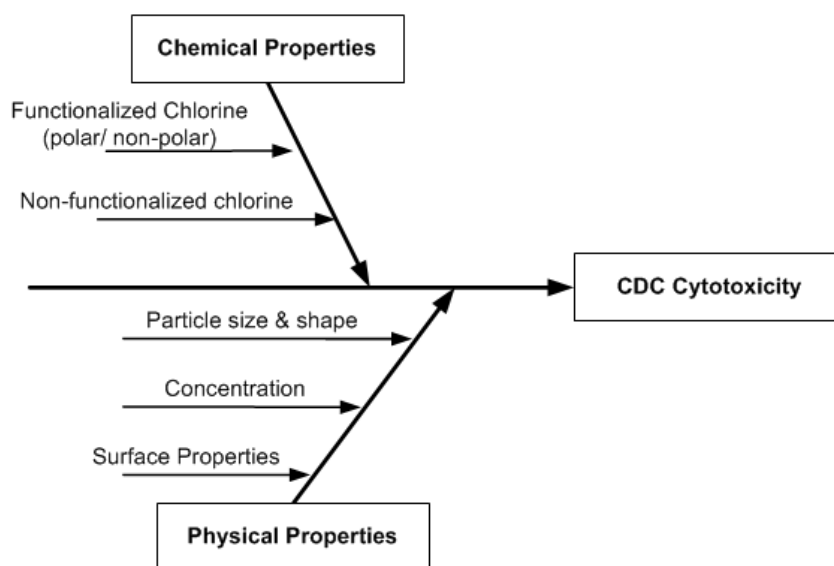


Figure 24: Fish Bone Diagram of CDC Cytotoxicity

Experiments were conducted to study the effect of chemical and physical properties independently on CDC cytotoxicity. To study the effect of chemical properties (residual chlorine), CDC powder were treated in a high temperature (1400 °C) vacuum furnace for 8 hours to remove all the residual chlorine. EDS analysis of the furnace treated CDC confirmed that chlorine was not detected at a test method detection limit of 0.1 wt %.

To study the effect of physical properties, submicron particles in the CDC sample were removed using high speed centrifugation to increase the magnitude of the gravitational field (See Section 4.4, Indirect Contact Cytotoxicity for CDC Powder). SEM analysis of furnace treated CDC samples with and without centrifugation confirmed that sub-micron particles were removed via the centrifugation step, as shown in Figures 25 and 26.

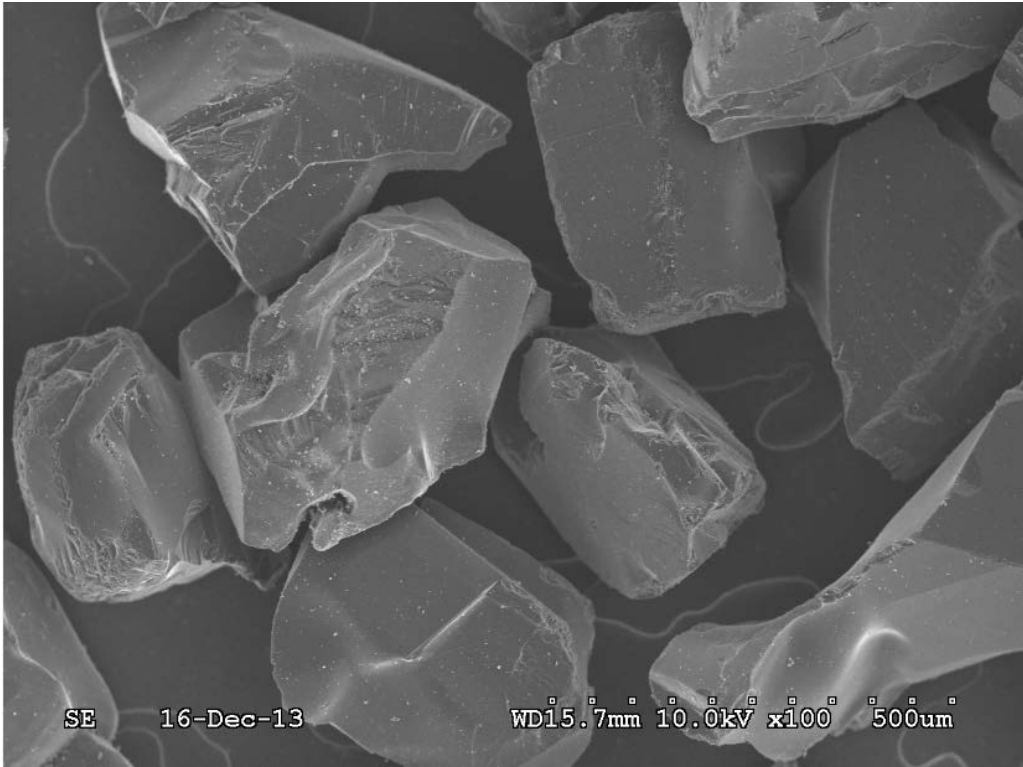


Figure 25: SEM Image of Furnace Treated CDC Sample – Visible Sub-micron Particles

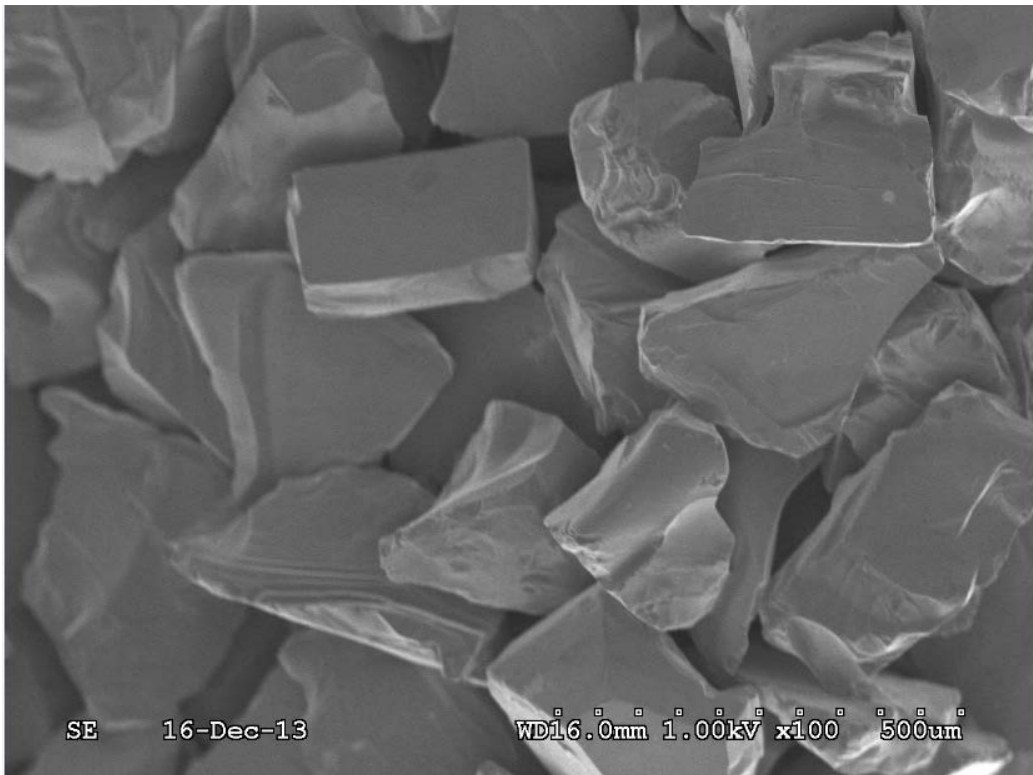


Figure 26: SEM Image of Centrifuged CDC Sample – No Sub-micron Particles

Biocompatibility of the CDC powder samples (“as-is”, with furnace treatment and/or centrifuged) were tested following the procedures described in Section 4.4, Indirect Contact Cytotoxicity for CDC powder.

Figure 27 shows the quantitative cytotoxicity result of the CDC powder samples. Each sample was tested in 4 replicates (n = 4) and standard deviations are shown as the error bars on the figure. The test result shows that both the furnace treated and centrifuged CDC samples are not cytotoxic, and sub-micron CDC particles are cytotoxic only when residual chlorine is present. This result is consistent with the finding from the previous CNT cytotoxicity study where the study concluded that frustrated phagocytosis is uncommon in a CNT dimension < 5 μm [42]. Additionally, this result confirms that biocompatible CDC powder can be produced using the extreme post-chlorination treatment to remove the residual chlorine.

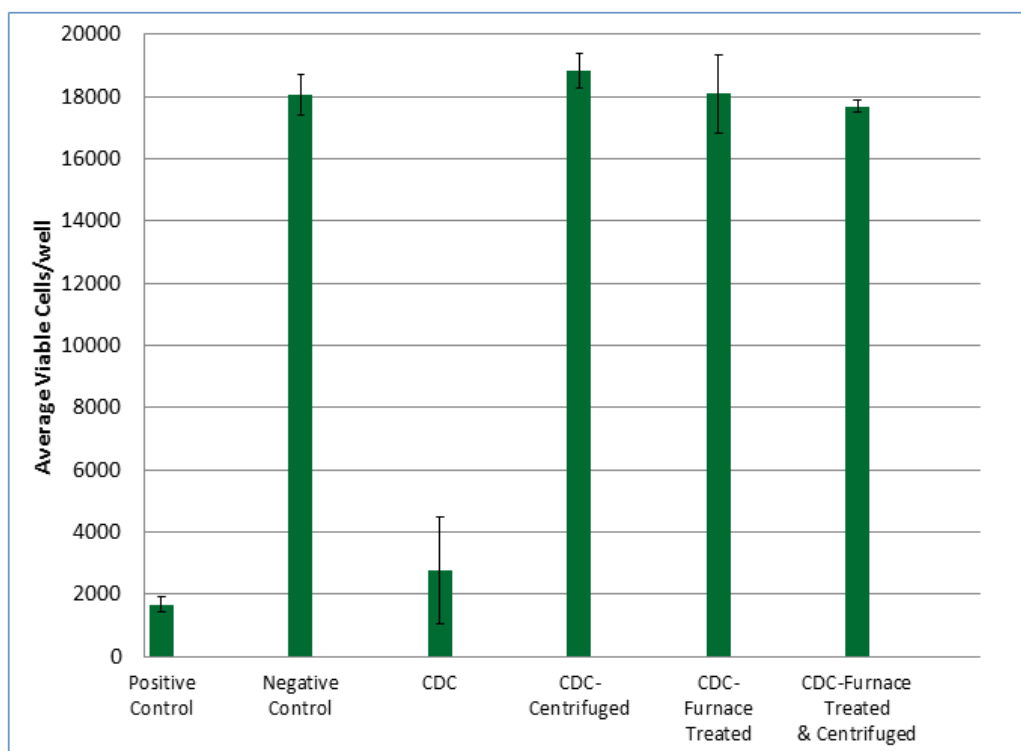


Figure 27: Cytotoxicity of CDC Powder Samples

Fluorescence images (qualitative cytotoxicity result) for the CDC and furnace treated CDC samples are shown in Figure 28. The fluorescence images show that CDC powder sample is cytotoxic where almost all the cells were dead, as shown by the red color round cells. On the other hand, the images show healthy live cells for the furnace treated CDC powder sample, as shown by the green spindle shape cells. Collectively, the qualitative result is consistent with the quantitative cytotoxicity result therefore verified the result.

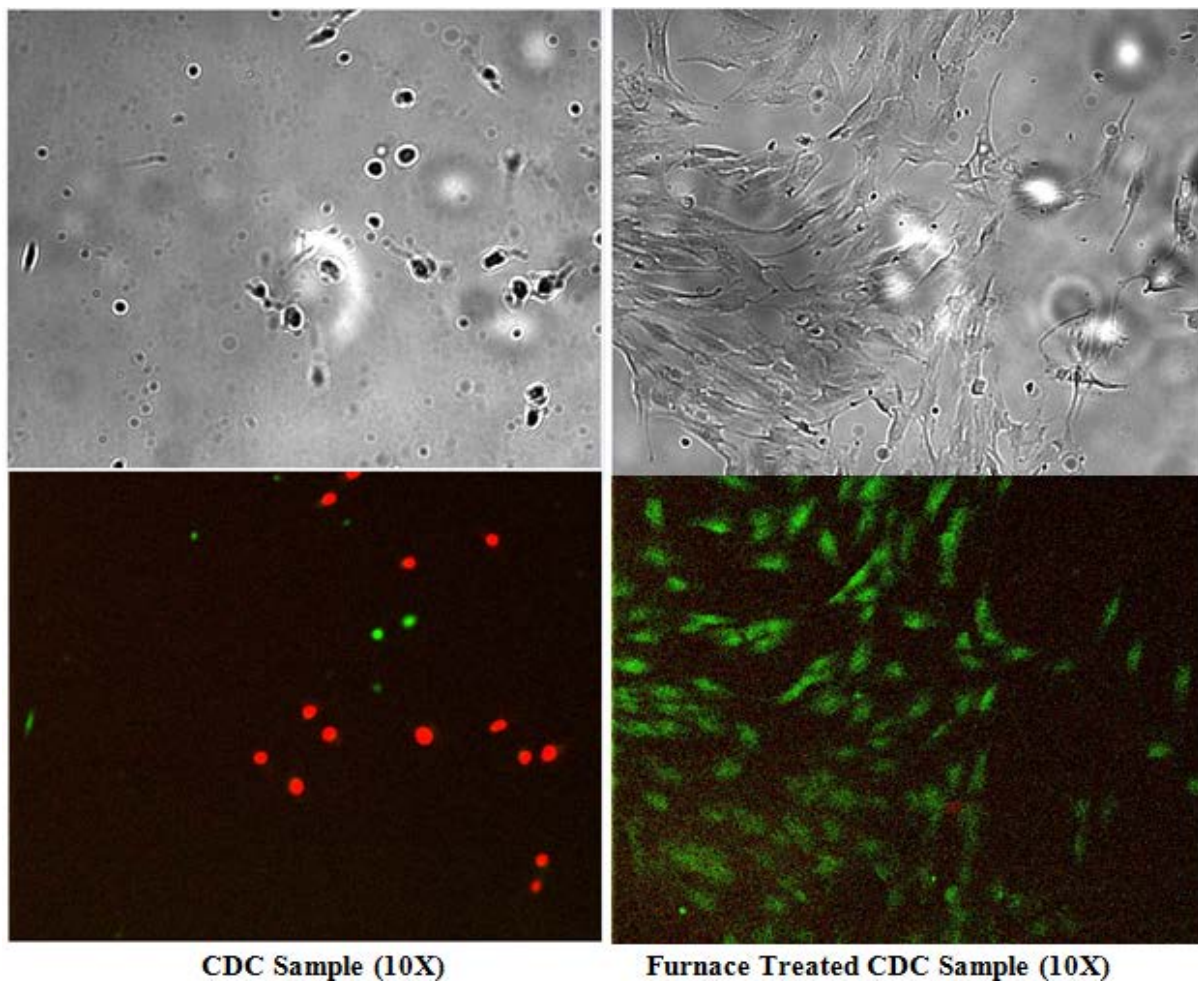


Figure 28: Fluorescence Images of CDC Powder Samples

Table 6 summarizes the EDS analysis result for the CDC powder samples before and after extraction, with or without centrifugation. Five to ten scans were taken for each sample for the EDS analysis. Minimum and maximum values for each sample are listed in the table for comparison purposes. The data show that the residual chlorine in the CDC sample and CDC samples after extraction, with or without centrifugation are very similar. This data indicates that extraction in cell culture medium at 37°C for 3 days did not appear to remove significant amount of chlorine even though the sample extract was colorless, indicating acidic as the cell culture medium contains Phenol Red indicator. This data also confirms that the additional washing/centrifugation steps did not remove significant amount of chlorine and support the hypothesis that the residual chlorine in CDC could be chemically bonded.

Sodium (Na) and aluminum (Al) are components of PBS and cell culture medium therefore it is not surprising to see some residual PBS and cell culture medium elements in the CDC wet cake samples after extraction.

Table 6: EDS Analysis Result for the CDC Powder Samples Before and After Extraction

Sample	Min, Max of 5-10 tests	C	O	Si	Na	Cl	Al
		w/w %					
CDC	Max	99.0	11.8	1.0		2.0	
	Min	88.2	2.1	0.5		1.0	
CDC after extraction	Max	88.3	10.2		0.5	2.1	
	Min	87.8	9.5		0.5	1.5	
Centrifuged CDC after extraction	Max	94.0	13.6	1.8	0.8	2.6	0.6
	Min	84.2	4.5	0.6	0.3	1.1	0.6

In addition, SEM and EDS analysis were conducted to determine the chemical composition of the sub-micron particles. Figure 29 shows the high magnification SEM image and EDS spectrum for the CDC powder. As expected, sub-micron particles were visible on the CDC particle surface. EDS analysis on the sub-micron particles show no detectable difference between the CDC surface and the sub-micron particles where only C, O, and Cl were detected. The technique used to acquire the chemical composition was proven to be discriminative as it was able to detect composition difference between loose particles and the substrate on another CDC specimen obtained from a company in Europe.

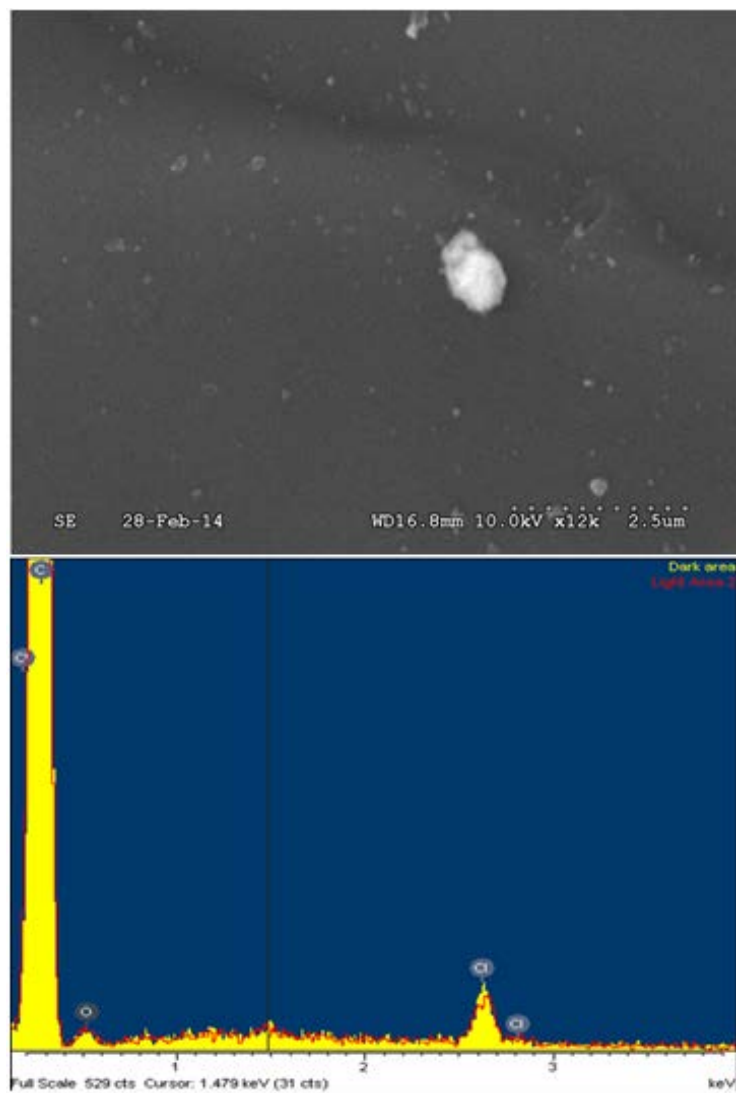


Figure 29: SEM and EDS for the Sub-Micron Particles

6.2 Determine the Effects of key CDC Processing Parameters on Tribological Properties of CDC Specimens under Physiological Simulated Conditions

The key processing parameters studied include chlorination temperature, chlorination time, post chlorination treatment gas mixture, and post chlorination treatment time, as summarized in Table 7.

Table 7: Summary of Processing Parameters Studied

Processing Parameter	Units	Level 1	Level 2	Level 3
Chlorination and Post Treatment Times	Hour	≤ 8, 8	19, 24	
Chlorination Temperature	°C	1000	1100	-
Post Chlorination Treatment Gas	-	5% H ₂ -Ar	5 % NH ₃ -Ar	Vacuum
Post Chlorination Treatment Time	Hour	3	8	24

A full blown design of experiment (DOE) was not conducted to study all the potential main and secondary interactions between the parameters. Instead, the study was conducted in a step-wise manner where the design of the study was determined based on the outcome of the previous set of experiments, also known as the one-factor-at-a-time (OFAT) experiments. There is no doubt that a DOE is a much more superior approach than an OFAT approach. However, a DOE approach requires a lot more experiments which can be very resource draining and not feasible at times. In this study, the OFAT experiments are summarized as following, in a sequential manner:

- Effect of chlorination and post treatment times (≤ 8, 8 vs. 19, 24 hours)
- Effect of chlorination temperature (1000 vs. 1100 °C)
- Effect of post treatment gas mixture (H₂-Ar, NH₃-Ar, vacuum)
- Effect of post chlorination treatment time (3, 8 and 24 hours)

6.2.1 Effect of Polishing on Wear Rate

Previous studies concluded that CDC is a soft material that is highly lubricious [5] [8] [9] [10]. Therefore, surface roughness may not be as critical in terms of its effect on wear rate. To determine the effect of polishing on wear rate, tribological testing was conducted on 4 CDC specimens before and after polishing (See Section 4.10 for CDC polishing procedure). The tribological testing was done using the standard parameters listed below:

- Sliding frequency = 1 Hz
- Sliding distance = 3 mm
- Sliding time = 1 hour (3600 cycles)
- Normal load = 12.5 N

Wear rates for the specimens before and after polishing are tabulated in Table 8 and depicted in Figure 30. As shown that lower wear rates were consistently obtained from all the polished specimens. Each of the polished specimens was tested 2 to 4 times (n= 2 or 4) where the respectively standard deviation of the tests is shown as the error bars on the figure. It is believed that the polishing removed majority of the loosely adherent particles and allows more consistent evaluation of CDC microstructure effect on the wear rate. The loose particles once get into the BCS solution could act as third party particles and promote mechanical wear during the tribological testing therefore resulted in the higher wear rate values observed in the unpolished specimens. Based on this finding, all the specimens were polished prior to the tribological testing for the remaining studies in this research.

Table 8: Summary of Polishing Effect Data

Non-Polished Specimen	# of test	Wear rate, mm ³ /cycle	Polished Specimen	# of test	Wear rate, mm ³ /cycle	Standard Deviation
CDC-14	n = 1	4.56E-07	CDC-14	n = 2	1.77E-07	1.18E-07
CDC-17	n = 1	2.08E-07	CDC-17	n = 2	6.57E-08	1.59E-08
CDC-21	n = 1	3.18E-07	CDC-29 (same as CDC-21)	n = 2	1.02E-07	2.61E-08
CDC-22	n = 1	4.28E-07	CDC-22	n = 4	2.33E-07	5.73E-08

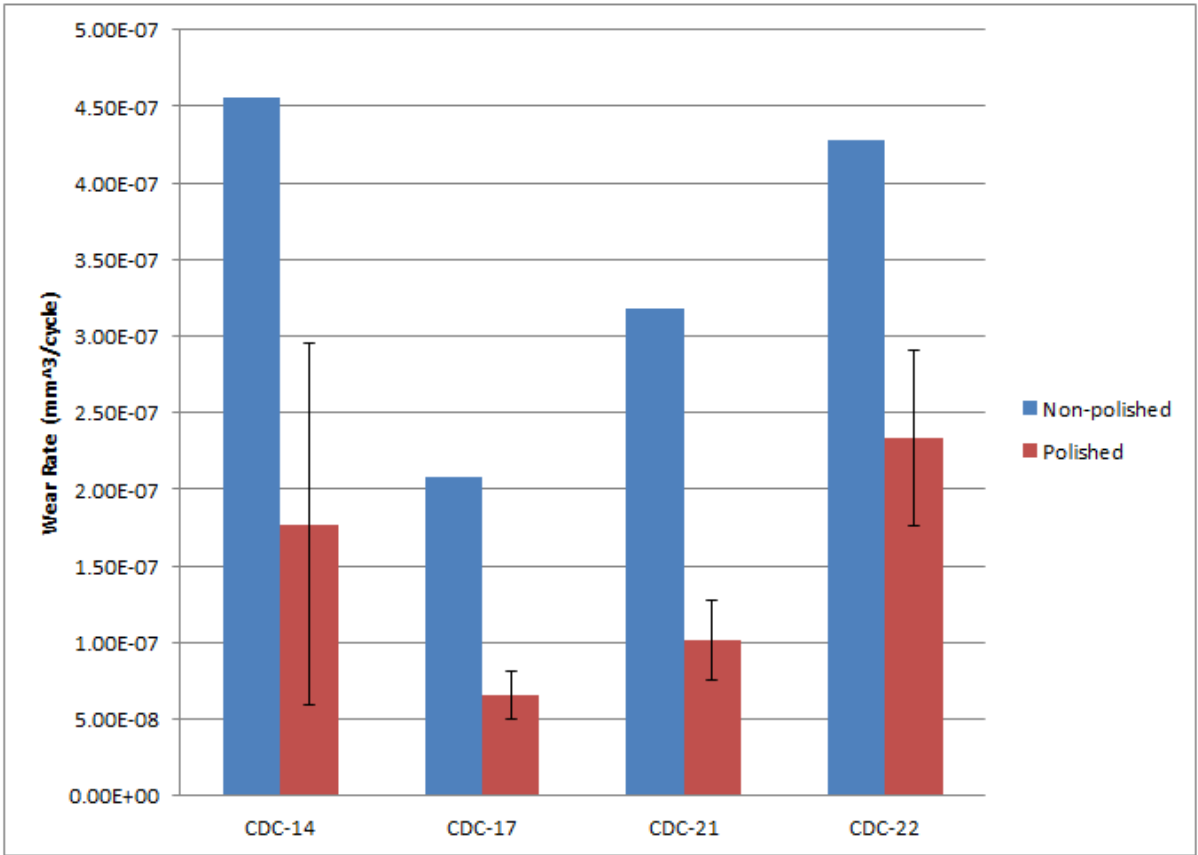


Figure 30: Wear Rate of CDC Specimens before and after Polishing

6.2.2 Effect of Sliding Frequency on Wear Rate

Biomechanical analysis of hip joints during normal gait cycle revealed that longer than 3 Hz is representing standing action [57]. It is well accepted that 1 Hz is representative of normal walking action. However, human hip joints may experience higher frequency during more aggressive activities such as running, jumping, sudden fall, and etc. Therefore, it is interesting to see the effect of sliding frequency on CDC wear rate. In this portion of the study, each specimen was tested at 3 sliding frequencies (10 Hz, 5 Hz and 1 Hz) for a total of 3600 cycles for each test. A sliding distance of 3mm and a normal load of 12.5 N were used in all the tests. Ti6Al4V and UHMWPE specimens were also tested in this study for comparison purposes. Some of the specimens were tested for 2-3 replicates ($n = 2$ or 3). Wear rate and standard deviation values for the tests are summarized in Table 9 and visually depicted in Figure 31.

As can be seen that different sliding frequencies has the most impact on the wear rates of Ti6Al4V specimens where higher wear rates were obtained at higher sliding frequencies. On the contrary, UHMWPE and CDC wear rates were not affected by the different sliding frequencies. It is well known that different sliding frequencies give different dwell times where a higher frequency gives a shorter dwell time. A short dwell time could impact the ability of oxide film formation on the Ti6Al4V specimens therefore resulted in higher wear rates due to tribocorrosion. The effect could be compounded as there could be a synergistic effect between tribocorrosion and mechanical wear [48]. Both UHMWPE and CDC specimens are non-corrosive materials with mechanical wear as the primary wear mechanism. Hence, it is conceivable that different dwell times have negligible impact on the wear rate of UHMWPE and CDC specimens.

Table 9: Summary of Sliding Frequency Effect on Wear Rate

Specimen	Normal load, N	Frequency, Hz	Stroke length, mm	Test duration, min	# of Test, n	Avg.Wear rate, mm ³ /cycle	Stdev
Ti6Al4V	10	10	3	6	2	1.32E-05	5.38E-06
	10	5	3	12	2	1.08E-05	1.30E-05
	10	1	3	60	2	6.35E-06	4.45E-06
UHMWPE	10	10	3	6	2	2.93E-06	2.41E-06
	10	5	3	12	2	3.25E-06	1.88E-06
	10	1	3	60	2	2.63E-06	1.33E-06
CDC-17	10	10	3	6	1	2.18E-07	-
	10	5	3	12	1	1.08E-07	-
	10	1	3	60	3	9.07E-08	4.48E-08
CDC-23	10	10	3	6	1	4.16E-07	-
	10	5	3	12	1	2.08E-07	-
	10	1	3	60	2	2.28E-07	1.05E-07
CDC-22	10	10	3	6	1	3.67E-07	-
	10	5	3	12	1	2.71E-07	-
	10	1	3	60	2	2.49E-07	8.50E-08
CDC-24	10	10	3	6	1	3.72E-07	-
	10	5	3	12	1	3.29E-07	-
	10	1	3	60	2	1.32E-07	2.06E-08
CDC-25	10	10	3	6	1	1.85E-07	-
	10	5	3	12	1	2.35E-07	-
	10	1	3	60	1	1.71E-07	-
CDC-26	10	10	3	6	1	2.20E-07	-
	10	5	3	12	1	3.42E-07	-
	10	1	3	60	1	3.61E-07	-

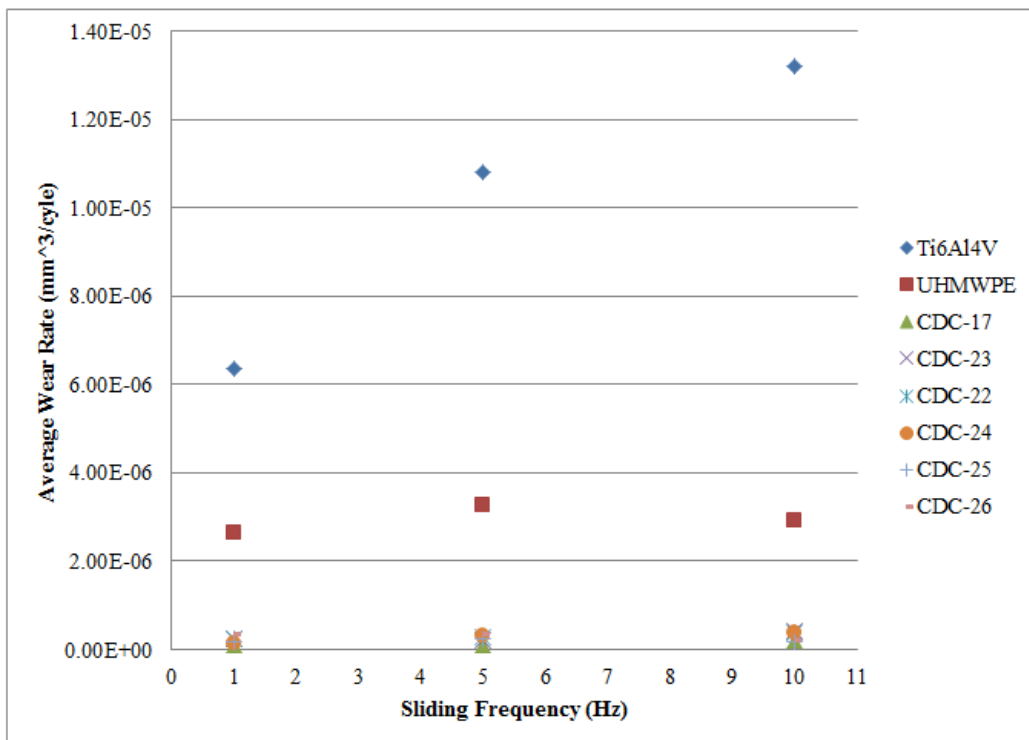


Figure 31: Wear rate of CDC and Standard Specimens at Different Sliding Frequencies

6.2.3 Effect of Sliding Time/Cycle on Wear Rate

It is well accepted that ~ 1 million step cycles is representing one year of in vivo use [57]. However, 1 million cycles at sliding frequency of 1 Hz means a total testing time of 11.6 days. To make effective use of time, the effect of sliding time on wear rate was studied to determine the appropriate testing time for the initial screening tests in this research. In this part of the research, CDC specimens and standard materials (Ti6Al4V and UHMWPE) were tested for 60, 120, 240, and 480 minutes or sliding cycles. A sliding frequency of 1 Hz, sliding distance of 3 mm and a normal load of 12.5 N were used for all the tests. Multiple replicates were conducted for some of the specimens. All the test conditions, wear rates and standard deviations are summarized in Table 10. Additionally, the wear rate results are visually presented in Figure 32.

Higher wear rates were observed at lower sliding times for all type of specimens. It should be pointed out that the CDC specimens have significantly lower wear rates as compared to the wear rates of Ti6Al4V and UHMWPE specimens. The higher wear rates observed at lower sliding times in all the specimens could be explained by the high initial wear, also known as the run-in-period. The effect of this severe initial wear will be diminished (or diluted) with increasing sliding time/cycle. As a result, sliding times of 60 and 120 minutes provide more discriminative wear rates and could indicate the enhanced tribological properties of CDC and the effect of processing parameters on wear rate. It is understood that the lower testing time will give lower wear volume and therefore higher variability in the wear volume measurement.

A testing time of 60 minutes was used as the standard testing time for the vast majority tests in this research. Multiple replicates were done for these 60-minute tests to address the wear volume measurement variability.

Table 10: Summary of Sliding Time Effect on Wear Rate

Specimen	Normal load, N	Frequency, Hz	Stroke length, mm	Test duration, min	Test cycles	# of Test, n	Avg. wear rate, mm ³ /cycle	Standard deviation
Ti6Al4V	12.5	1	3	60	3600	2	6.35E-06	4.45E-06
	12.5	1	3	240	14400	1	7.30E-07	-
	12.5	1	3	480	28800	1	8.29E-07	-
UHMWPE	12.5	1	3	60	3600	2	2.63E-06	1.33E-06
	12.5	1	3	120	7200	1	1.09E-06	-
	12.5	1	3	240	14400	1	7.16E-07	-
	12.5	1	3	480	28800	1	2.79E-07	-
CDC-17	12.5	1	3	60	3600	3	9.07E-08	4.48E-08
	12.5	1	3	240	14400	1	4.25E-08	-
	12.5	1	3	480	28800	1	4.20E-08	-
CDC-23	12.5	1	3	60	3600	2	2.28E-07	1.05E-07
	12.5	1	3	120	7200	1	1.03E-07	-
	12.5	1	3	240	14400	1	7.15E-08	-
	12.5	1	3	480	28800	1	5.78E-08	-
CDC-22	12.5	1	3	60	3600	2	2.49E-07	8.50E-08
	12.5	1	3	120	7200	1	1.58E-07	-
	12.5	1	3	240	14400	1	8.02E-08	-
	12.5	1	3	480	28800	1	4.47E-08	-
CDC-24	12.5	1	3	60	3600	2	1.32E-07	2.06E-08
	12.5	1	3	120	7200	1	9.00E-08	-
	12.5	1	3	240	14400	1	7.65E-08	-
	12.5	1	3	480	28800	1	4.91E-08	-
CDC-25	12.5	1	3	60	3600	1	1.71E-07	-
	12.5	1	3	120	7200	1	1.09E-07	-
	12.5	1	3	240	14400	1	8.23E-08	-
CDC-26	12.5	1	3	60	3600	1	3.61E-07	-
	12.5	1	3	120	7200	1	9.60E-08	-
	12.5	1	3	240	14400	1	9.26E-08	-
	12.5	1	3	480	28800	1	2.47E-08	-
CDC-29	12.5	1	3	60	3600	2	1.02E-07	2.61E-08
	12.5	1	3	120	7200	1	4.54E-08	-
CDC-30	12.5	1	3	60	3600	1	1.44E-07	-
	12.5	1	3	120	7200	1	6.76E-08	-
CDC-1b	12.5	1	3	60	3600	2	1.08E-07	5.79E-08
	12.5	1	3	120	7200	1	5.50E-08	-

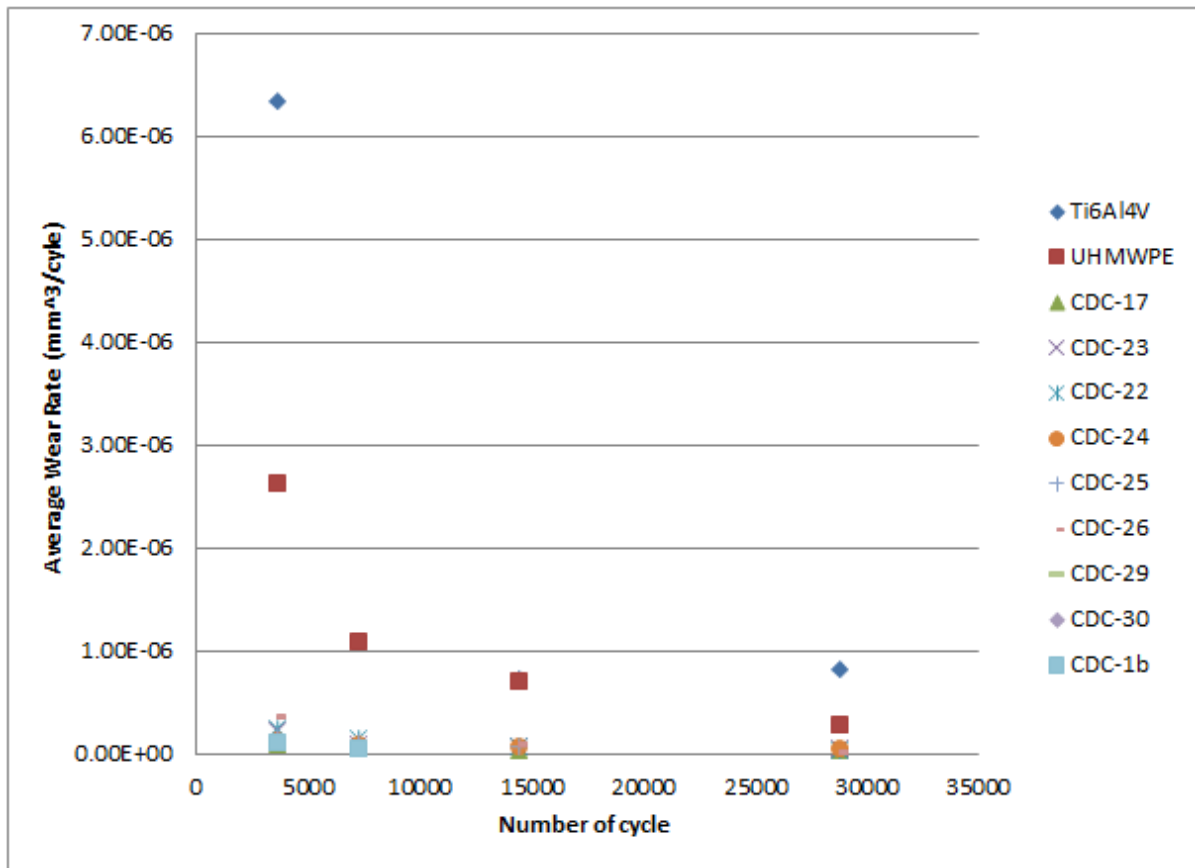


Figure 32: Wear rate of CDC and Standard Specimens at Different Sliding Time/Cycle

6.2.4 Effect of Processing Parameters on Friction Coefficient and Wear Rate

As shown that, wear rates of CDC specimens are significantly lower than the wear rates of UHMWPE and Ti6Al4V. Additionally, it was determined that lower sliding times gave more discriminative wear rates among the specimens tested therefore could be used to determine the low wear rate differences among the CDC specimens that were produced from different processing parameters.

As mentioned that an OFAT approach was used to study the effects of key processing parameters on wear rate. The key parameters studied and the respective experiments are summarized in Table 11. The OFAT experiments are listed in Table 12. Tribological test

results and SEM images can be found in Table 13 and Figures 33-38. The test results include (1) Maximum friction coefficient (CoF-max), (2) Average final friction coefficient (CoF-end), (3) Wear rate, and (4) Standard deviation values.

Table 11: Summary of Processing Parameters Studied and the Respective Experiments

Chlorination time, hr	Chlorination temp, °C	Post treatment gas	Post treatment time	Run ID
8	1000	-	-	CDC-16
≤ 8	1000	H ₂	8	CDC-14, CDC-17
19	1000	-	-	CDC-29
19	1000	H ₂	24	CDC-22, CDC-19
19	1000	Vac	24	CDC-24
19	1000	NH ₃	24	CDC-27
19	1100	-	-	CDC-30
19	1100	H ₂	24	CDC-25
19	1100	Vac	24	CDC-26
19	1100	NH ₃	24	CDC-28
8	1100	Vac	3	CDC-1b
19	1000	NH ₃	< 4	CDC-23

Table 12: Summary of OFAT Experiments

Processing Parameter	Levels		
	8 hours	19 hours	
Effect of chlorination and post treatment times	CDC-16	CDC-29	
	CDC-14, CDC-17	CDC-19 and CDC-22	
Effect of chlorination temperature	1000°C	1100°C	
	CDC-29 CDC-19 and CDC-22	CDC-30 CDC-25	
Effect of post treatment gas mixture	H ₂ -Ar	NH ₃ -Ar	Vacuum
	CDC-19 and CDC-22 CDC-25	CDC-27 CDC-28	CDC-24 CDC-26
Effect of post chlorination treatment time	3 hours	8 hours	24 hours
	CDC-1b and CDC-23	CDC-17	CDC-19 and CDC-22

Table 13: Summary of Processing Parameters Effect on CDC Wear Rate

Specimen	Cl2 temp, C	Cl2 time, hr	Post treatment gas	Post treatment time, hr	Post treatment temp, C	CoF-max	CoF-end	Wear rate, mm ³ /cycle	# of Test, n	Avg.Wear rate, mm ³ /cycle	Standard Deviation
CDC-14*	1000	5	H2	8	800	0.42	0.38	2.61E-07	2	1.77E-07	1.18E-07
	1000	5	H2	8	800	0.43	0.42	9.33E-08			
CDC-17	1000	8	H2	8	1000	0.48	0.39	5.44E-08	3	9.07E-08	4.48E-08
						0.45	0.35	7.69E-08			
						0.45	0.41	1.41E-07			
CDC-19	1000	19	H2	24	800	0.74	0.72	2.46E-07	2	2.17E-07	4.05E-08
						0.62	0.62	1.89E-07			
CDC-23	1000	19	NH3	4	800	0.62	0.60	1.54E-07	2	2.28E-07	1.05E-07
						0.57	0.55	3.02E-07			
CDC-22	1000	19	H2	24	800	0.56	0.54	3.09E-07	2	2.49E-07	8.5E-08
						0.49	0.46	1.89E-07			
CDC-24	1000	19	Vac	24	800	0.62	0.59	1.17E-07	2	1.32E-07	2.06E-08
						0.54	0.50	1.46E-07			
CDC-25	1100	19	H2	24	800	0.58	0.55	1.71E-07	1	1.71E-07	-
CDC-26	1100	19	Vac	24	800	0.62	0.61	3.61E-07	1	3.61E-07	-
CDC-29	1000	19	-	-	-	0.62	0.59	1.20E-07	2	1.02E-07	2.61E-08
						0.48	0.45	8.31E-08			
CDC-30	1100	19	-	-	-	0.68	0.66	1.44E-07	1	1.44E-07	-
CDC-1b	1100	8	Vac	3	800	0.56	0.51	6.72E-08	2	1.08E-07	5.79E-08
						0.62	0.54	1.49E-07			

Processing Times Effect on Wear Rate - Figure 33 shows the average wear rate of CDC specimens produced from short and long processing times. Short and long processing times represent 8 hours of chlorination time followed by 8 hours of post treatment time, and 19 hours of chlorination time followed by 24 hours of post treatment time, respectively. The same chlorination temperature (1000 °C) and post treatment gas mixture (H₂-Ar) were used in this set of experiments. It should be mentioned that CDC-29 was only chlorinated with no post treatment. It represents the chlorinated state of CDC-19 and CDC-22, and has a total processing time of 19 hours which is closer to the total short processing time of 16 hours. Substantial standard deviation values were obtained from the replicates of the tests which could be attributed to the low wear rates (higher measurement variability) and the fact that the replicates were conducted at months apart where other test variables such as BCS solution quality, specimen integrity and etc, could play a role. In general, no significant different was observed from the wear rates of CDC specimens produced from short and long processing times.

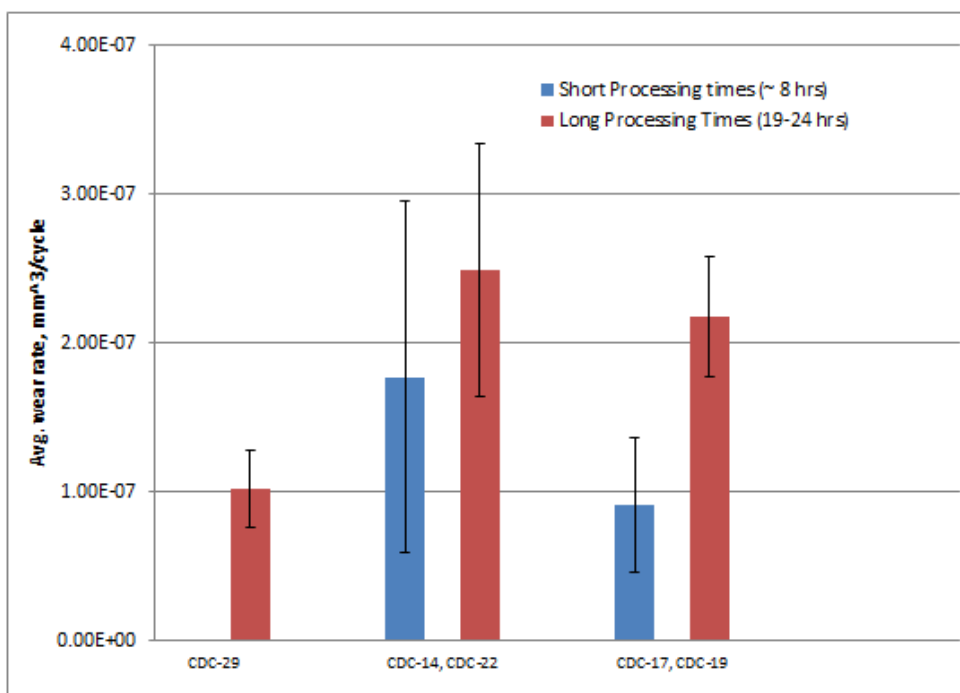


Figure 33: Wear rate of CDC Specimens at Different Processing Times

Chlorination Temperature Effect on Wear Rate - Previous study reported that rhombohedral crystalline graphitic structure was produced at a chlorination temperature of 1200°C and therefore improved the tribological properties of CDC due to the self-lubricating properties of rhombohedral crystalline graphitic structure [13]. However, another study reported that chlorination temperature beyond 1000°C result in CDC with predominantly graphitic structure and therefore shrinkage of the material [30]. Two temperatures, 1000 °C and 1100°C, was studied in this research to further investigate the effect of chlorination temperature on CDC wear rate.

CDC specimens chlorinated at the 2 temperatures before (CDC-29, CDC-30) and after post treatment (CDC-19, CDC-22, CDC-25) were tested using the standard tribological testing conditions (1 Hz, 3 mm, 12.5 N and 3600 cycles). As shown in Figure 34, no noticeable different in wear rate was observed among the 2 set of specimens that were produced at the 2 temperatures.

It should be pointed out that, some shallow and light cracks were observed on the CDC specimens chlorinated at 1000°C for 19 hours and post chlorination treated for 24 hours. On the other hand, more severe cracks were observed on CDC specimens produced from chlorination temperature of 1100°C, most noticeably on CDC-25 (chlorinated at 1100°C and post chlorination treated for 24 hours). SEM images of these CDC specimens are shown in Figure 35. It is believed that the cracks were caused by shrinkage of the CDC microstructure when converting to the most thermodynamic stable form, the graphitic structure. The result suggests that the CDC microstructure form conversion is a function of temperature and time.

Review of tribological data for the CDC specimens with and without post chlorination hydrogen treatment revealed that the post treatment did not reduce the friction coefficient

and/or wear rate of the CDC specimen, which is inconsistent with the finding from the previous study.

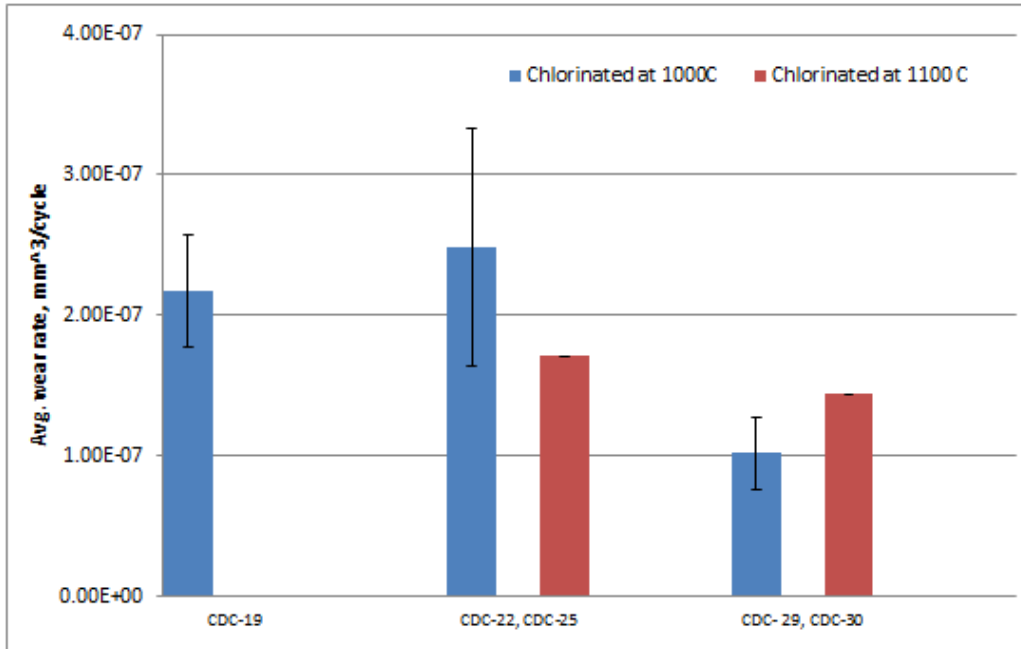


Figure 34: Wear rate of CDC Specimens at Different Chlorination Temperatures

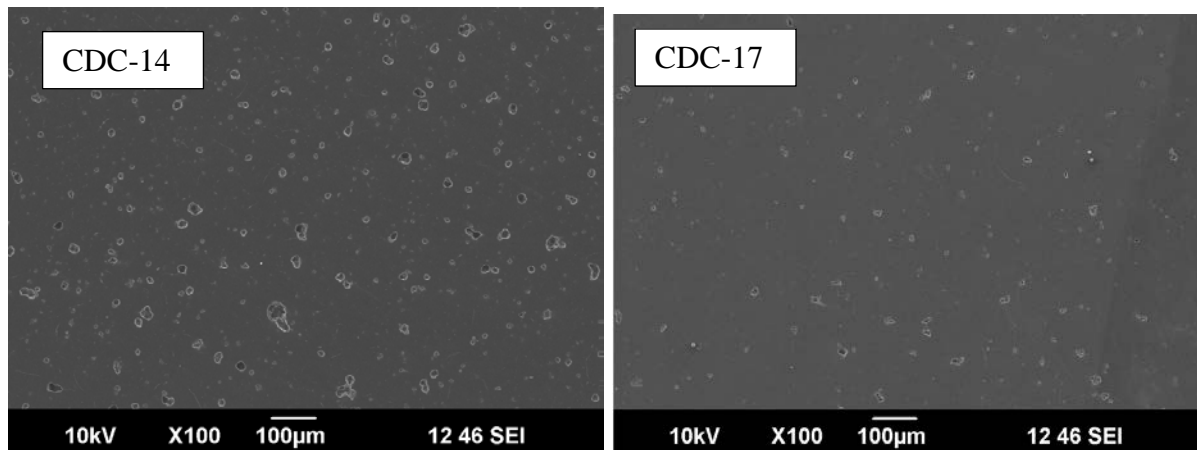


Figure 35: SEM Images of CDC Specimens at 100x Magnification

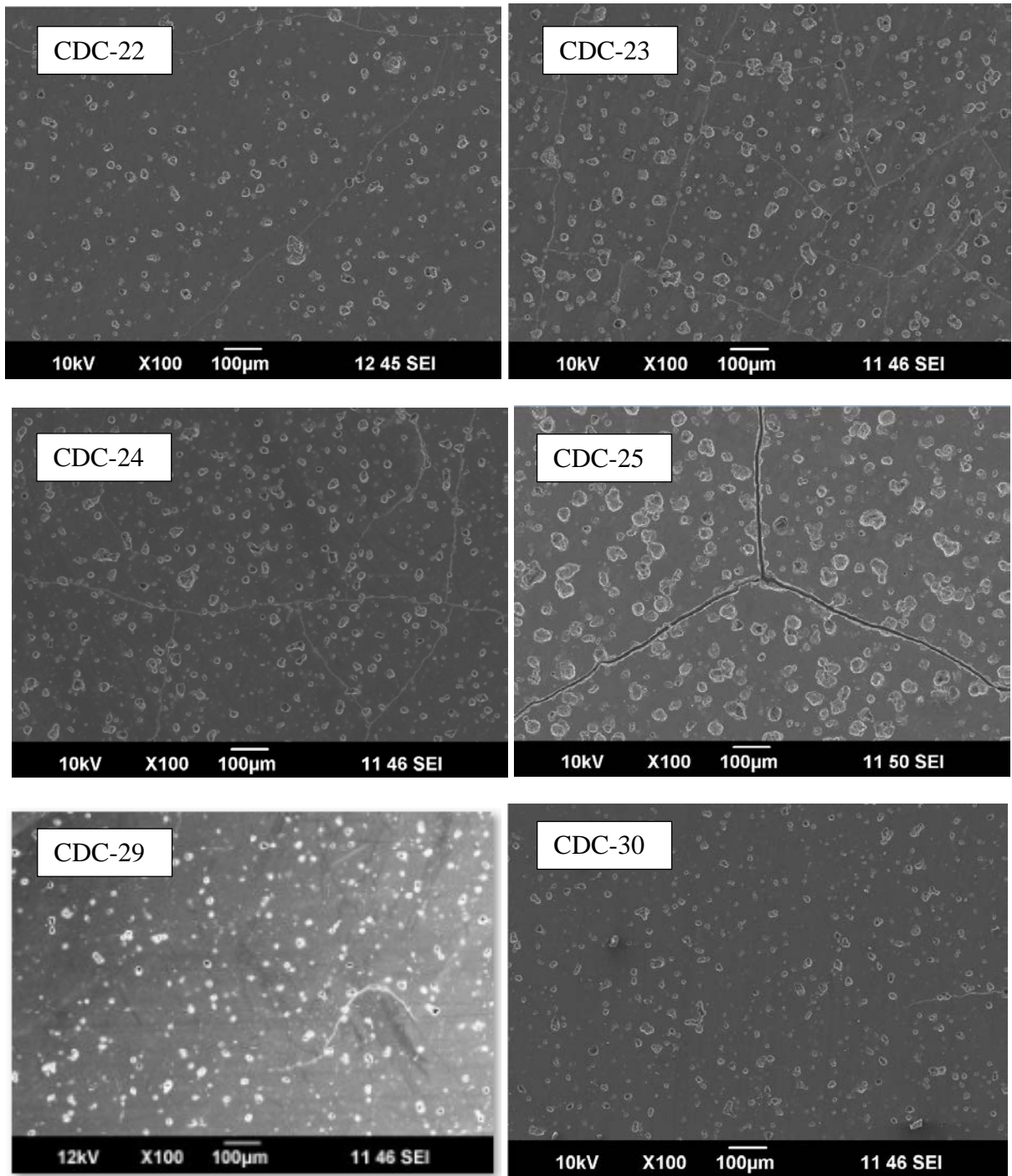


Figure 35: SEM Images of CDC Specimens at 100x Magnification (cont'd)

Post Treatment Gas Mixture Effect on Wear Rate - As known that gas treatment is a commonly used method to change the surface chemistry of materials. For an example, some of the commercially available tissue culture plates are vacuum gas plasma treated to improve cell attachment. It was reported that ammonia treatment leads to increased protein adsorption at neutral pH [58]. In this study, post treatment with 5% H₂-Ar, 5% NH₃-Ar and vacuum were studied. Long processing times (19 hours chlorination and 24 hours post treatment times) were used for this set of experiments to produce thicker layer of CDC since no significant different in wear rate was found between the short and long processing times. The experiments were conducted at chlorination temperature of 1000°C (H₂: CDC-19, CDC-22; NH₃: CDC-27; vacuum: CDC-24) and 1100°C (H₂: CDC-25; NH₃: CDC-28; vacuum: CDC-26).

The CDC specimens treated in 5% NH₃-Ar (CDC-27 and CDC-28) were severely cracked where the CDC layers were completely delaminated upon rubbing, therefore were not tested for tribological properties. SEM images of CDC-28 are shown in Figure 36. EDS analysis of CDC-28 revealed that only C, O, Cl and Si (substrate effect) are present on the specimen surface. The EDS result is summarized in Table 14. Wear rates of CDC specimens treated with 5% H₂-Ar and vacuum are shown in Figure 37. Once again, no significant different in wear rate was observed from the CDC specimens treated with 5% H₂-Ar and vacuum.

Table 14: EDS Result for CDC-28

Element	Spectrum 1	Spectrum 2	Spectrum 3
	Weight%		
C	94.51	94.8	96.44
O	5.49	4.72	3.56
Si		0.24	
Cl		0.23	
Total	100	99.99	100

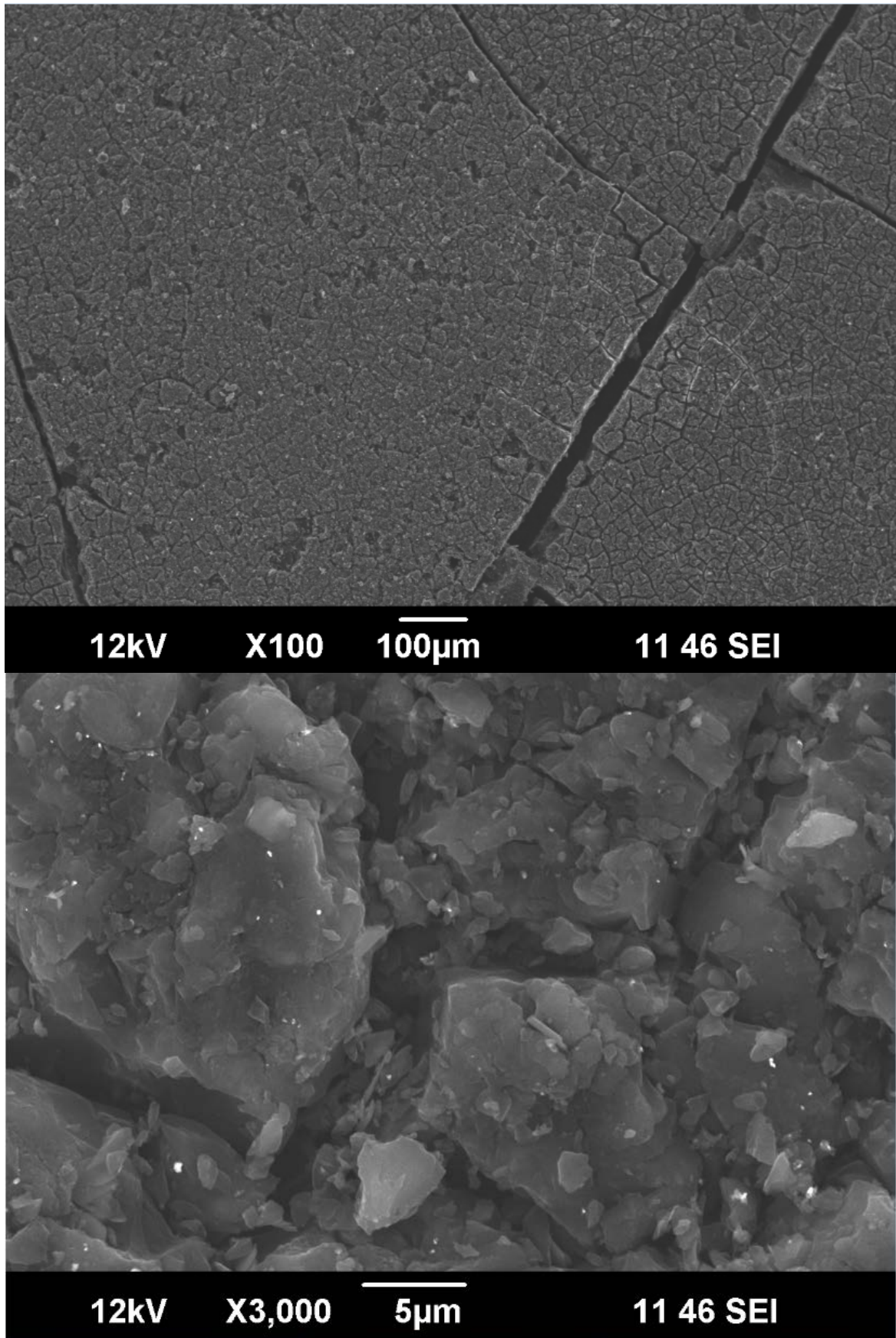


Figure 36: SEM Images of CDC-28

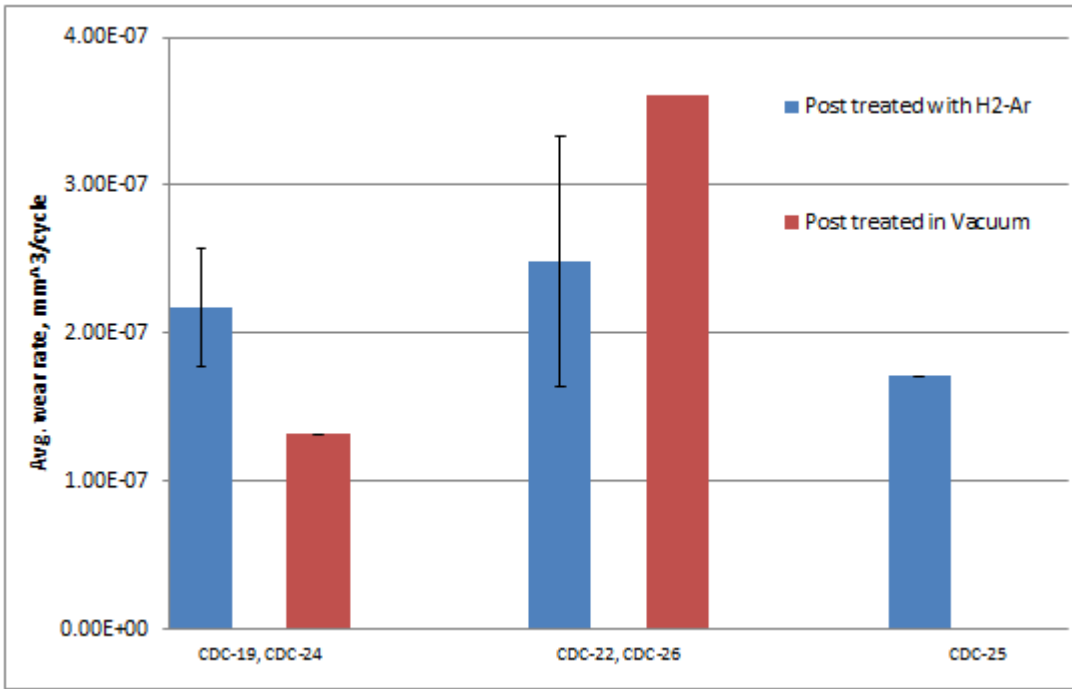


Figure 37: Wear rate of CDC Specimens with Different Post Treatment Gas Mixtures

Experimental data up to this point show that:

- Short vs. long chlorination times did not appear to impact the CDC wear rate. Some light cracks were observed on the specimens produced from the long processing times.
- Chlorination temperature at 1000°C and 1100°C with long chlorination times did not seem to impact the CDC wear rate, however, cracks were observed on the specimens produced at chlorination temperature of 1100°C.
- Post chlorination treatment with H₂ and vacuum using the long processing times produced CDC specimens with similar wear rates.
- CDC specimens treated by NH₃ post treatment with the long processing times were severely cracked.

With these findings, the next 2 questions were:

- (1) The surface cracking at chlorination temperature of 1100°C, was it due to the higher temperature or the long post treatment time? Will the specimen still be cracked if it was produced at 1100°C but post treated for a short period of time. To answer this question, CDC-1b was produced using chlorination temperature of 1100°C and vacuum post treated for 3 hours.
- (2) The crack phenomenon on the specimens treated by NH₃ was it due to the post treatment gas mixture or the long post treatment time. For this, CDC-23 was produced using chlorination of 1000°C and NH₃ post treated for < 4 hours.

No crack was observed on both CDC-1b and CDC-23 which indicates that the crack phenomenon is a function of temperature, treatment gas and time, and the phenomenon could be alleviated by shorter processing time. Wear rates of these CDC specimens were compared to the CDC specimens produced at chlorination temperature of 1000°C with short (CDC-17) and long (CDC-19 and CDC-22) processing times as shown in Figure 38. Again, no significant different in wear rate was observed.

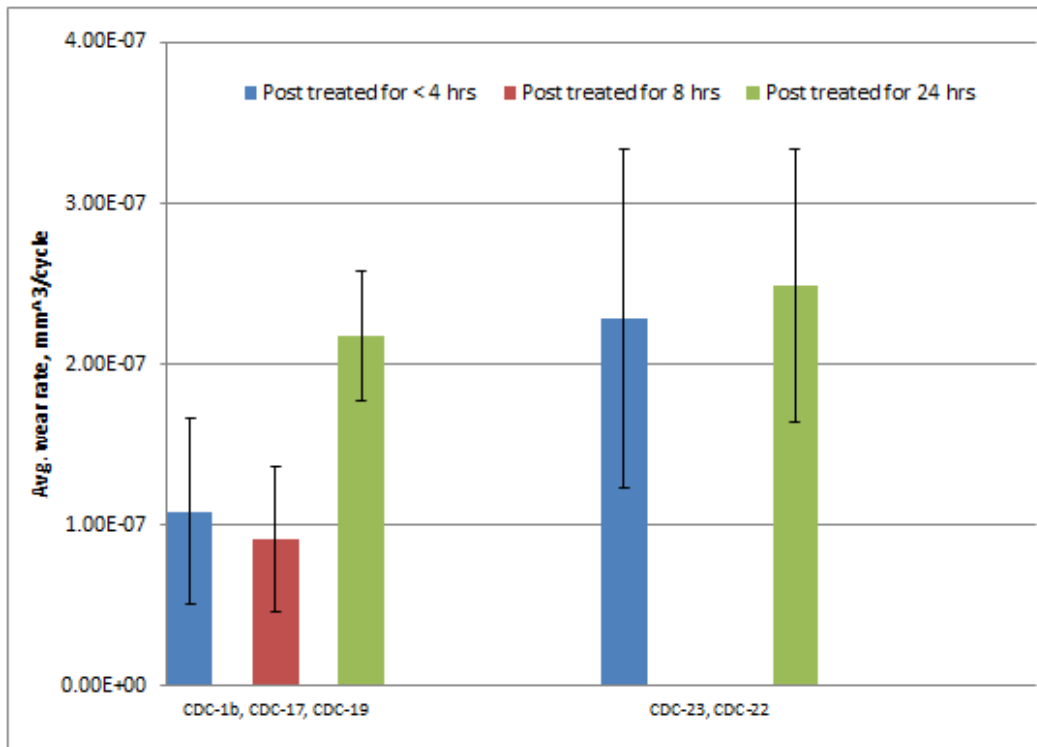


Figure 38: Wear rate of CDC Specimens with Different Post Treatment Times

Collectively, the data show that no detectable and measurable wear rate difference among the CDC samples produced from the different processing parameters studied. This also means that CDC with excellent wear rate can be produced via a wide range of parameters.

To further confirm this finding, tribological testing with 100,000 sliding cycles was conducted on the 2 CDC specimens produced at 1000°C with the short (CDC-17) and long (CDC-19) processing times. Each specimen was tested in two replicates ($n = 2$). Due to the long testing time (~ 27.8 hours), it was noticed that the BCS solution was thickening over the testing period due to evaporation. As known that given a constant surface area, the evaporation rate is primarily affected by the temperature and humidity in the air/environment. Friction coefficient curves for the tests are shown in Figure 39 where evident of BCS solution thickening over the testing period can be deduced from the increased of the curves. Note that, CDC-19 Trial 1 exhibited higher friction coefficient values as compared to the other tests, and something happened at around 1000 minutes where there was a sudden drop in the

friction coefficient values. It is believed that the sudden drop was due to drying out of the BCS solution. As a result, CDC delamination was observed on the wear scar of CDC-19 Trial 1, which was likely occurred when lifting the alumina ball from the specimen therefore the wear scar was not further analyzed. On the contrary, CDC-19 Trial 2 exhibited slightly higher friction coefficient values in the beginning of the test as compared to the CDC-17 tests, however, there was not much increase in the friction coefficient values over the testing period. This clearly shows the effect of testing environment on BCS evaporation rate and therefore the protein concentration which directly impacts the friction coefficient and the wear rate. The effect of protein on wear rate and friction coefficient is documented in the next section. In general, CDC's wear rate increases with protein concentration. Given that, the wear rate results in this study should represent the absolute worst case as the testing environment was not controlled and the protein concentration increased over the testing period.

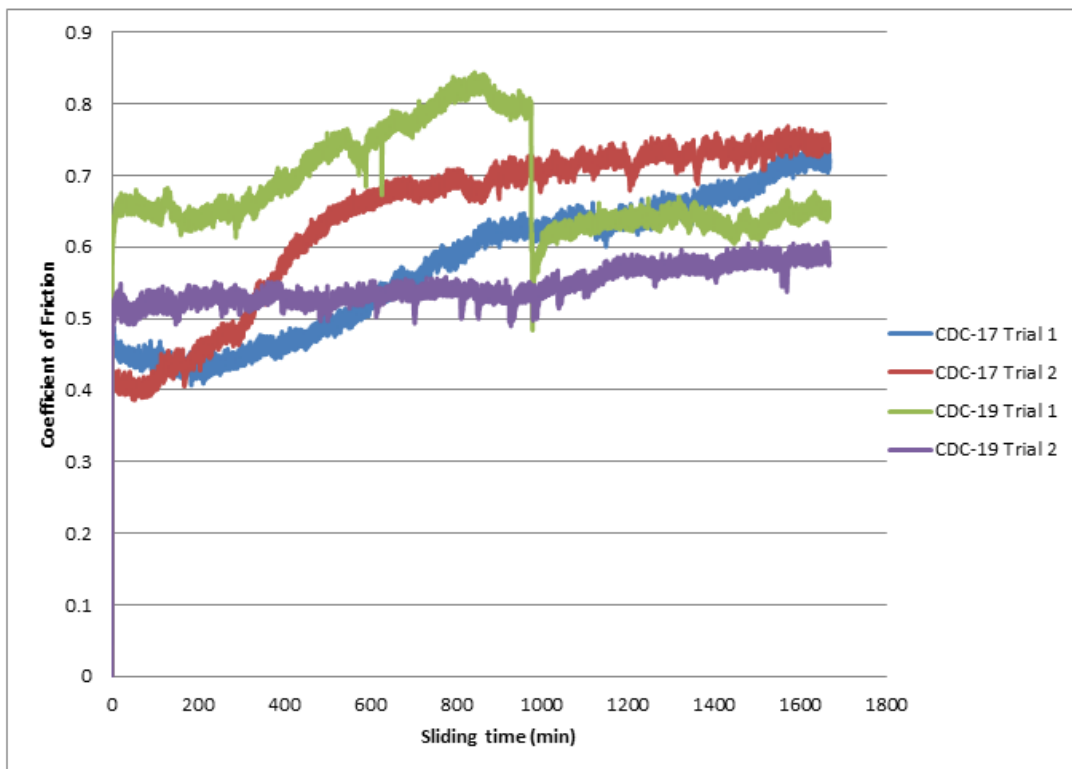


Figure 39: Friction Coefficient Curves for CDC-17 and CDC-19 in BCS Solution

Wear rate results and Zygo images of the wear scars are presented in Figures 40 and 41, respectively. A slightly lower wear rate was observed for CDC-19 as compared to the wear rate of CDC-17. This is probably due to the lower evaporation rate/lower protein concentration for the CDC-19 test. Despite the testing environment variability, the wear rates of the CDC specimens are still significantly lower than the wear rate of CoCrMo.

The Zygo images show that CDC-17 exhibited more uniform surface as compared to CDC-19, a replicate run of CDC-22. As shown in Figure 35, some shallow and light cracks were observed from the CDC specimens produced from chlorination temperature of 1000°C with long processing times (CDC-22, CDC-23, and CDC-24) while no crack was observed from the CDC specimens produced from the same temperature with short processing times (CDC-14 and CDC-17). It appeared that the shallow and light cracks did not significantly affect the CDC wear rate.

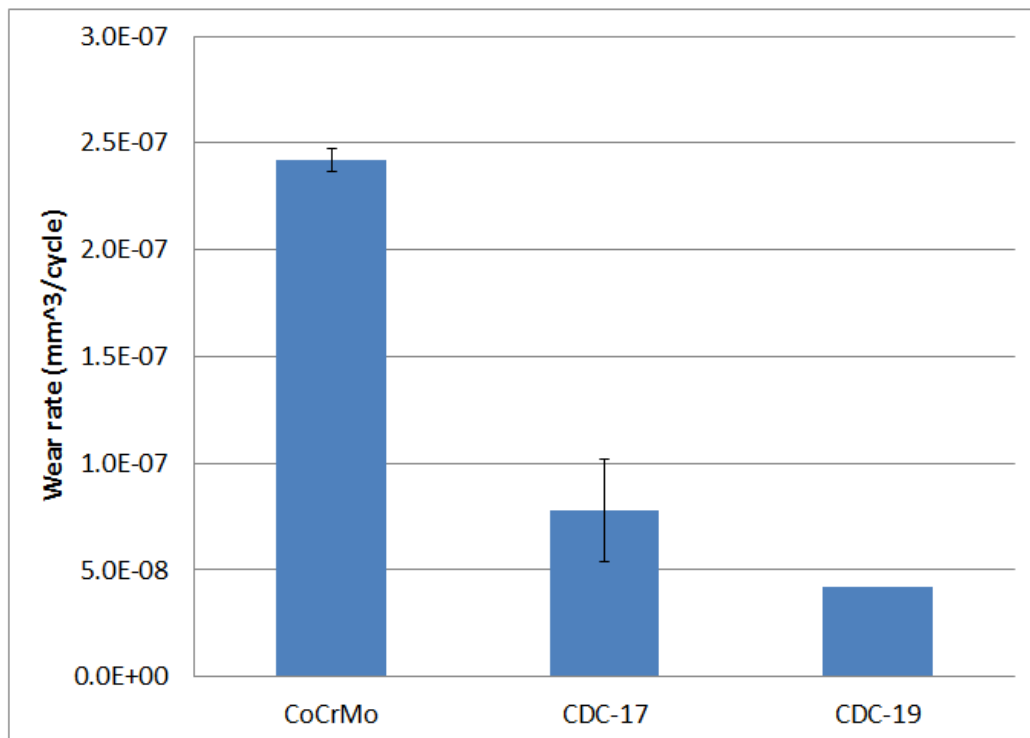


Figure 40: 100,000 Cycle Wear Rate Comparison between CDC-17 and CDC-19

CDC-17

CDC-19

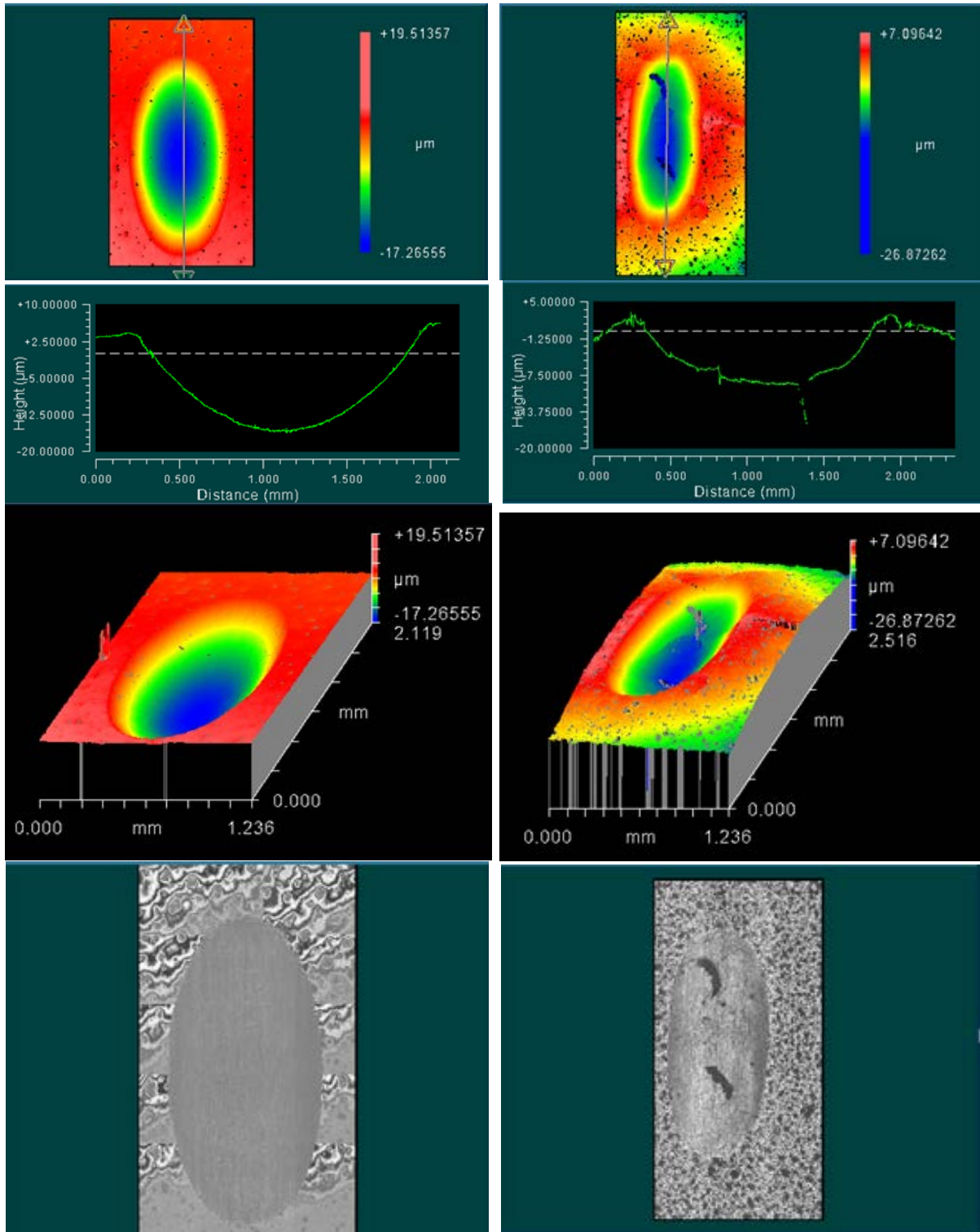


Figure 41: Zygo Images of 100,000 Sliding Cycles Wear Scars

6.2.5 Effect of Protein on Friction Coefficient and Wear Rate

As mentioned that protein concentration and the adherence of proteins to the material surface could effectively increase surface roughness and reduce the effectiveness of lubricant film thickness. A study of PTFE wear against stainless steel reported that higher wear rates were observed with increasing protein concentration [59]. Two other studies reported reduced wear of CoCrMo with increasing protein concentration as protein can effectively reduce the corrosion potential [48] [60]. CDC surface characterization to better understand protein adsorption ability was studied in this portion of the study. In addition, tribological testing was conducted with the two extreme CDC specimens (CDC-17 and CDC-19) using BCS and distilled water as the tribological testing solutions. The BCS solution has a protein concentration of 30g/L and a pH value of 7.6. The distilled water contains 0 g/L of protein and a pH of 6.8-7.0.

Protein adsorption testing was conducted using PierceTM Bicinchoninic Acid (BCA) protein assay kit. Please refer to section 5.6 for the testing procedures. Table 15 summarizes the adsorbed protein concentration, standard deviation of the protein concentration and the corresponding wear rates for the CDC specimens. Figure 42 shows the protein adsorption result for CDC specimens. A plot of average wear rate vs. adsorbed protein is shown in Figure 43.

The result shows that only a small amount ($194\text{-}517\ \mu\text{g/mL} \equiv 9\text{-}25\%$) of bovine serum albumin (BSA) protein was adsorbed on the CDC surface. The BCS solution contained $\sim 2100\ \mu\text{g/mL}$ of BSA protein. No definitive correlation between adsorbed protein and wear rate was observed in Figure 43.

Table 15: Summary of Protein Adsorption Test Result

Specimen	Protein Concentration ($\mu\text{g}/\text{mL}$)	stdev	Avg. wear rate, mm^3/cycle
CDC-13	278	25	3.46E-07
CDC-14	243	28	1.77E-07
CDC-1B	173	29	1.08E-07
CDC-17	260	26	9.07E-08
CDC-22	232	29	2.49E-07
CDC-23	301	34	2.28E-07
CDC-24	517	38	1.32E-07
CDC-25	195	26	1.71E-07
CDC-26	307	33	3.61E-07
CDC-29	230	31	1.02E-07
CDC-30	194	31	1.44E-07

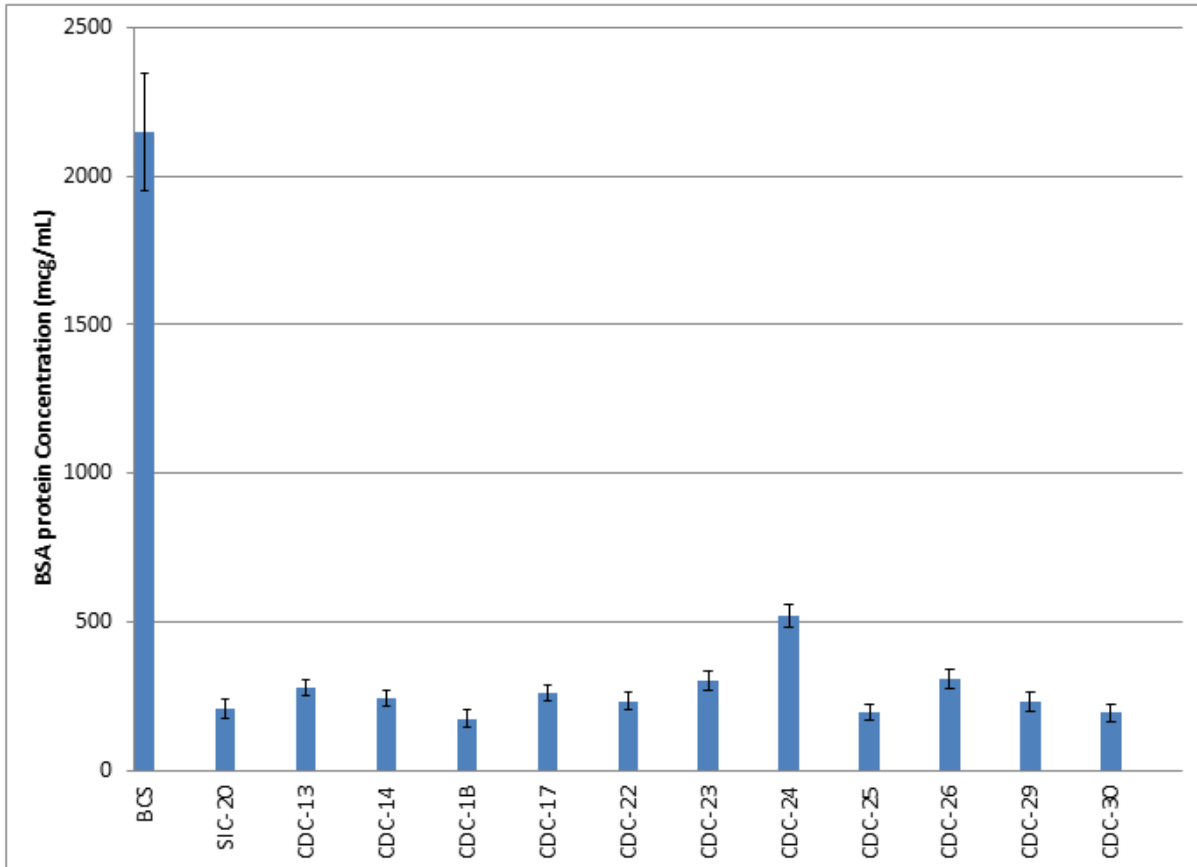


Figure 42: Protein Adsorption Result for CDC Specimens

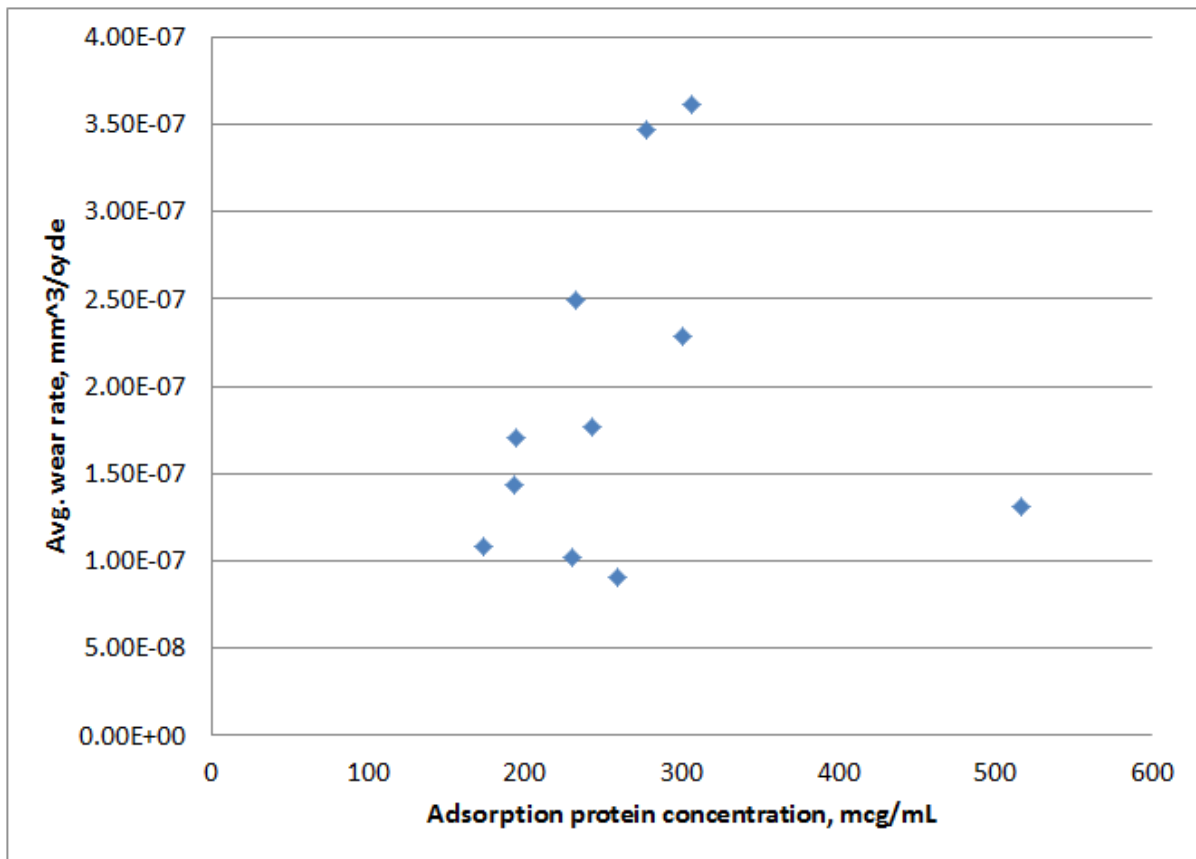


Figure 43: Average Wear Rate vs. Adsorbed Protein for CDC Specimens

The averaged wear rates and standard deviations for the tribological tests in BCS and distilled water are summarized in Table 16 and visually depicted in Figure 44. Lower wear rates were obtained from distilled water tests for both CDC-17 and CDC-19. This result is consistent with the PFTE study where higher wear was observed with increasing protein concentration. The presence of protein could increase the CDC surface roughness and reduce the effectiveness of lubricant film thickness. Reviews of friction coefficient (CoF) curves for these runs, as shown in Figure 45, found that CoF reduced with sliding time for the runs conducted in distilled water while CoF stayed constant throughout the testing period for the runs conducted in BCS.

Table 16: Summary of Protein Concentration Effect on Wear Rate

Specimen	Testing Solution	Avg. Friction Coefficient	Wear rate, mm ³ /cycle	Avg. Wear rate, mm ³ /cycle	Standard Deviation
CDC-17	BCS	0.46	5.44E-08	6.57E-08	1.59E-08
			7.69E-08		
CDC-19	BCS	0.84	2.46E-07	2.17E-07	4.05E-08
			1.89E-07		
CDC-17	H2O	0.44	4.83E-08	4.86E-08	3.93E-10
			4.89E-08		
CDC-19	H2O	0.65	1.25E-07	1.35E-07	1.41E-08
			1.45E-07		

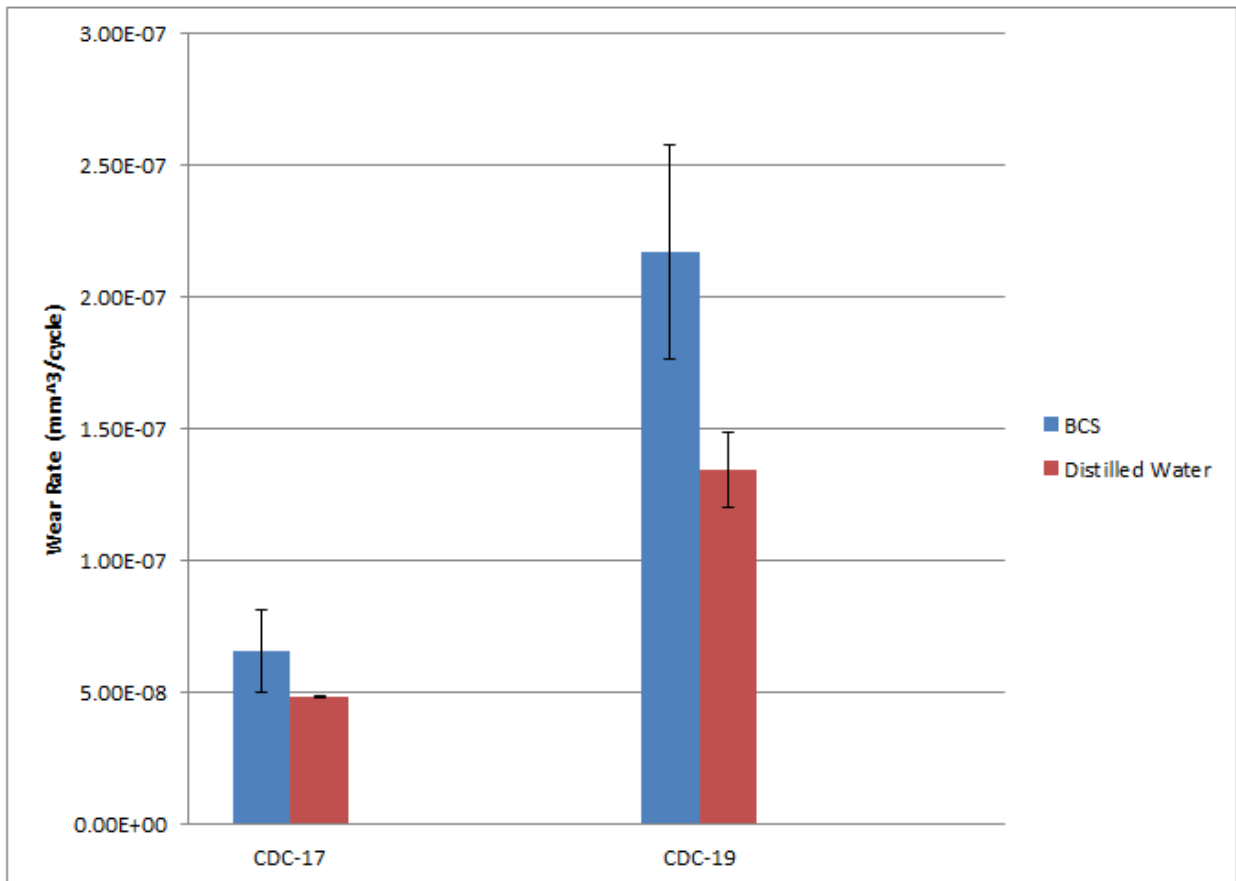


Figure 44: Summary of Protein Concentration Effect on Wear Rate

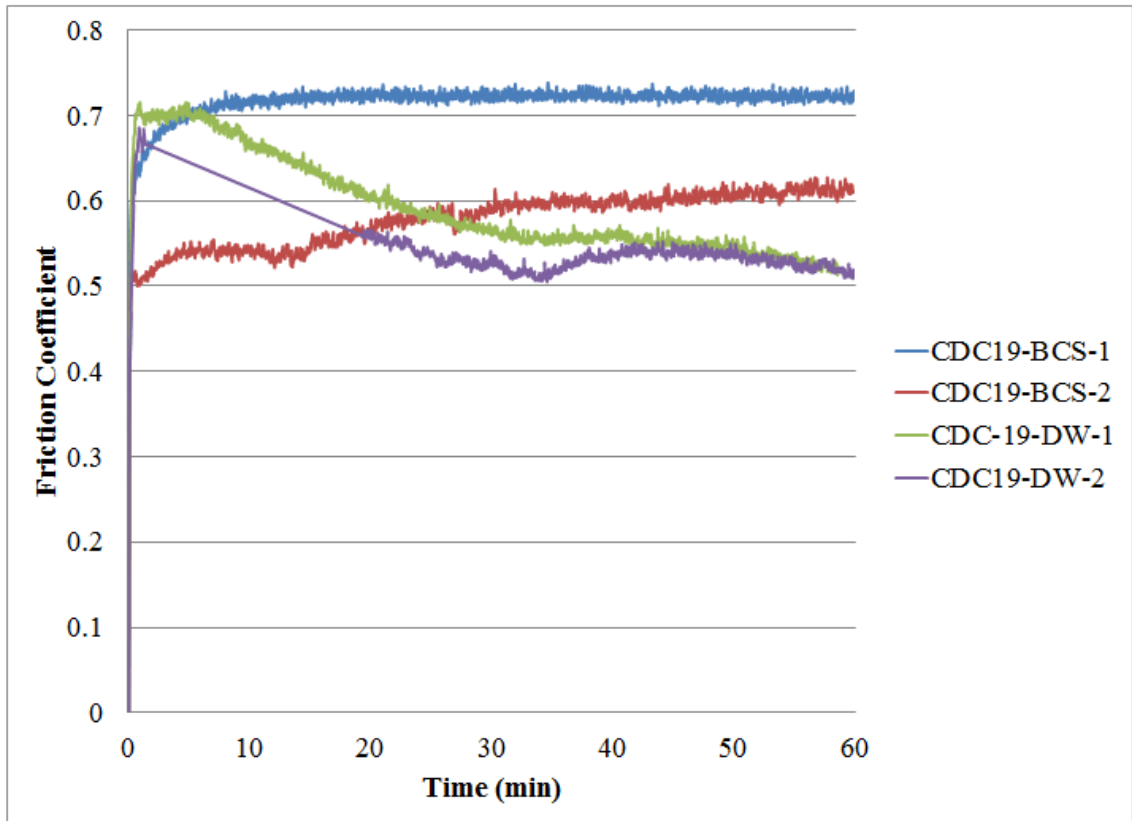


Figure 45: Effect of Protein Concentration on Friction Coefficient Curves

To further confirm this finding, tribological testing with 100,000 sliding cycles was conducted with CDC-19 using BCS and distilled water as the lubricant. Friction coefficient and wear scar data are tabulated in Table 17, and depicted in Figures 46 and 47. The result is consistent with the finding from the 3600 sliding cycles runs (Figure 44) therefore confirming the test result.

Table 17: Summary of Protein Concentration Effect on Wear Rate (100,000 Cycle)

Specimen	Wear rate (mm ³ /cycle)	Standard deviation
CDC-19 (BCS as lubricant)	4.20E-08	7.77817E-11
	4.21E-08	
CDC-10 (Distilled water as lubricant)	2.09E-08	1.9799E-10
	2.11E-08	

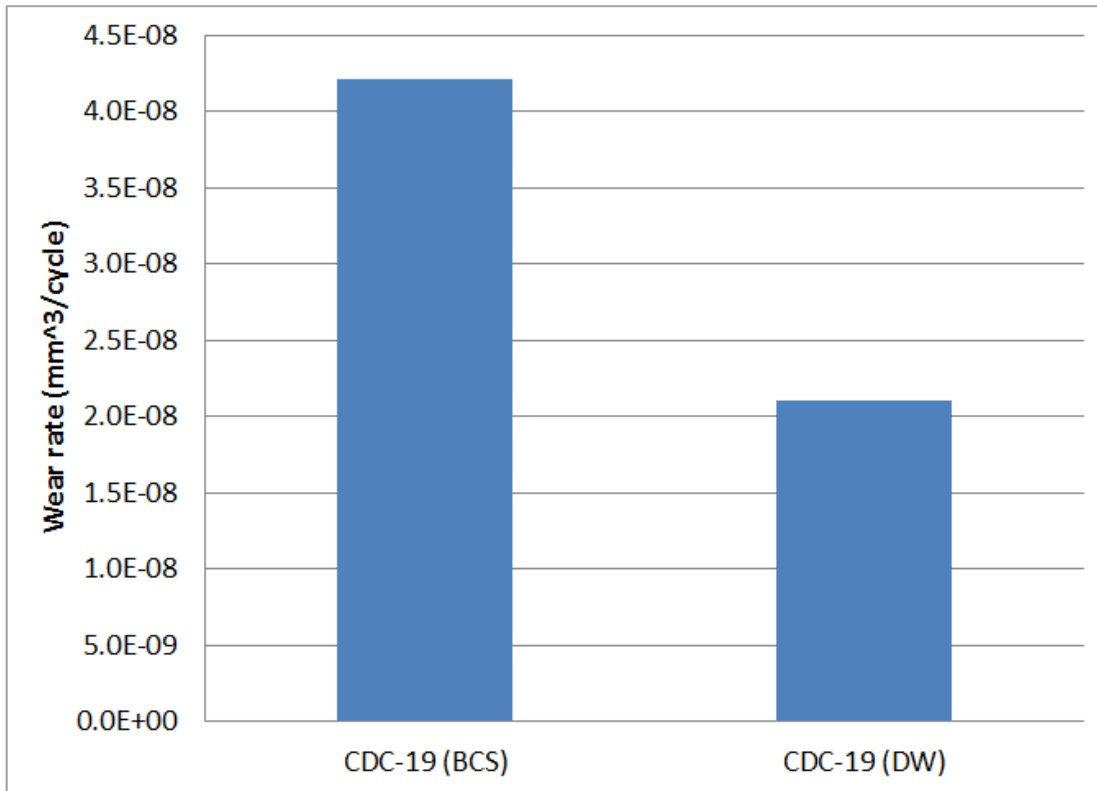


Figure 46: Summary of Protein Concentration Effect on Wear Rate (100,000 Cycles)

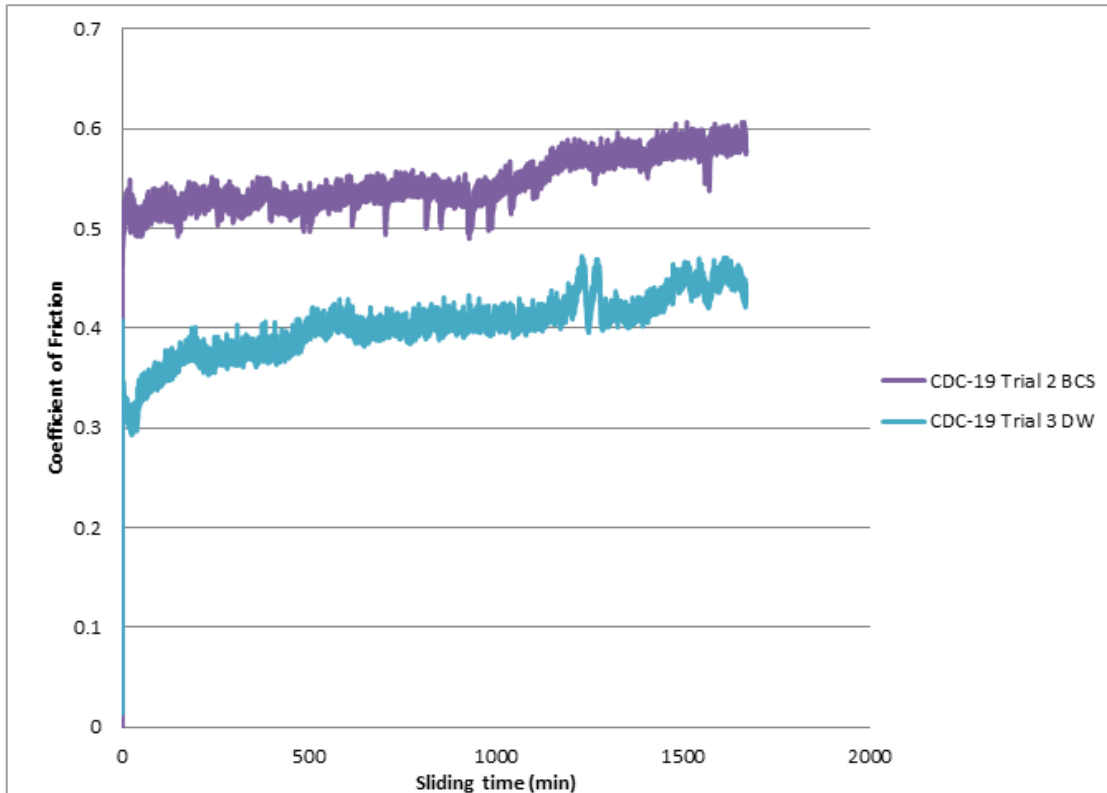


Figure 47: Effect of Protein Concentration on Friction Coefficient Curves (100,000 Cycles)

6.2.6 Comparison of 100,000 Sliding Cycles Data between CDC and CoCrMo

The CDC and CoCrMo specimens were tested in 2 different (but comparable) tribometer apparatus. BCS solutions with 30g/L of protein and alumina balls were used as the sliding counterpart for both the tests. The tribometer used for the CDC specimens is described in Section 4.9 (Bio-tribological Test). In general, the wear tests were conducted using a normal load of 12.5 N, sliding frequency of 1 Hz, and sliding distance of 3 mm, and with 9 mm diameter alumina balls sliding on CDC surfaces for 100,000 cycles.

For the CoCrMo, a cylindrical pin of CoCrMo with 12mm diameter were articulated against a 28 mm diameter alumina ball in a custom designed pin-on-ball set up [48]. The contact surface of the CoCrMo pin was polished to a surface roughness of 9.4 ± 2.6 nm Ra using standard metallographic methods [60]. To summarize, the wear tests were conducted using a ball rotation of $\pm 15^\circ$, a normal load of 16 N and at 1 Hz for 100,000 cycles.

A summary of the wear test conditions, and the corresponding initial Hertzian contact pressures and the wear rate results are presented in Table 18. As shown that for both CDC and CoCrMo, the initial Hertzian contact pressures for the linear reciprocating tribometer are significantly higher than the initial Hertzian contact pressures for the custom designed tribometer. Therefore, it can be concluded that the testing conditions for the linear reciprocating tribometer are more severe than the testing conditions for the custom designed tribometer. Despite with the more severe testing conditions, CDC still exhibit significantly lower wear rate as compared to the wear rate of CoCrMo, as shown in Figure 48.

Table 18: Summary of 100,000 Cycle Wear Test Conditions and Results for CDC and CoCrMo

Linear reciprocating tribometer	Sphere Counterpart (2)	Flat Sample (1)	
	Alumina ball	CDC	CoCrMo
Radius, r (mm)	4.5	0	0
Young's modulus, E (GPa)	350	25	241
Poisson ratio, ν	0.3	0.3	0.3
Mean Pressure (GPa)	-	285	947
Maximum Pressure (GPa)	-	428	1420
Wear Rate, mm^3/cycle		$7.8\text{E-}08 \pm 5.4\text{E-}09$	Not tested
Custom designed tribometer	Sphere Counterpart (2)	Flat Sample (1)	
	Alumina ball	CDC	CoCrMo
Radius, r (mm)	14	0	0
Young's modulus, E (GPa)	350	25	241
Poisson ratio, ν	0.3	0.3	0.3
Mean Pressure (GPa)	-	145	482
Maximum Pressure (GPa)	-	218	724
Wear Rate, mm^3/cycle		Not tested	$2.4\text{E-}07 \pm 2.4\text{E-}08^*$

* Calculated from weight loss values of 187.03 g and 1.87.5 g, and a density of 8.30 g/cm^3

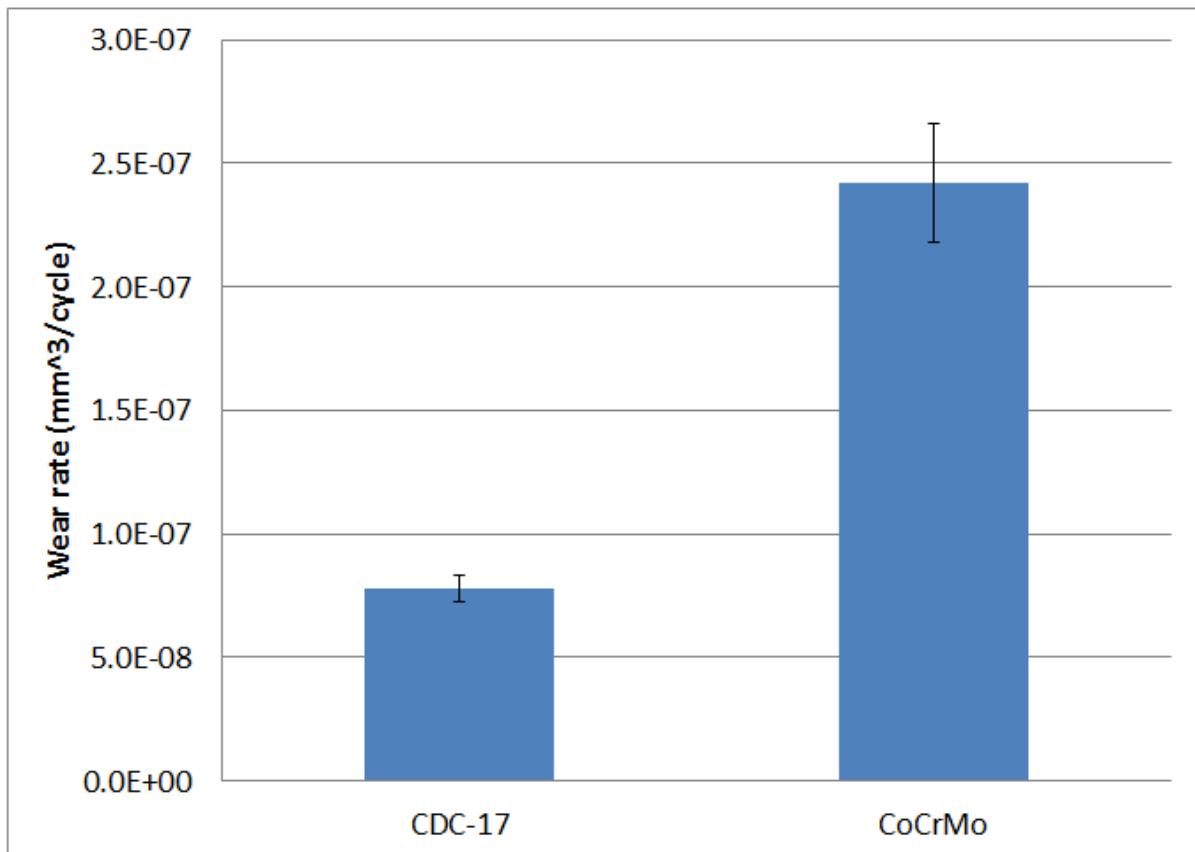


Figure 48: Comparison of 100,000 Cycle Wear Test Results between CDC-17 and CoCrMo

6.2.7 Wear volume of the Counterpart (alumina ball)

Due to the hardness difference between the test specimens and the alumina balls, and the mechanical action during the tribological test, some degrees of wear is expected on the alumina balls. Hardness and wear volume/rate values for SiC and CDC specimens are summarized in Table 19 and Figure 49. As expected that, alumina ball sliding on SiC resulted in a higher wear volume on the alumina ball while lower wear volumes were observed for alumina ball sliding on CDC specimens. This could be due to the fact that SiC is much harder than alumina and CDC is a lot softer than the alumina ball. In addition, similar wear volumes were obtained for the CDC specimens sliding for 28,800 and 100,000 cycles. This result supports the hypothesis that CDC will form a smooth layer after the run-in-period and further reduce the friction coefficient and wear on the contacting parts.

Table 19: Summary of Hardness and Wear Result on the Alumina Balls [61]

Material	Hardness (GPa)		
Alumina ball	11 -14.4		
SiC	27 - 28		
CDC	~ 2		
Specimen	Sliding cycle	Wear volume (mm³)	Wear rate (mm³/cycle)
SiC-18	28,800	0.000163	5.66E-09
CDC-22	28,800	0.000040	1.39E-09
CDC-25	28,800	0.000073	2.53E-09
CDC-19	100,000	0.000025	2.50E-10
CDC-19 (DW)	100,000	0.000030	3.00E-10

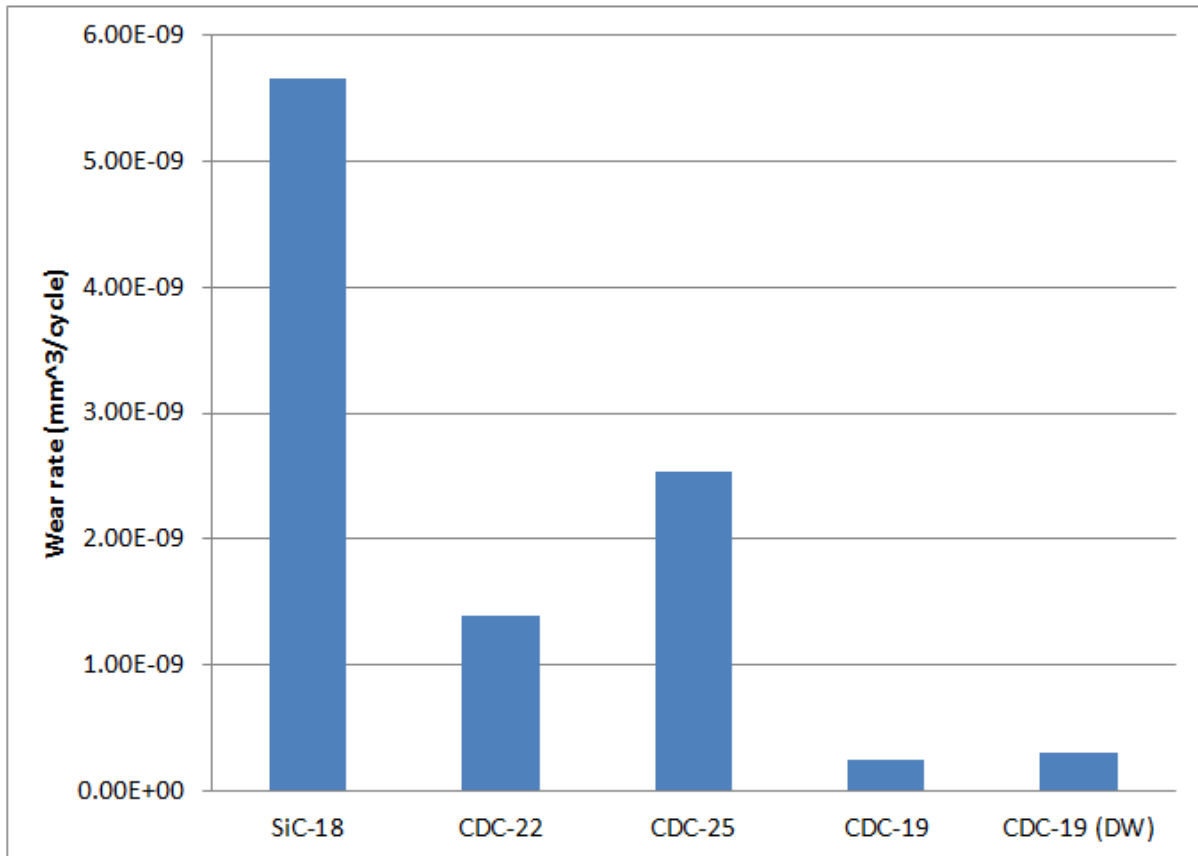


Figure 49: Wear Result on the Alumina Balls

6.3 Determine the Effect of Post Chlorination Treatments on the Biocompatibility of the CDC Specimens.

In this research, biocompatibility was determined by cell viability, which is defined as the number of healthy cells in a 96-well or on the test specimen. Four tests utilized 2 cell viability assays were completed for the study in order to confirm the test results of the individual test/assay. To recapture, the 4 test are:

- Indirect contact cytotoxicity test – high cell seeding density with 2 days exposure time
- Indirect contact cell proliferation – low cell seeding density and cell viability was determined over 7 days

- Direct contact cytotoxicity test - high cell seeding density and cell viability was determined after 2 days
- Direct contact cell proliferation test – low cell seeding density and cell viability was determined after 7 days

And, the 2 assays are (1) Quantitative cell viability using CCK-8, and (2) Qualitative cell viability using live/dead cell viability kit. To minimize the test method variability and standardization of the test result for ease of comparison, all the quantitative cell viability results are presented in percentage of the negative control result, UHMWPE.

It should be reiterated that, prolonged extraction times and higher solid-to-solvent ratio than the recommended conditions listed in ISO were used in this study because the CDC specimens are not very toxic so the severe conditions are needed to give discriminative test results. Test procedure details can be found in section 4.5 through section 4.8.

For the biocompatibility study, CDC specimens with and without post treatment were tested for cell viability, as summarized in Table 20. CDC-7 was chlorinated at 1000°C for 5 hours with no post treatment whereas CDC-13 and CDC-14 were also chlorinated at 1000°C for 5 hours plus 8 hours of hydrogen treatment. Both CDC-29 and CDC-30 were chlorinated for 19 hours at 1000°C and 1100°C, respectively. In short, CDC specimens chlorinated similarly are listed on the same row under the respectively post treatment column.

CDC-27 and CDC-28 were chlorinated for 19 hours at 1000°C and 1100°C, respectively. Both specimens were treated in NH₃ for 24 hours. However, the specimens were severely cracked therefore were not furthered evaluated.

Table 20: Summary of CDC Specimens with and without Post Treatment

Chlorinated CDC	H ₂ Treated CDC	Vacuum Treated CDC	NH ₃ Treated CDC
CDC-7	CDC-13, CDC-14		
CDC-29	CDC-19	CDC-24	CDC-23, CDC-27*
CDC-30	CDC-25	CDC-26, CDC-1b	CDC-28*

* Specimen damaged and was not tested.

6.3.1 Effect of Hydrogen Post Treatment on Biocompatibility of CDC Specimens

Quantitative test results for hydrogen treated specimens are summarized in Table 21 and visually depicted in Figure 50. Appropriate test system response and background response were confirmed based on the desired positive control and negative control results where a lot of viable cells were detected from the negative control specimen and very few viable cells were detected from the positive control specimen. As expected, cell culture medium (media control) control shows slightly higher viable cell count as compared to the negative control.

Titanium type V alloy (Ti6Al4V), one of the materials used in commercial hip implants, shows comparable biocompatibility result as the negative control for the indirect contact cytotoxicity test. However, it exhibited only 75-90% cell viability for the indirect contact cell proliferation test, a more stringent test than the cytotoxicity test.

The indirect contact cell proliferation test was executed with prolonged extraction time (7 days vs. 3 days in the indirect contact cytotoxicity test vs. ISO recommendation of 1 day) and higher solid-to-solvent ratio (7.5-15 cm²/mL vs. ISO requirement of < 6 cm²/mL) therefore should be more indicative than the indirect contact cytotoxicity test.

For the cell proliferation test, each of the 96-well was seeded with 2200 cells. At day 4, cell growth was observed on all the specimens except for the positive control. However, cell reduction was observed on all the CDC specimens on day 7, although the degrees of reduction were different among the CDC specimens. Less than 50% of viable cell was observed from CDC-7, CDC-29 and CDC-30, the specimens with no hydrogen post treatment. CDC-13 and CDC-14 exhibited over 100% of viable cell at day 7, followed by CDC-19 with 86% viable cell then CDC-25 with 58% viable cell. Test results with similar trend were obtained from the indirect contact cytotoxicity test therefore confirming the test result. Collectively, the test results show that post chlorination hydrogen treatment improved the biocompatibility of the CDC specimens, and the treatment effect is higher on the CDC specimens produced from the short processing times (with thinner CDC layer).

Table 21: Summary of Hydrogen Post Treatment Effect on Biocompatibility of CDC

Specimen	Indirect Contact Cytotoxicity-Day 2		Indirect C. Proliferation- Day 4		Indirect C. Proliferation- Day 7	
	% Cell Viability	Stdev	% of Cell Viability	Stdev	% of Cell Viability	Stdev
Media Control	102	6	113	6	102	6
Ti6Al4V	103	2	74	4	89	3
Negative Control	100	2	100	14	100	3
Positive control	3	1	7	9	2	2
CDC-7	-	-	120	18	47	10
CDC-29	6	0	109	3	48	4
CDC-30	5	1	91	5	39	4
CDC-13	95	2	110	2	104	6
CDC-14	99	5	117	3	111	7
CDC-19	86	2	128	4	86	6
CDC-25	-	-	81	4	58	6

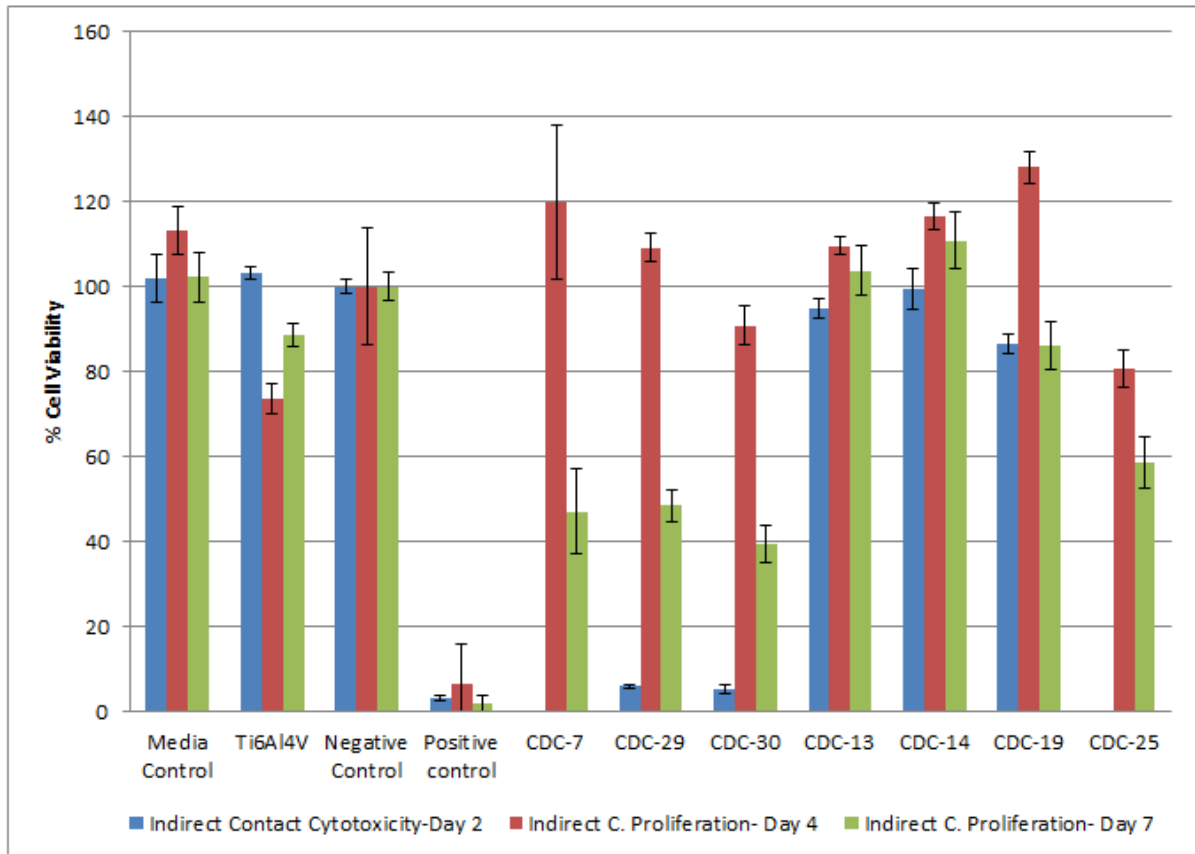


Figure 50: Summary of Hydrogen Post Treatment Effect on Biocompatibility

EDS analysis of these CDC specimens revealed that the biocompatibility results are somewhat correlating to the amount of residual chlorine in the CDC specimens. A summary of the EDS test result is provided in Table 22 and depicted in Figure 51.

Table 22: EDS Test Result for CDC Specimens with and without Hydrogen Treatment

Specimen	C	O	S	Cl	Al	Fe	Si	Na	Ca	Cu	Tm	SUM	Avg. Cl	% Viable cell of PE
	w/w %													
CDC-13	86.14	6.28	0.70				6.28	0.23	0.36			99.99	0.0	104
	85.49	4.17	0.53				9.29	0.20	0.32			100.00		
	83.93	6.32	0.92				8.61	0.22				100.00		
CDC-14	88.46	9.92	1.30					0.33				100.01	0.7	111
	84.77	12.57	1.36	0.71	0.59							100.00		
	88.05	10.35	1.32					0.28				100.00		
CDC-19	78.11	16.52	2.33	1.58						1.45		99.99	1.1	86
	92.02	7.19		0.79								100.00		
	92.45	6.72		0.82								99.99		
CDC-25	93.20	6.27		0.53								100.00	0.6	58
	99.29			0.71								100.00		
	92.73	6.60		0.66								99.99		
CDC-29	97.26		0.14	2.13			0.07				0.40	100.00	2.3	48
	85.58	9.83	0.54	2.60	0.25		1.06	0.15				100.01		
	97.78			2.22								100.00		
CDC-30	92.16	6.42		1.41								99.99	1.9	39
	84.90	11.49	1.32	2.29								100.00		
	89.11	8.08	0.38	1.91								99.48		

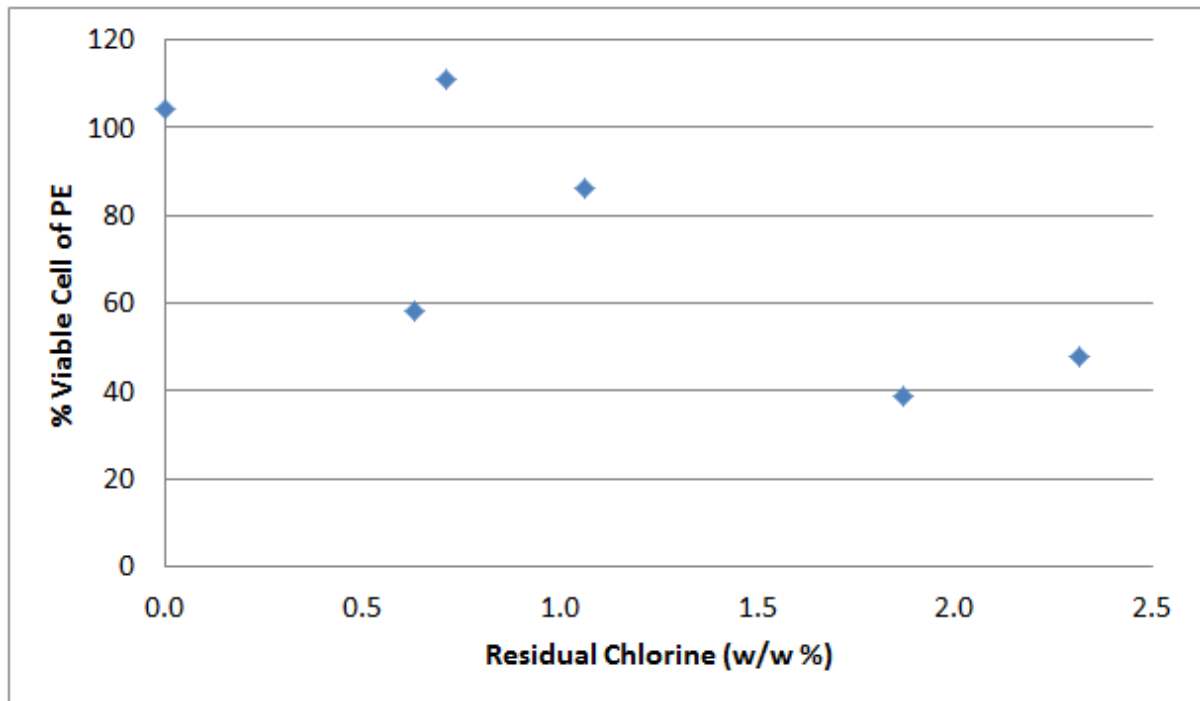


Figure 51: Percent Viable Cell of PE vs. Residual Chlorine for Hydrogen Treated Specimens

Direct contact cytotoxicity test was conducted on Ti6Al4V, CDC-29, CDC-30, CDC-13, CDC-19 and CDC-25 and the resultant fluorescence images for the test are presented in Figures 52-57. In addition, direct contact cell proliferation test was conducted on Ti6Al4V, CDC-13 and CDC-19 and the respective fluorescence images are shown in Figure 58-60.

In general, predominantly live cells with some dead cells are shown on all the images including the CDC samples with no hydrogen post treatment (CDC-29 and CDC-30). This result is not too surprising since it was learned that the CDC samples are not very toxic and more stringent extraction and cytotoxicity test conditions were required for the indirect cytotoxicity and cell proliferation tests to be discriminative.

As known that the most challenging factor in live-cell imaging is control of cell culture environment, from cell staining to cell imaging, to maintain overall cell health and prevent false negative result (cell death causes by the artifact). Additionally, live-cell imaging is extremely analyst technique dependent and is a highly subjective qualitative test. For an example, the imaging cell density result is affected by cell seeding technique and the selection of area (view) to image. Therefore, live-cell imaging should always be done in conjunction to another test to verify the test result.

Based on the imaging result and considering the nature of live-cell imaging, it is reasonable to believe that all the CDC specimens tested in this section are relatively biocompatible.

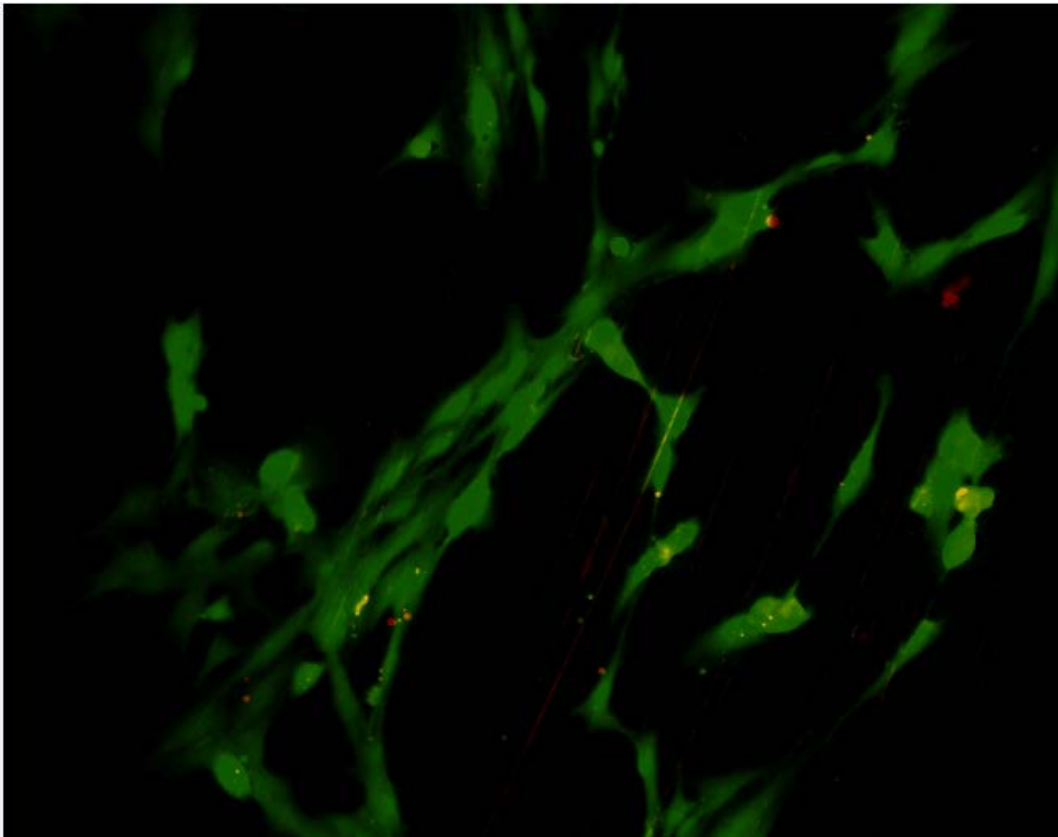
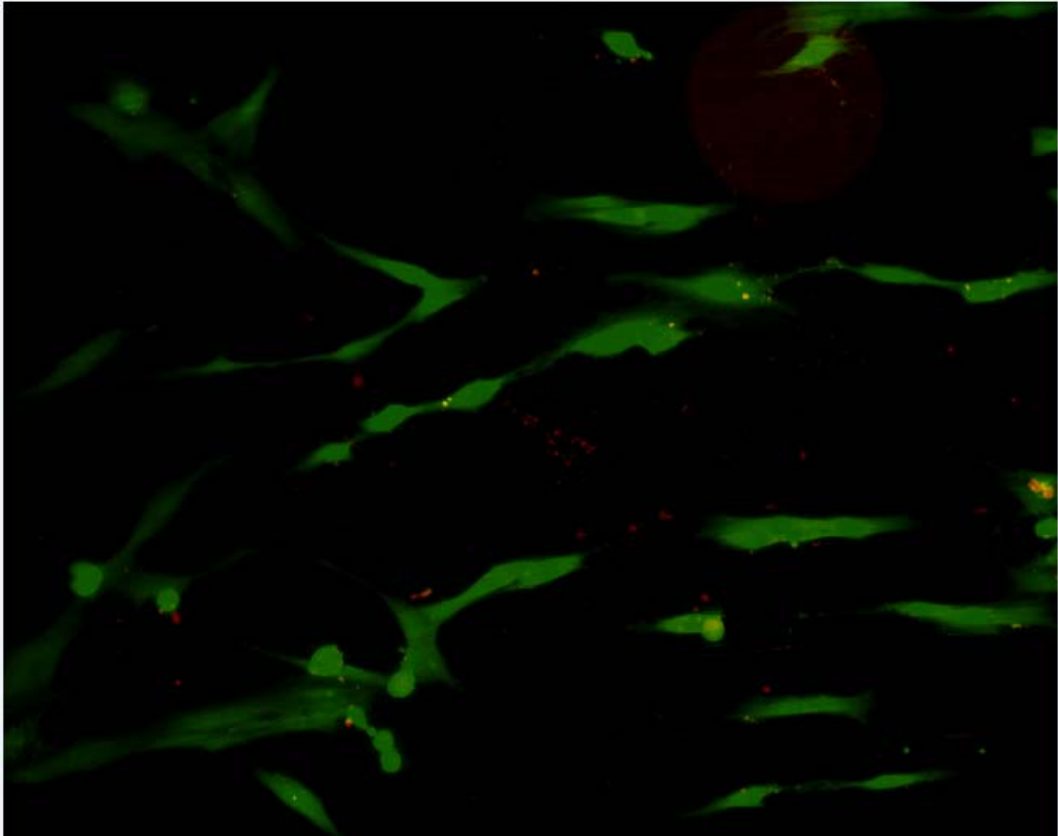


Figure 52: Fluorescence Images for Ti6Al4V at Day 2 of Cytotoxicity Test

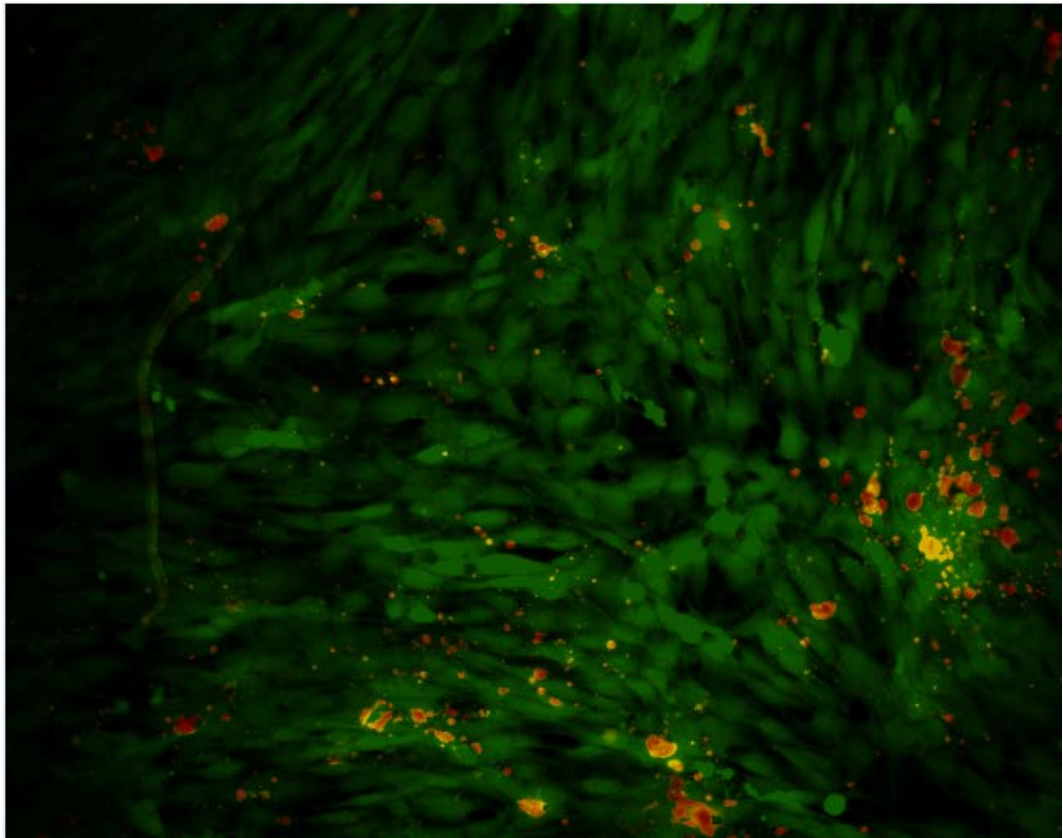
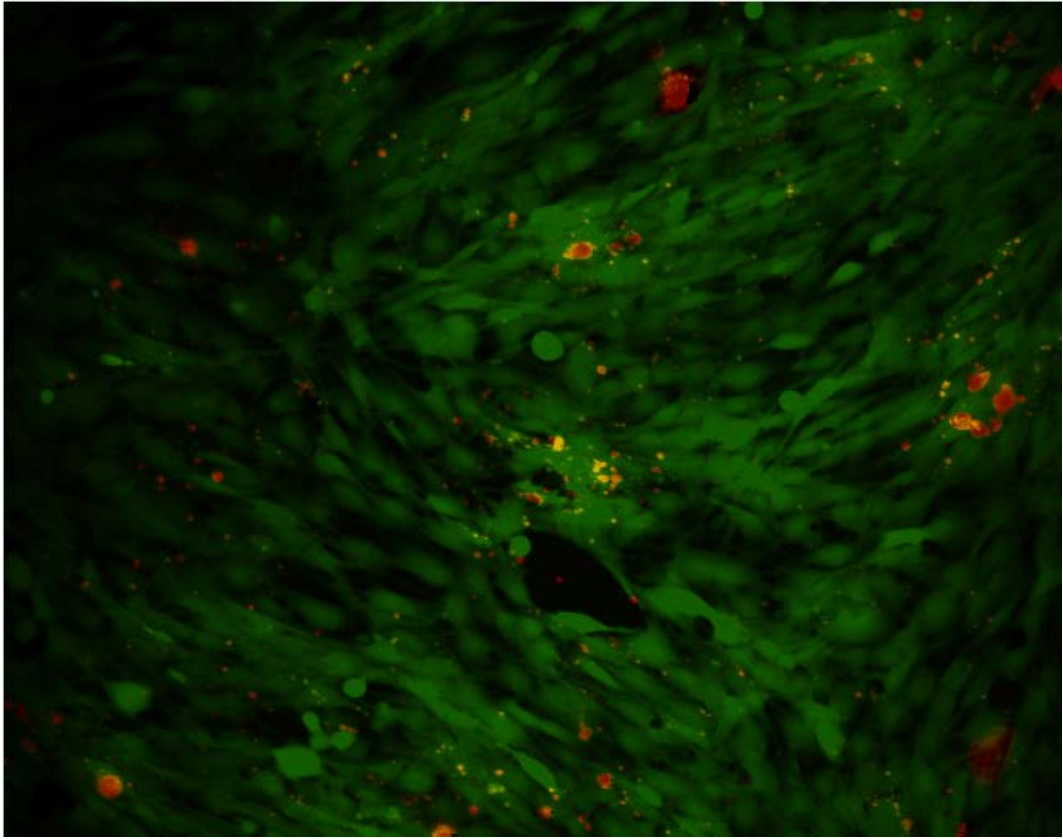


Figure 53: Fluorescence Images for CDC-29 at Day 2 of Cytotoxicity Test

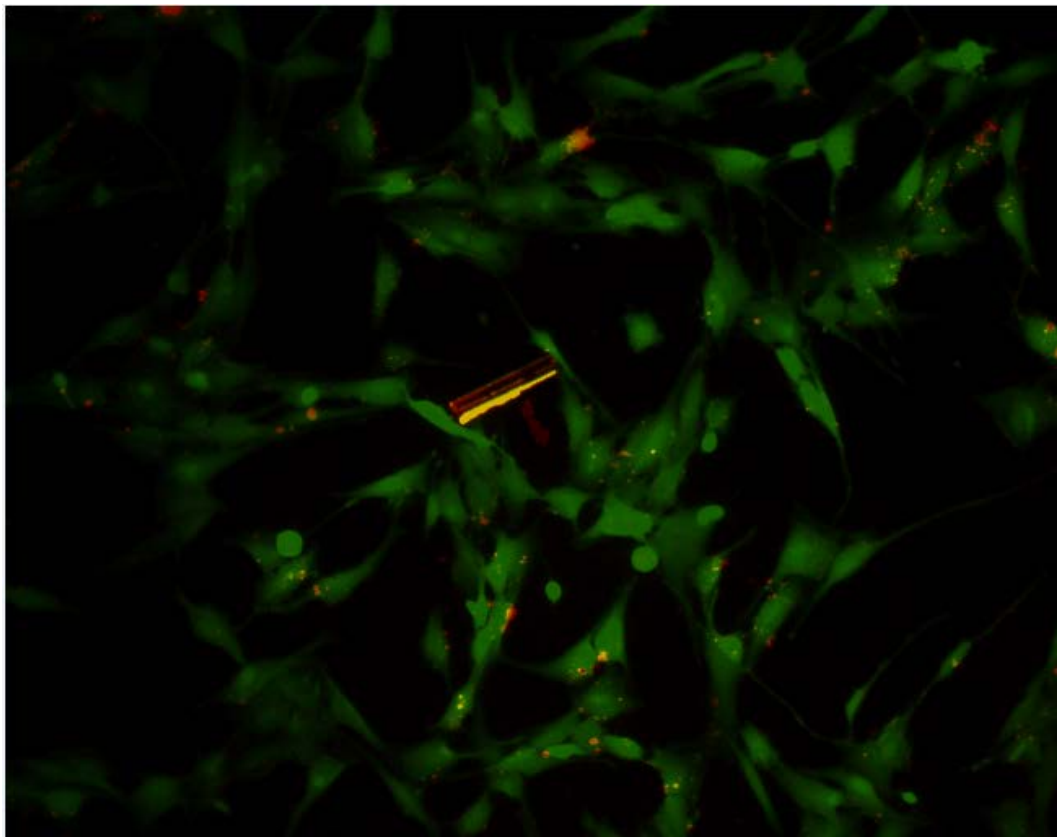
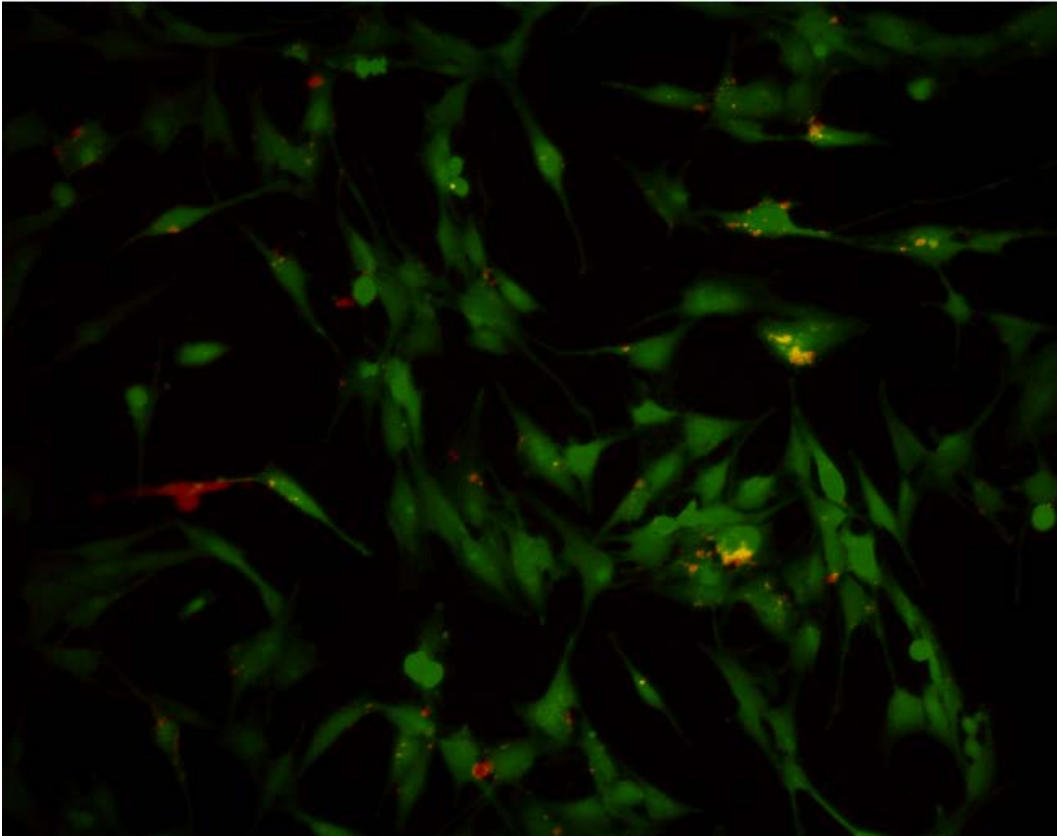


Figure 54: Fluorescence Images for CDC-30 at Day 2 of Cytotoxicity Test

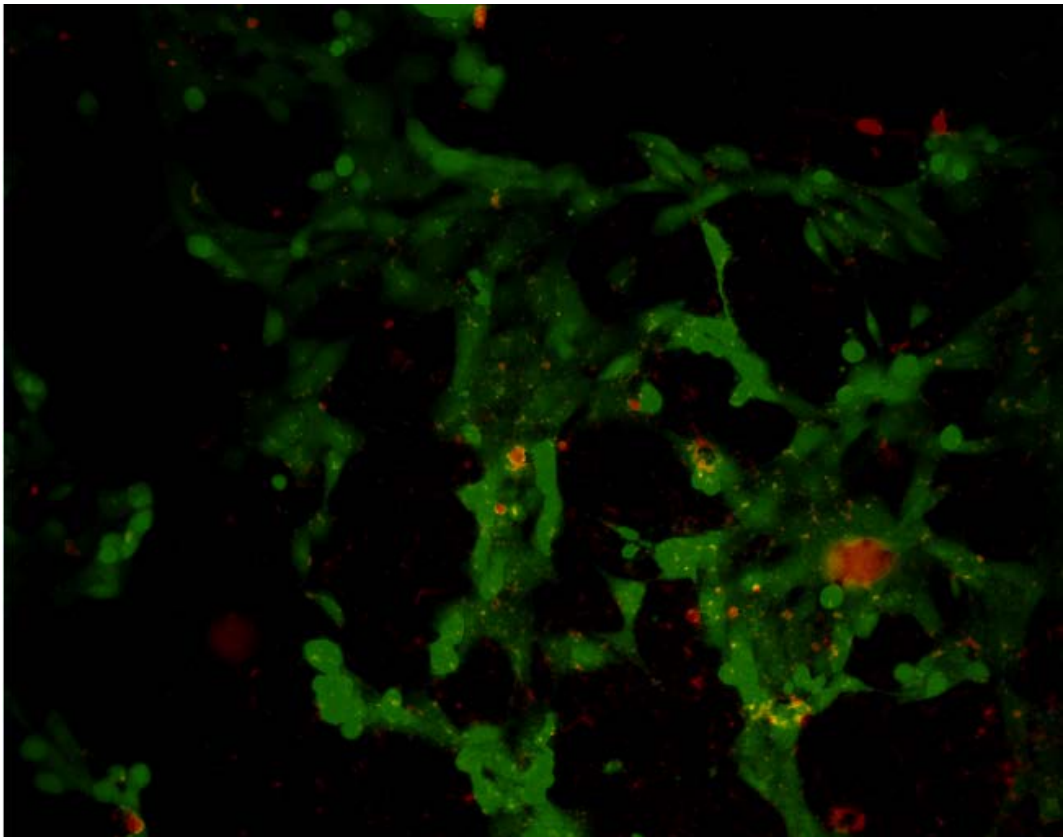
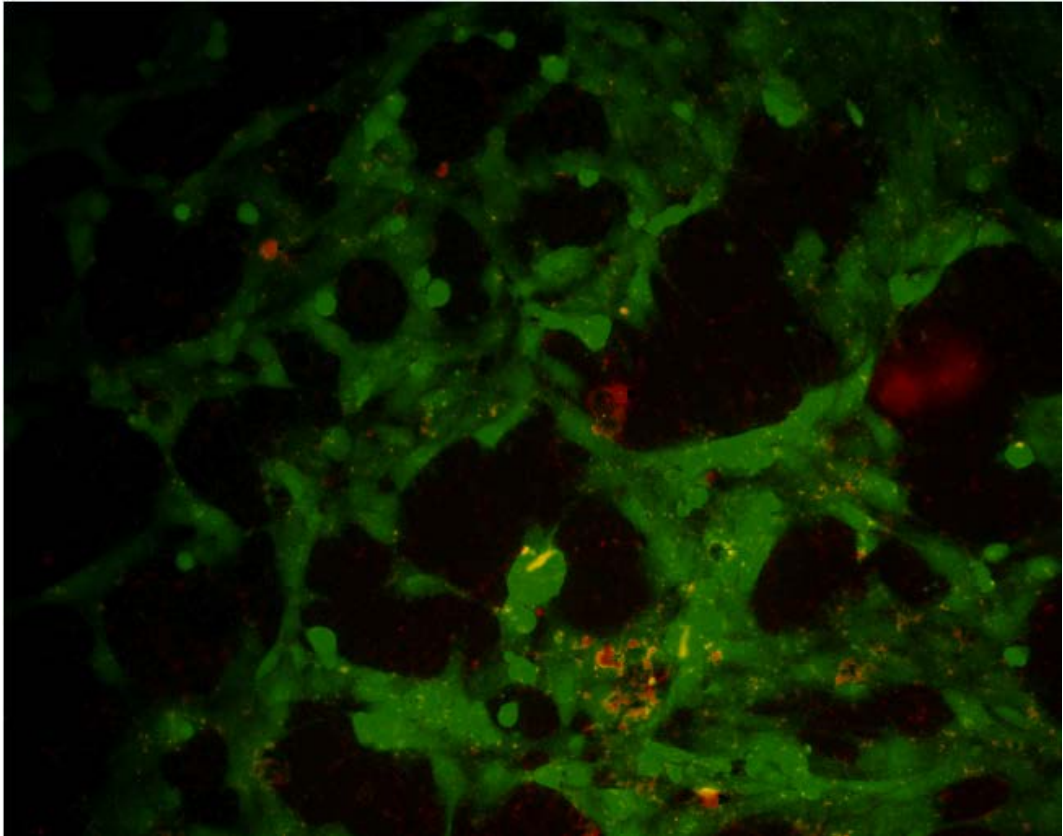


Figure 55: Fluorescence Images for CDC-13 at Day 2 of Cytotoxicity Test

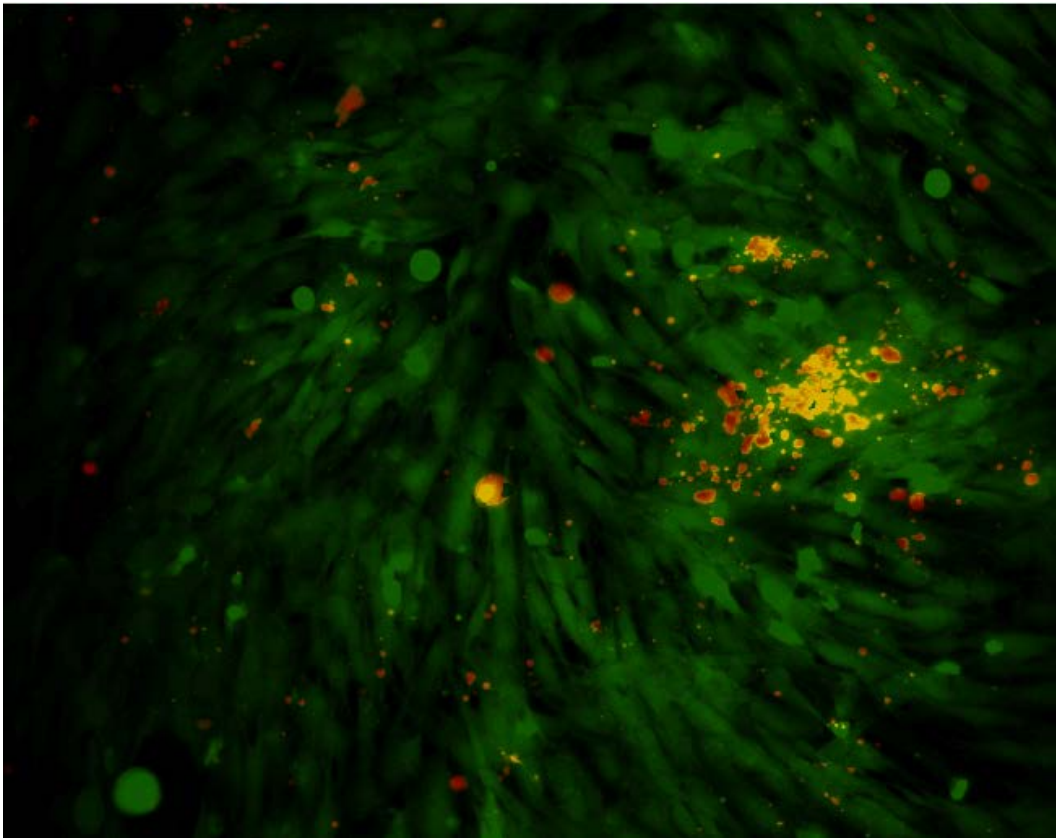
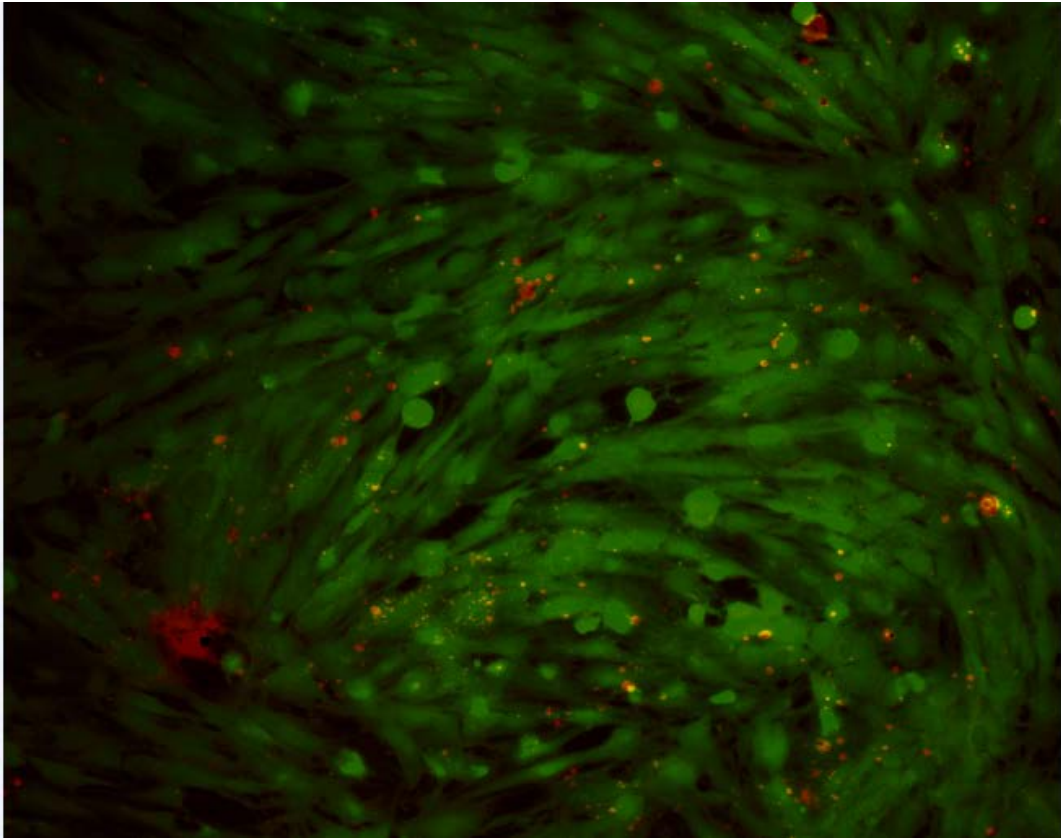


Figure 56: Fluorescence Images for CDC-19 at Day 2 of Cytotoxicity Test

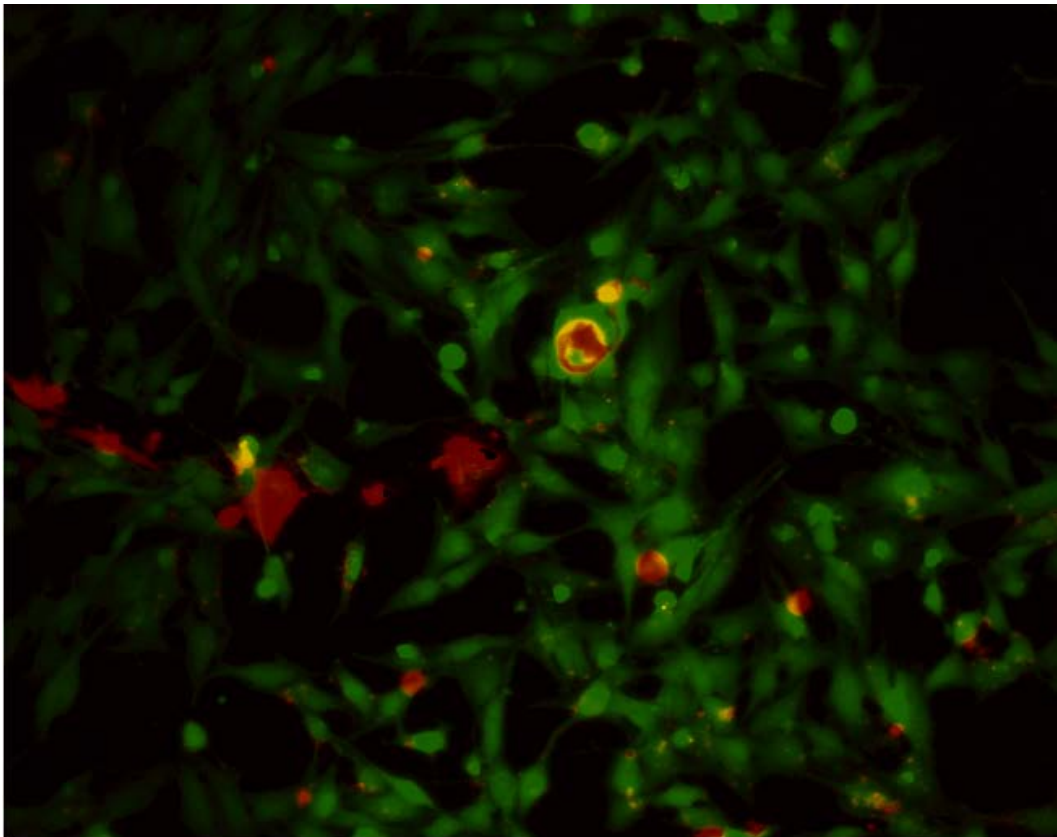
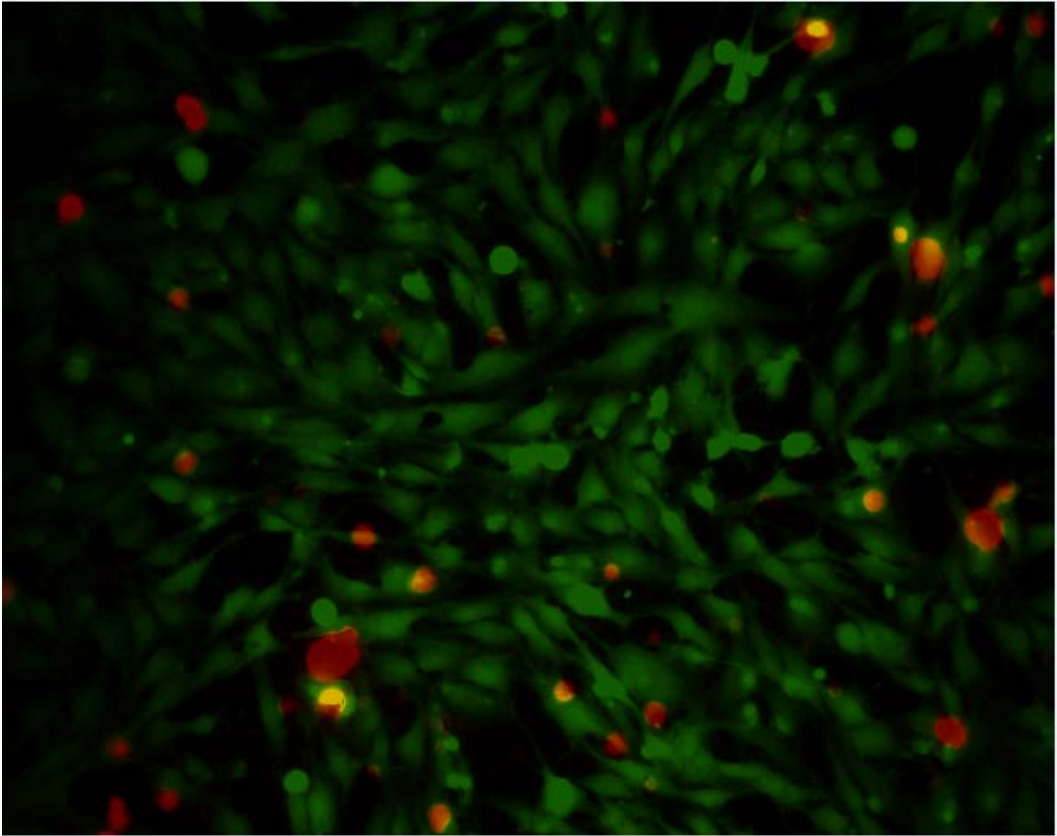


Figure 57: Fluorescence Images for CDC-25 at Day 2 of Cytotoxicity Test

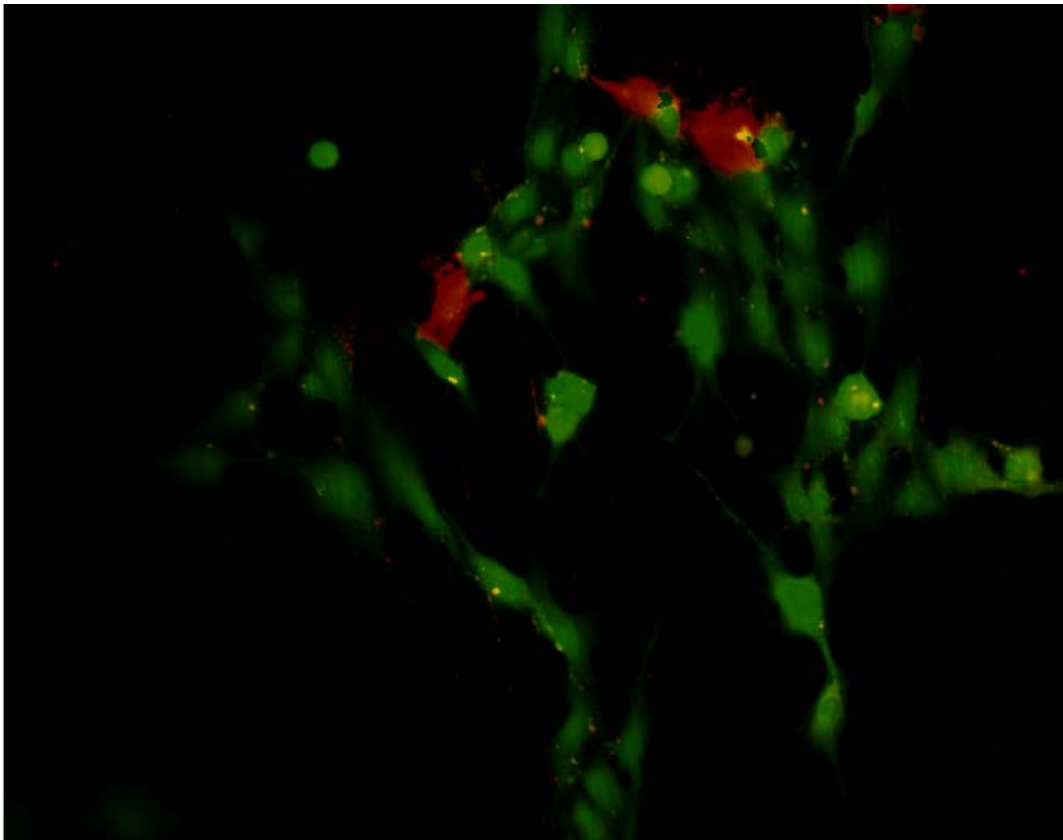
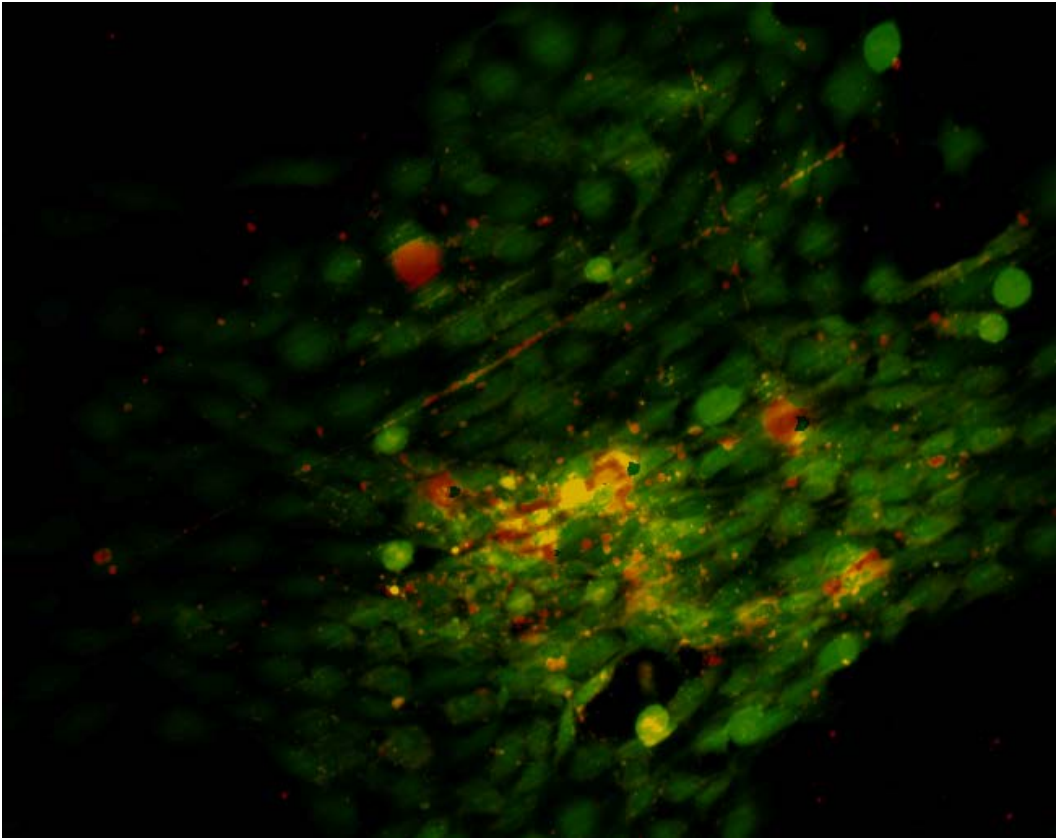


Figure 58: Fluorescence Images of Ti6Al4V at Day 7 of Cell Proliferation Test

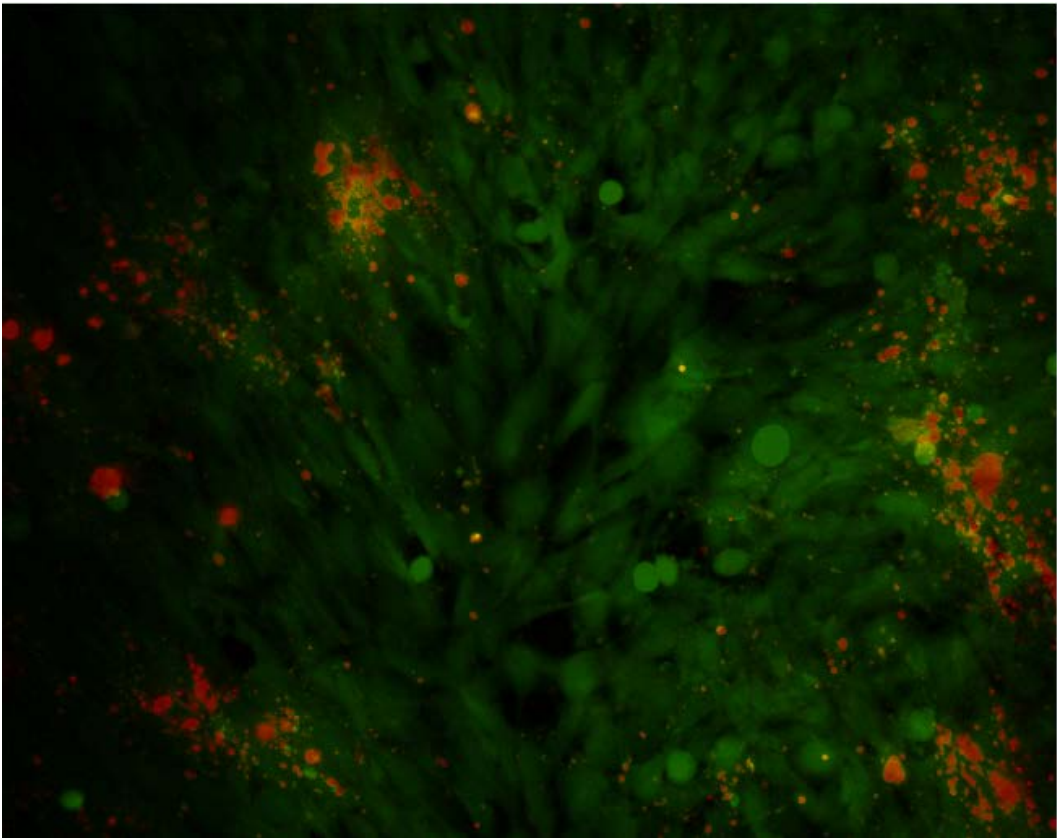
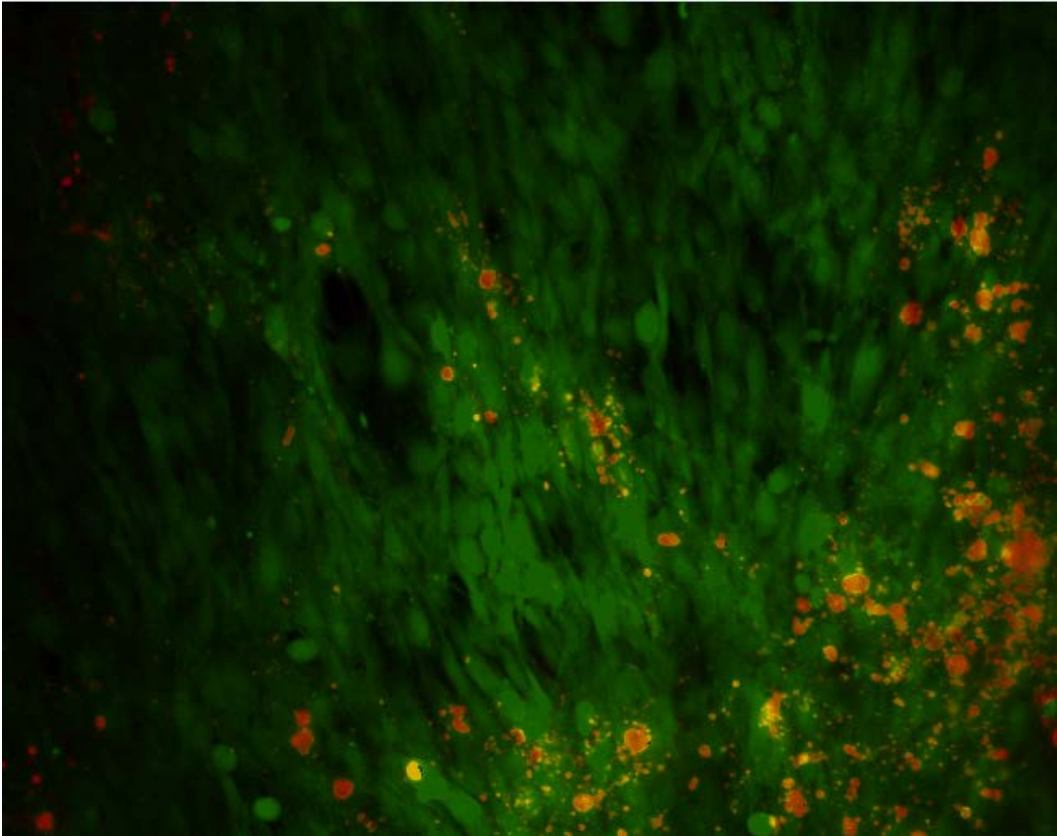


Figure 59: Fluorescence Images of CDC-13 at Day 7 of Cell Proliferation Test

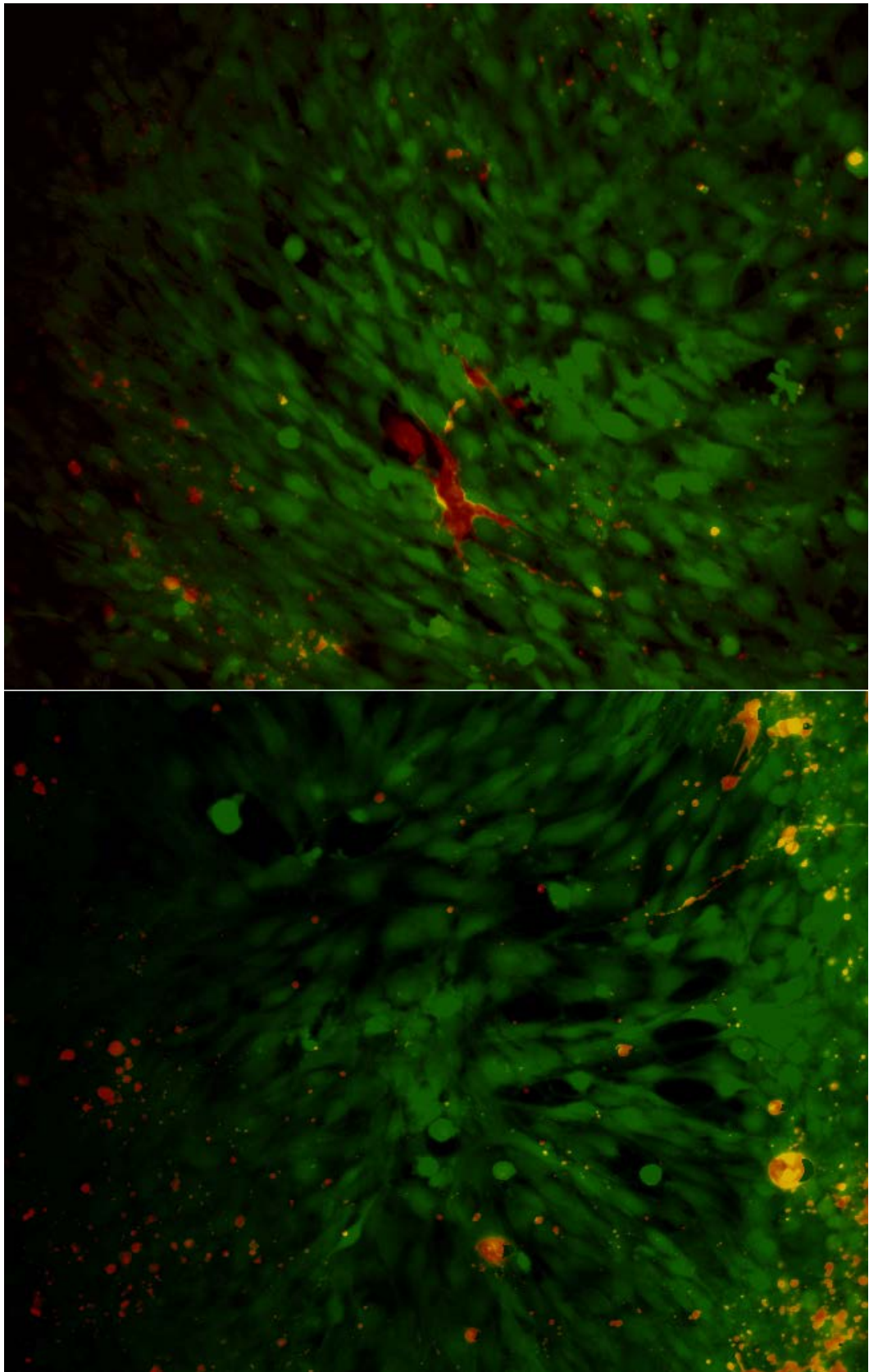


Figure 60: Fluorescence Images of CDC-19 at Day 7 of Cell Proliferation Test

6.3.2 Effect of Vacuum Post Treatment on Biocompatibility of CDC Specimens

Quantitative test results for vacuum treated specimens are summarized in Table 23 and visually depicted in Figure 61. The indirect contact cytotoxicity result shows that the chlorinated CDC samples (CDC-29 and CDC-30) and the vacuum treated CDC samples (CDC-24, CDC-26 and CDC-1b) are cytotoxic.

For the indirect contact cell proliferation test, cell growth was observed on day 4 for all the CDC samples and viable cell reduction to < 50% was observed for all the CDC samples at day 7. This result is rather interesting. Further study should include study of mechanism of cell death to determine whether the death was due to apoptosis or necrosis. Apoptosis is programmed cell death to remove unwanted cells during normal development, and can also occur when a cell is undergoing a period of stress and damaged beyond repair [62]. On the other hand, necrosis is traumatic cell death and occurs due to toxins, infection or trauma [62].

In summary, the test results show that vacuum treated CDC samples are not as biocompatible as the negative control and the Ti4Al4V samples. Additionally, the vacuum treated CDC samples exhibited similar cytotoxicity as the chlorinated CDC samples, and more biocompatible than the positive control sample.

Table 23: Summary of Vacuum Post Treatment Effect on Biocompatibility of CDC

Specimen	Indirect Contact Cytotoxicity-Day 2		Indirect C. Proliferation- Day 4		Indirect C. Proliferation- Day 7	
	% Cell Viability	Stdev	% of Cell Viability	Stdev	% of Cell Viability	Stdev
Media Control	102	6	113	6	102	6
Ti6Al4V	103	2	74	4	89	3
Negative Control	100	2	100	14	100	3
Positive control	3	1	7	9	2	2
CDC-29	6	0	109	3	48	4
CDC-30	5	1	91	5	39	4
CDC-24	5	1	78	11	33	6
CDC-26	-	-	90	6	49	2
CDC-1b	8	3	102	16	53	6

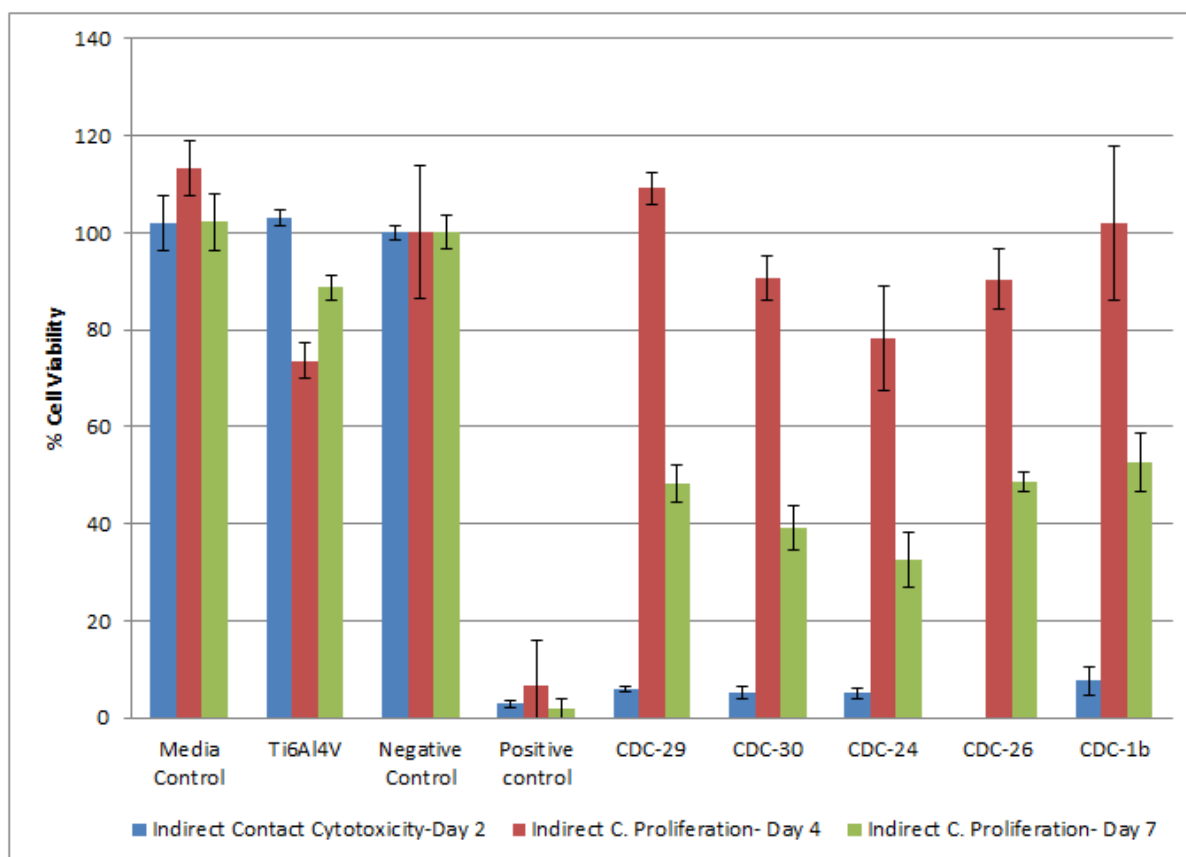


Figure 61: Summary of Vacuum Post Treatment Effect on Biocompatibility of CDC

EDS analysis results for the vacuum treated CDC samples are shown in Table 24. Significant lower levels (≤ 0.5 vs ≥ 1.9 w/w%) of residual chlorine were observed from the vacuum treated CDC samples as compared to the chlorinated (with no post treatment) samples. As shown that residual chlorine was not detected in CDC-24 and some of the scans for CDC-26 and CDC-1b. In general, low levels of residual chlorine was detected on the vacuum treated samples and the level varied depending on the location of the scan. Despite the low level of residual chlorine, the vacuum treated samples are cytotoxic and the toxicity level is comparable to the chlorinated samples. This could be due to the fact that all the vacuum treated samples were cracked and submicron CDC particles could get into the extraction solution during the biocompatibility testing and resulted cytotoxicity. This hypothesis is supported by the earlier finding in this research where it was demonstrated that submicron CDC particles are cytotoxic only when residual chlorine is present.

Table 24: EDS Test Result for CDC Specimens with and without Vacuum Treatment

Specimen	C	O	S	Cl	Al	Fe	Si	Na	Ca	Cu	Tm	SUM	Avg. Cl	% Viable cell of PE
	w/w %													
CDC-24	88.52	11.48										100.00	0.0	33
	81.06	18.94										100.00		
	87.04	12.07			0.9							100.01		
CDC-26	80.92	17.22	0.54	0.35	0.39		0.59					100.01	0.4	49
	96.61	2.92	0.54									100.07		
	85.53	11.94	0.58	0.36	0.23		0.8	0.14		0.43		100.01		
CDC-1b	91.32	8.21	0.48									100.01	0.5	53
	88.39	9.73	1.33		0.26		0.3					100.01		
	89.44	9.72	0.33	0.5								99.99		
CDC-29	97.26		0.14	2.13			0.07				0.4	100.00	2.3	48
	85.58	9.83	0.54	2.6	0.25		1.06	0.15				100.01		
	97.78			2.22								100.00		
CDC-30	92.16	6.42		1.41								99.99	1.9	39
	84.9	11.49	1.32	2.29								100.00		
	89.11	8.08	0.38	1.91								99.48		

CDC-24 and CDC-26 were tested with direct contact cytotoxicity and fluorescence images for the cytotoxicity test can be found in Figures 62-63. Detached live cells (as shown by the

round shape cells) and dead cells are shown on these figures therefore confirming the quantitative cytotoxicity result.

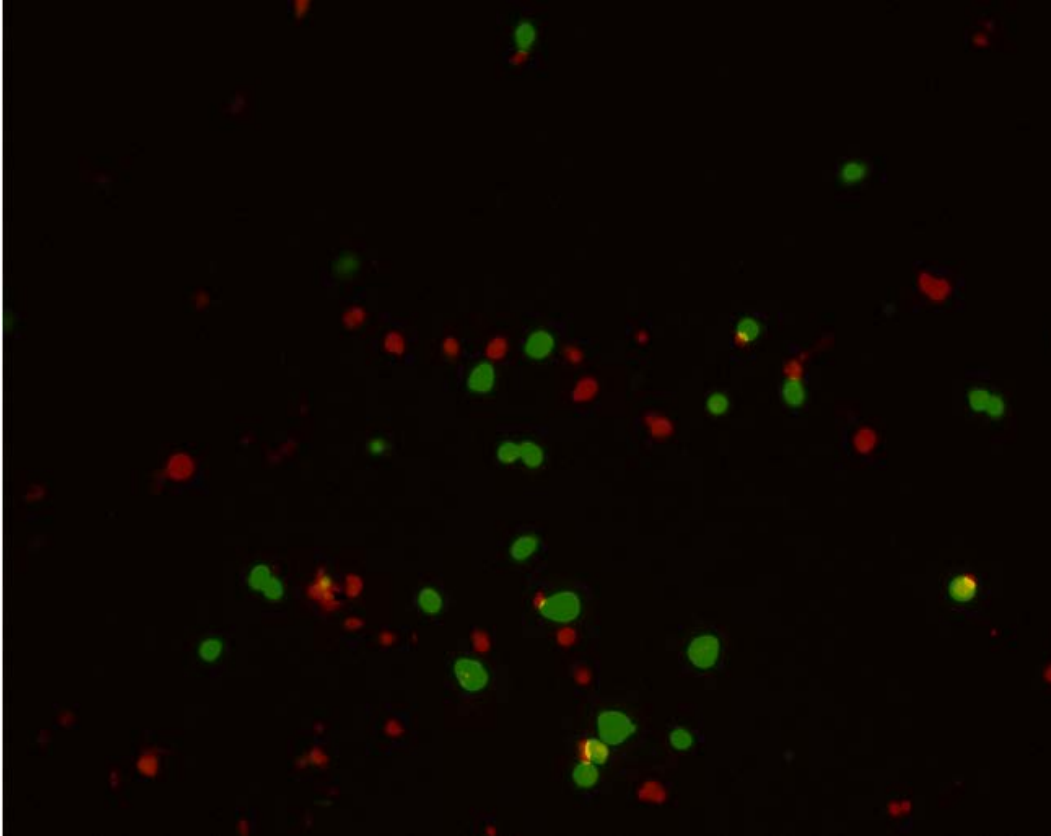


Figure 62: Fluorescence Image for CDC-24 at Day 2 of Cytotoxicity Test

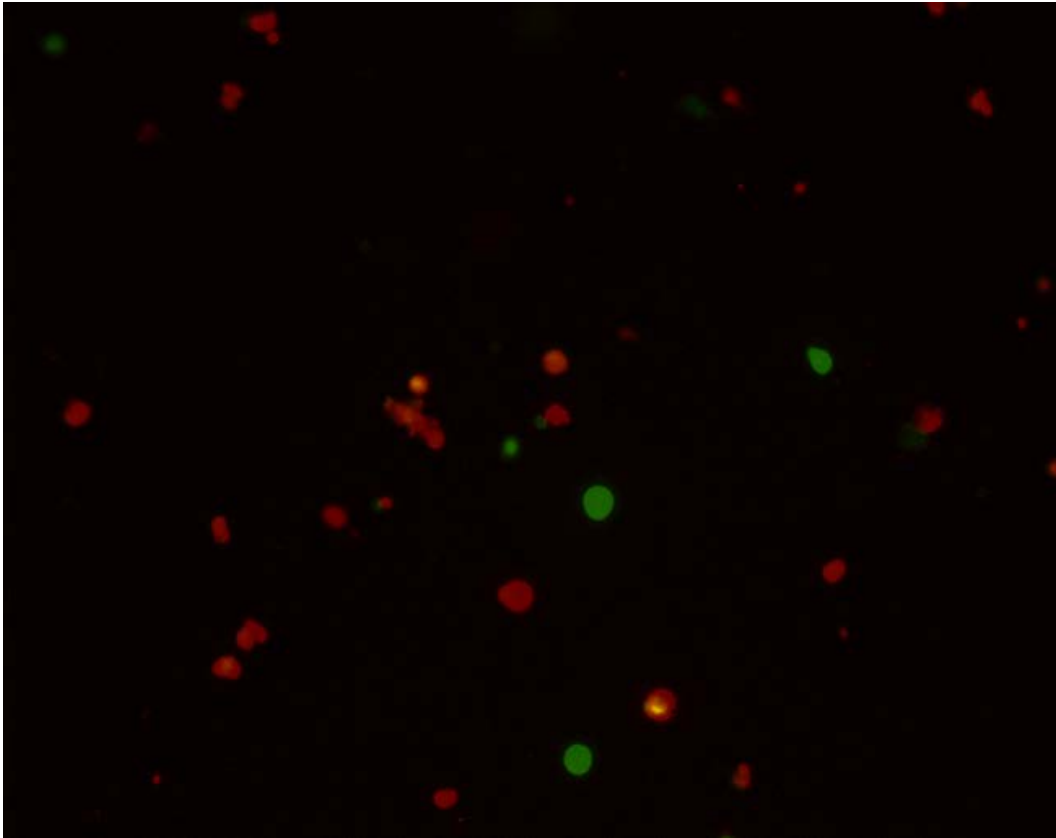


Figure 63: Fluorescence Images for CDC-26 at Day 2 of Cytotoxicity Test

6.3.3 Effect of Ammonia Post Treatment on Biocompatibility of CDC Specimens

As mentioned that 2 out of the 3 ammonia treated CDC specimens were severely cracked therefore were not further evaluated. Quantitative biocompatibility test results for the remaining ammonia treated specimen (CDC-23) and the respective chlorinated specimen (CDC-29) are summarized in Table 25 and illustrated in Figure 64. Both the indirect contact cytotoxicity and cell proliferation results show that the ammonia treated sample is cytotoxic with toxicity level similar to the positive control.

Table 25: Summary of Ammonia Post Treatment Effect on Biocompatibility of CDC

Specimen	Indirect Contact Cytotoxicity-Day 2		Indirect C. Proliferation- Day 4		Indirect C. Proliferation- Day 7	
	% Cell Viability	Stdev	% of Cell Viability	Stdev	% of Cell Viability	Stdev
Media Control	102	6	113	6	102	6
Ti6Al4V	103	2	74	4	89	3
Negative Control	100	2	100	14	100	3
Positive control	3	1	7	9	2	2
CDC-29	6	0	109	3	48	4
CDC-23	6	2	10	9	3	2

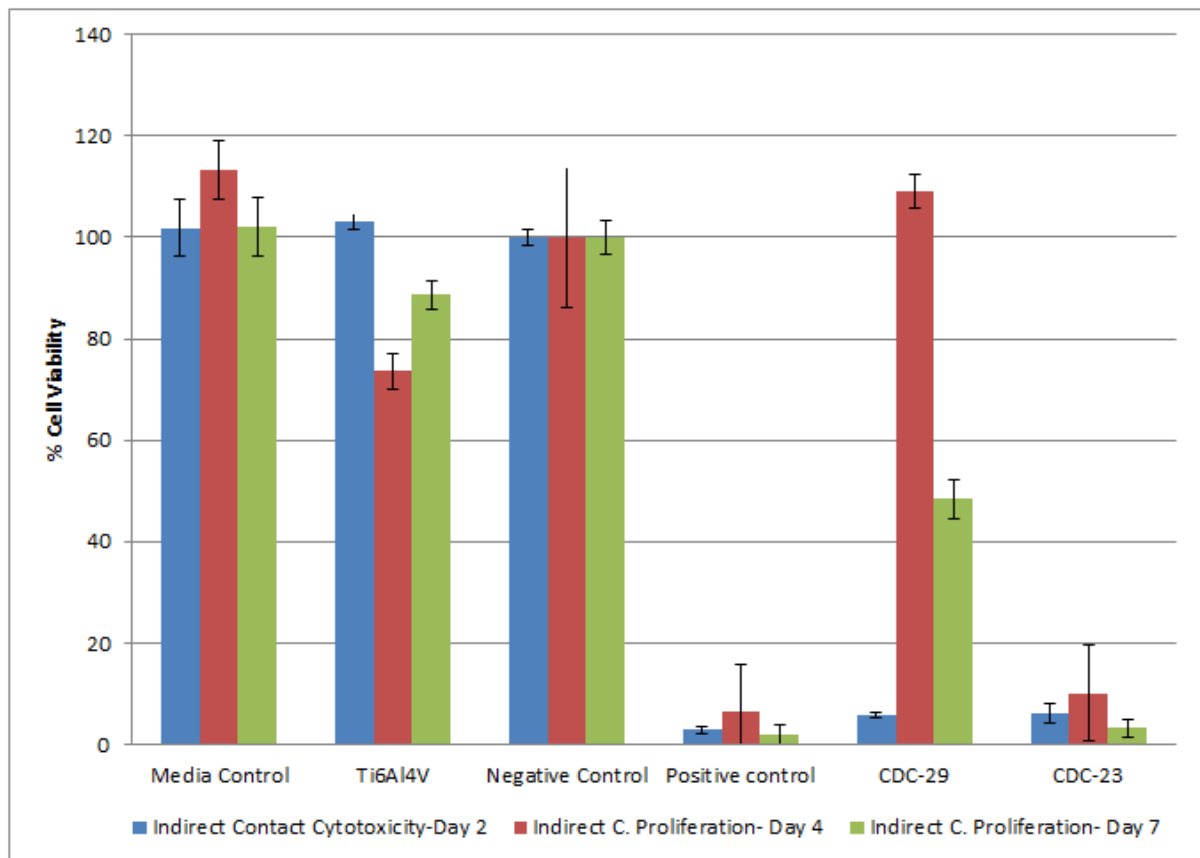


Figure 64: Summary of Ammonia Post Treatment Effect on Biocompatibility of CDC

EDS analysis and biocompatibility results for the ammonia treated CDC sample are shown in Table 26. The results show that the ammonia treatment was able to remove significant amount of residual chlorine in CDC samples, and there is no unexpected chemical composition on the treated CDC samples. Despite the finding, the amount treated sample is very toxic, significantly more toxic than the chlorinated CDC samples with no post treatment (CDC-29 and CDC-30).

CDC-23 was tested with direct contact cytotoxicity test and the resultant fluorescence images for the cytotoxicity test are presented in Figure 65. Detached live cells (shown by round cells) and dead cells are shown on these figures therefore confirming the quantitative cytotoxicity result.

Table 26: EDS Test Result for CDC Specimens with and without Ammonia Treatment

Specimen	C	O	S	Cl	Al	Fe	Si	Na	Ca	Cu	Tm	SUM	Avg. Cl	% Viable cell of PE
	w/w %													
CDC-23	90.79	8.28		0.92								99.99	0.77	3
	86.20	11.99	0.28	0.73	0.57			0.23				100.00		
	91.11	8.23		0.66								100.00		
CDC-28	94.51	5.49										100.00	0.23	-
	94.80	4.72		0.23			0.24					99.99		
	96.44	3.56										100.00		
CDC-29	97.26		0.14	2.13			0.07				0.4	100.00	2.3	48
	85.58	9.83	0.54	2.6	0.25		1.06	0.15				100.01		
	97.78			2.22								100.00		
CDC-30	92.16	6.42		1.41								99.99	1.9	39
	84.90	11.49	1.32	2.29								100.00		
	89.11	8.08	0.38	1.91								99.48		

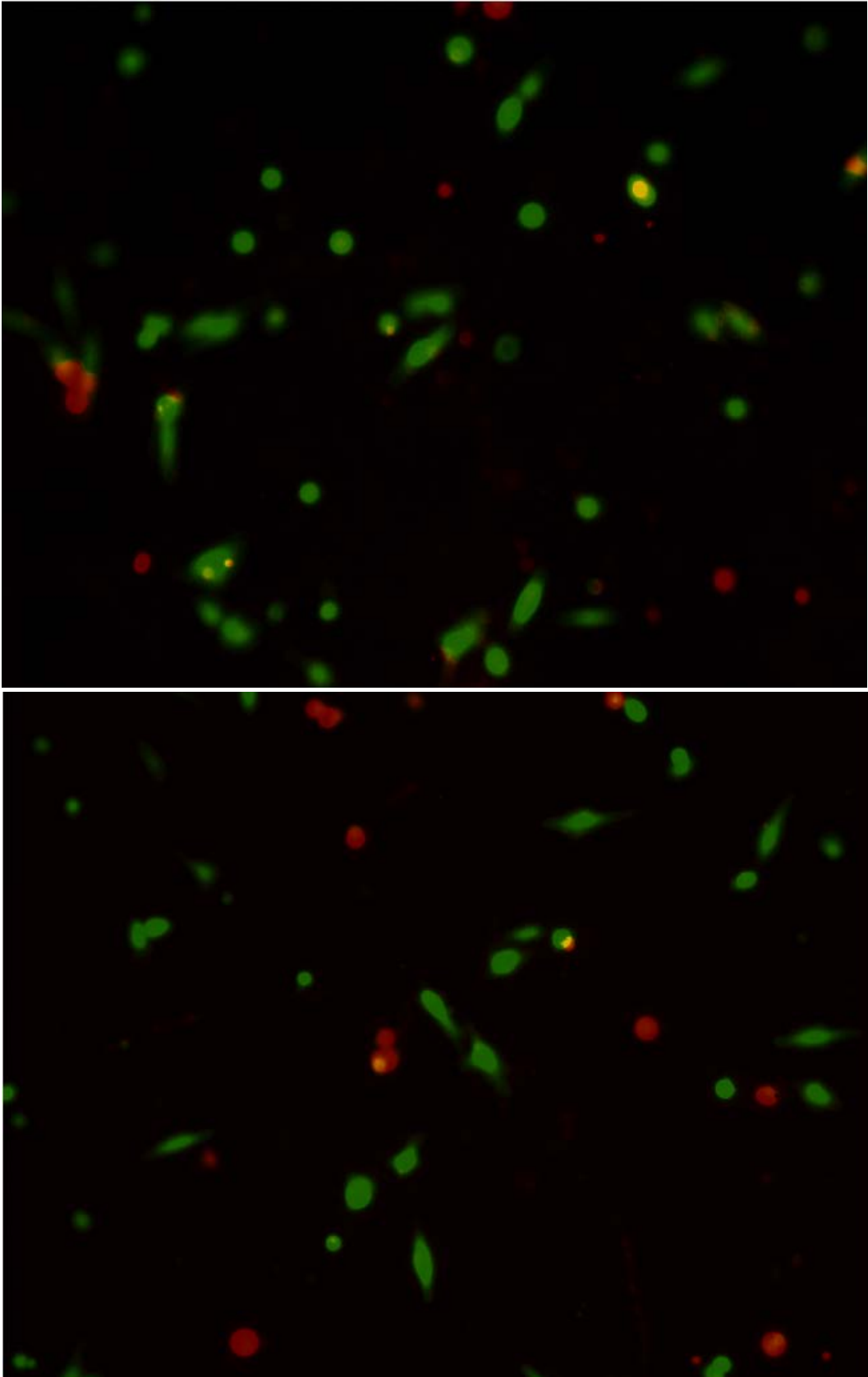


Figure 65: Fluorescence Images for CDC-23 of Cytotoxicity Test

7.0 CONCLUSIONS

The research was conducted in three parts:

Part 1: Determine the effects of residual chlorine and sub-micron CDC particles on the biocompatibility of CDC powder.

Part 2: Determine the effects of key CDC processing parameters on the tribological properties of CDC specimens under physiological simulated conditions.

Part 3: Determine the effects of post-chlorination treatments on the biocompatibility of the CDC specimens.

In Part 1, experiments were conducted to study the effect of residual chlorine and submicron particles independently on CDC cytotoxicity. High temperature (1400°C) vacuum treatment and high speed centrifugation were used to remove residual chlorine and submicron particles from the CDC samples. Subsequently, energy dispersive spectroscopy (EDS) analysis of the furnace-treated and centrifuged CDC samples confirmed the complete removal of residual chlorine and submicron CDC particles in the treated samples. Indirect cytotoxicity tests were conducted on CDC powder and furnace-treated CDC sample, both with and without centrifugation. The test results showed that both the furnace-treated (no residual chlorine) and centrifuged (no submicron particles) CDC samples were not cytotoxic, and the submicron CDC particles are cytotoxic only when residual chlorine is present.

Scanning electron microscopy (SEM) and EDS analysis results confirmed that there was no detectable chemical compositional difference between the submicron particles and the CDC

layer. Additionally, the analysis results indicated that the extraction and the additional centrifugation/washing steps did not remove a significant amount of residual chlorine from the CDC samples, therefore supporting previous findings that the residual chlorine is chemically bonded to the CDC structure.

In Part 2, tribological test variables such as polishing of specimens, sliding frequencies, and sliding time were studied to determine the appropriate test parameters for this research. It was learned that CDC specimens should be lightly polished to remove loosely adhered particles before their use in tribological testing to allow consistent evaluation of CDC microstructure effect on the wear rate. As expected, the different sliding frequencies (different dwell times) studied had negligible impact on the wear rate of CDC and on ultra-high molecular weight polyethylene (UHMWPE) specimens as these materials are non-corrosive and do not need a minimum time to form an oxide layer. In addition, higher wear rates were observed at lower sliding times for all types of specimens (UHMWPE, titanium and CDC). It is believed that this was due to the higher initial wear rate, also known as the “run-in-period”. Given this, a short sliding time of 60 minutes was used as the standard testing time in hope of observing more discriminative wear rates.

The effects of chlorination temperature (1000°C and 1100°C), chlorination time (≤ 8 hours and 19 hours) and post-chlorination treatment gas mixture (H_2 , NH_3 and vacuum) on wear rate were studied. In general, the experimental data showed no significant wear rate difference from CDC produced as the result of:

- Long vs. short processing times
- Chlorination temperature of 1000°C vs. 1100°C
- Post-chlorination treatment with H_2 and vacuum

However, SEM analysis revealed that the extensive processing conditions (long processing time and high temperature) resulted in cracks on the CDC layer which was believed to be caused by shrinkage of CDC microstructure when it was converting to the graphitic structure. Additionally, the results also indicated that the form transformation was a function of post-treatment gas mixture, with NH_3 being the most aggressive.

The effect of protein concentration in the tribological testing solution on wear rate was studied using bovine calf serum (BCS) solution (30 g/L of protein) and distilled water (0 g/L of protein). Lower wear rate and friction coefficient were obtained on the tests conducted in distilled water. The finding was confirmed by conducting 100,000 Cycle (27.8 hours) sliding tests, and further investigated with protein adsorption test using PierceTM Bicinchoninic Acid (BCA) protein assay kit. The test results showed that only a small amount of BSA protein (9-25 %) was adsorbed on the CDC surface. It is possible that the presence of protein increased the CDC surface roughness and reduced the effectiveness of the lubricant film thickness, therefore resulting in a higher wear rate.

CDC wear rates were compared to CoCrMo (the “gold standard” of existing hip implants) wear rates tested under comparable testing apparatus and conditions. This comparison showed that CDC exhibited significantly lower wear rate when compared to the wear rate of CoCrMo.

Due to the hardness difference between the test specimens and the alumina balls, and the mechanical action applied during the tribological test, some wear on the alumina balls were observed. To support the hypothesis that CDC will form a smooth layer after the run-in period, wear volumes on the alumina balls after selected tribological test were measured. As expected, sliding relatively hard SiC on the alumina balls resulted in a higher wear volume

when compared to that observed for CDC specimens sliding on alumina balls. Additionally, similar wear volumes were obtained for the CDC specimens sliding for 28,800 and 100,000 cycles, which indicates further reduction of the friction coefficient and wear on the contacting components.

In Part 3, the effect of post-chlorination hydrogen treatment on biocompatibility of CDC specimens were studied using 4 tests and 2 cell viability assays. It was learned that the CDC specimens were not very toxic, therefore more severe testing conditions were needed to produce discriminative test results. Collectively, the test results indicated that the post-chlorination hydrogen treatment improved the biocompatibility of the CDC specimens, and the treatment effect was more pronounced on the CDC specimens produced from the short processing times, which should have thinner CDC layers. Overall, it can be concluded that the CDC layers are relatively biocompatible. CDC layers with similar biocompatibility as the Ti6Al4V alloys can be produced by the selected chlorination conditions and post-chlorination hydrogen treatment.

The effect of post-chlorination vacuum treatment on the biocompatibility of CDC specimen was also studied. Study results showed that the vacuum treatment appeared to be able to remove a significant amount of residual chlorine in CDC samples, however the resultant CDC samples were still cytotoxic. It is believed that the cytotoxicity of the vacuum treated CDC samples was due to the presence of submicron CDC particles in the samples; visible cracks in the samples indicated that the integrity of the samples was compromised.

The effect of post-chlorination ammonia treatment on the biocompatibility of CDC specimen was also studied. Study results showed that the ammonia treatment appeared to be able to remove significant amount of residual chlorine in CDC samples, but the resultant CDC

sample was very cytotoxic. EDS analysis of the ammonia treated sample showed that the treatment did not generate unexpected chemical composition.

Conclusion:

Biocompatible CDC layers can be produced by modulating chlorination conditions and application of a post-chlorination hydrogen treatment. Excessive processing conditions (high temperature and long processing time) are not recommended as these will affect the integrity of the resulting CDC layer.

8.0 REFERENCES

- [1] Y. Liao, R. Pourzal, M. Wimmer, J. Jacobs, A. Fischer and L. Marks, "Graphitic Tribological Layers in Metal-on-Metal Hip Replacements," *Science*, vol. 334, pp. 1687-1690, 2011.
- [2] "American Academy of Orthopedic Surgeons Web site," December 2011. [Online]. Available: <http://orthoinfo.aaos.org/topic.cfm?topic=a00377>. [Accessed 26 August 2014].
- [3] C. Brockett, S. Williams, Z. Jin, G. Isaac and J. Fisher, "Friction of Total Hip Replacements With Different Bearings and Loading Conditions," *Journal of Biomedical Materials Research Part B: Applied Biomaterials*, 2007.
- [4] H. Malchau and P. Herberts, "Prognosis of Total Hip Replacement," in *the 65th Annual Meeting of the American Academy of Orthopaedic Surgeons*, New Orleans, USA, 1998.
- [5] D. A. Ersoy, M. J. McNallan and Y. Gogotsi, "Carbon Coatings Produced by High Temperature Chlorination of Silicon Carbide Ceramics," *Material Research Innovation*, vol. 5, pp. 55-62, 2001.
- [6] S. Welz, M. J. McNallan and Y. Gogotsi, "Carbon Structures in Silicon Carbide Derived Carbon," *Materials Processing Technology*, vol. 179, pp. 11-22, 2006.

- [7] M. J. McNallan, D. Ersory, R. Zhu, A. Lee, C. White, S. Welz, Y. Gogotsi, A. Erdemir and A. Kovalchenko, "Nano-structured Carbide-Derived Carbon Films and Their Tribology," *Tsinghua Science and Technology*, vol. 10, no. 6, 2005.
- [8] B. Carroll, Y. Gogotsi, A. Kovalchenko, A. Erdemir and M. J. McNallan, "Effect of Humidity on the Tribological Properties of Carbide-Derived Carbon (CDC) Films on Silicon Carbide," *Tribology Letters*, vol. 15, pp. 51-55, July 2003.
- [9] A. Erdemir, A. Kovalchenko, M. J. McNallan, S. Welz, Y. Gogotsi and B. Carroll, "Effects of High-Temperature Hydrogenation Treatment on Sliding Friction and Wear Behavior of Carbide-Derived Carbon Films," *Surface and Coatings Technology*, vol. 188, pp. 588-593, 2004.
- [10] A. Erdemir, A. Kovalchenko, C. White, R. Zhu, A. Lee, M. J. McNallan, B. Carroll and Y. Gogotsi, "Synthesis and tribology of carbide-derived carbon films," *Applied Ceramic Society*, vol. 3, no. 3, p. 236–244, 2006.
- [11] H. J. Choi, H. T. Bae, J. K. Lee, B. C. Na, M. J. McNallan and D. S. Lim, "Sliding Wear of Silicon Carbide Modified by Etching with Chlorine At Various Temperatures," *Wear*, vol. 266, pp. 214-219, 2009.
- [12] F. Gao, J. Lu and W. Liu, "Tribological Behavior of Carbide-Derived Carbon Coating on SiC Polycrystal Against SAE52100 Steel in Moderately Humid Air," *Tribology Letter*, vol. 27, p. 339–345, 2007.

- [13] H. J. Choi, H. T. Bae and D. S. Lim, "Tribology of Carbon Layers Fabricated From SiC Exposed to Different H-2/Cl-2 Gas Mixtures," *Journal of Ceramic Processing Research*, vol. 10, pp. 330-334, 2009.
- [14] H. J. Choi, H. T. Bae, M. J. McNallan, Y. H. Sohn and D. S. Lim, "Effect of Hydrogen on The Physical and Mechanical Properties of Silicon Carbide-Derived Carbon Films," *Surface & Coatings Technology*, vol. 204, p. 1018–1021, 2009.
- [15] H. T. Bae, J. H. Jeong, H. J. Choi and D. S. Lim, "Fabrication and Tribological Characterization of Gradient Carbon Layer Derived From SiC-TiC Composites," *Journal of the Ceramic Society of Japan*, vol. 118, pp. 1150-1153, 2010.
- [16] J. Sui and J. Lu, "Formulated Self-Lubricating Carbon Coatings on Carbide Ceramics," *Wear*, vol. 271, p. 1974– 1979, 2011.
- [17] R. Zhu, "Effects of Residual Chlorine on Properties of Carbide-Derived-Carbon," Doctor of Philosophy in Materials Engineering in the Graduate College of the University of Illinois at Chicago, Chicago, IL, 2006.
- [18] Y. Gogotsi, R. K. Dash, G. Yushin, B. E. Carroll, S. R. Altork, S. Sassi-Gaha and R. F. Rest, "Bactericidal Activity of Chlorine-loaded Carbide-Derived Carbon Against Escherichia Coli and Bacillus Anthracis," *Published online - Wiley InterScience*, July 2007.

- [19] S. Yachamaneni, F. Yushin, S. H. Yeon, Y. Gogotsi, C. Howell, S. Sandeman, G. Phillips and S. Mikhalovsky, "Mesoporous carbide-derived carbon for cytokine removal from blood plasma," *Biomaterial*, vol. 31, pp. 4789-4794, 2010.
- [20] C. Brockett, S. Williams, Z. Jin , G. Isaac and J. Fisher, "Friction of Total Hip Replacements With Different Bearings and Loading Conditions," *Journal of Biomaterial*, p. DOI: 10.1002/jbm.b.30691., 2007.
- [21] "Wikipedia, Carbon," Wikimedia Foundation, August 18 2014. [Online]. Available: <http://en.wikipedia.org/wiki/Carbon>. [Accessed 24 August 2014].
- [22] W. Shao, P. Arghya, Y. Y. Mai, L. Rodes and S. Prakash, "Carbon Nanotubes for Use in Medicine: Potentials and Limitations," *INTECH Open Science-Open Mind*, 2013.
- [23] "Wikipedia, Carbon Nanotube," 15 August 2014. [Online]. Available: http://en.wikipedia.org/wiki/Carbon_nanotube. [Accessed 26 August 2014].
- [24] "Wikipedia, SiC," 8 August 2014. [Online]. Available: http://en.wikipedia.org/wiki/Silicon_carbide. [Accessed 26 August 2014].
- [25] R. Cheung, *Silicon Carbide Microelectromechanical systems for Harsh Environments*, ISBN: 978-1-86094-624-0, 2006.
- [26] T. Muranaka, Y. Kikuchi, T. Yoshizawa, N. Shirakawa and J. Akimitsu, "Superconductivity in Carrier-doped Silicon Carbide," *Science and Technology Advanced Material*, 2008.

- [27] J. Leis, A. Perkson, M. Arulepp, M. Kaarik and G. Svensson, "Carbon Nanostructures Produced by Chlorinating Aluminium Carbide," *Carbon*, vol. 39, pp. 2043-2048, 2001.
- [28] S. Dimovski, A. Nikitin, H. Ye and Y. Gogotsi, "Synthesis of Graphite by Chlorination of Iron Carbide at Moderate Temperature," *Journal of Materials Chemistry*, vol. 14, pp. 238-243, 2004.
- [29] V. Presser, M. Heon and Y. Gogotsi, "Carbide-derived carbons-from porous networks to nanotubes and graphene," *Advanced Functional Materials*, vol. 21, pp. 810-833, 2010.
- [30] "Wikipedia-CDC," 8 10 2013. [Online]. Available: http://en.wikipedia.org/wiki/Carbide-derived_carbon. [Accessed 27 August 2014].
- [31] T.Y.Kosolapova, Carbides properties, production and application, 1971.
- [32] S. Pathak, Z. G. Cambaz, S. R. Kalidindi, J. G. Swandener and Y. Gogotsi, "Viscoelasticity and high buckling stress of dense carbon nanotube brushes," *Carbon*, vol. 47, pp. 1969-1976, 2009.
- [33] D. Williams, "On the mechanisms of biocompatibility," *Biomaterials*, vol. 29, pp. 2941-2953, 2008.

- [34] A. K. Varkouhi, S. Foilard, T. Lammers, R. M. Schiffelers, E. Doris, W. E. Hennink and G. Storm, "SiRNA delivery with functionalized carbon nanotubes," *International Journal of Pharmaceutics*, vol. 416, pp. 419-425, 2011.
- [35] H. Chen, X. Ma, Z. Li, Q. Shi and W. Zheng, "Functionalization of single-walled carbon nanotubes enables efficient intracellular delivery of siRNA targeting MDM2 to inhibit breast cancer cells growth," *Biomed Pharmacother*, 2012.
- [36] H. Dumortier, S. Lacotte, G. Pastorin, R. Marega, W. Wu, D. Bonifazi, J. P. Briand, S. Muller and A. Bianco, "Functionalized carbon nanotubes are non-cytotoxic and preserve the functionality of primary immune cells," *Nano Letters*, vol. 6, pp. 1522-1528, 2006.
- [37] S. K. N. Wong, T. C. Jessop, P. A. Wende and H. Dai, "Nanotube molecular transporters: Internalization of carbon nanotube-protein conjugates into mammalian cells," *Journal of American Chemical Society*, vol. 126, pp. 6850-6851, 2004.
- [38] L. W. Zhang, L. Zeng, A. R. Barron and N. A. Monteiro-Riviere, "Biological interactions of functionalized single-wall carbon nanotubes in human epidermal keratinocytes," *Int J Toxicol.*, vol. 26, pp. 103-113, 2007.
- [39] P. H. Chen, K. M. Hsiao and C. C. Chou, "Molecular Characterization of toxicity Mechanism of Single-Walled Carbon Nanotubes," *Biomaterial*, vol. 34, 2013.

- [40] A. Hirose, A. Ono, M. Hirata-Koizumi, H. Serizawa, E. Kamata and T. Nishimura, "Repeated Dose 28-day Oral Toxicity Studies of Single- and Multi-walled Carbon Nanotubes in Rats," *Toxicology Letter*, 2011.
- [41] O. Vittorio, V. Raffa and A. Cuschieri, "Influence of purity and surface oxidation on cytotoxicity of multiwalled carbon nanotubes with human neuroblastoma cells," *Nanomedicine*, vol. 5, pp. 424-431, 2009.
- [42] K. L. Aillon, Y. Xie, N. El-Gendy, C. J. Berkland and M. L. Forrest, "Effects of nanomaterial physicochemical properties on in vivo toxicity," *Advanced Drug Delivery Reviews*, vol. 61, pp. 457-466, 2009.
- [43] C. P. Firme and P. R. Bandaru, "Toxicity issues in the application of carbon nanotubes to biological systems," *Nanomedicine*, vol. 6, pp. 245-256, 2010.
- [44] Z. M. Jin, M. Stone, E. Ingham and J. Fisher, "Biotribology," *Current Orthopaedics*, vol. 20, pp. 32-40, 2006.
- [45] D. Dowson and V. Wright, Introduction to the biomechanics of joints and joint replacements, London: Mechanical engineering publications Ltd, 1981.
- [46] S.-G. Ceramics, "Saint-Gobain Ceramics," [Online]. Available: <http://www.hexoloy.com/hexoloy-sic-physical-properties>. [Accessed 31 August 2014].

- [47] "ATI," ATI Allvac, 2014. [Online]. Available: <https://atimetals.com/products/Pages/co-based.aspx>. [Accessed 9 September 2014].
- [48] M. T. Mathew, J. J. Jacobs and M. A. Wimmer, "Wear-corrosion synergism in a CoCrMo hip bearing alloy is influenced by proteins," *Clinical Orthopaedics and Related Research*, p. 9, 2012.
- [49] I. 10993-5, *Biological evaluation of medical devices- Part 5: Tests for in vitro cytotoxicity*, 2009.
- [50] "Centrifugation Law," [Online]. Available: <http://www.monzir-pal.net/Bioseparation/Contents/Centrifugation%20Chapter.pdf>.
- [51] "Wiki-Stoke's law," Wikimedia, 5 May 2014. [Online]. Available: http://en.wikipedia.org/wiki/Stokes'_law. [Accessed 16 September 2014].
- [52] "Wikipedia; Raman Spectroscopy," Wikimedia Foundation, 9 September 2014. [Online]. Available: http://en.wikipedia.org/wiki/Raman_spectroscopy. [Accessed 11 September 2014].
- [53] CCK-8, "Cell Counting Kit-8 Protocol," [Online]. Available: http://www.dojindo.com/technicalmanual/manual_ck04.pdf. [Accessed 1 September 2014].

- [54] M. Probes, "LIVE/DEAD Viability/Cytotoxicity Kit for mammalian cells," 21 December 2005. [Online]. Available: <http://tools.lifetechnologies.com/content/sfs/manuals/mp03224.pdf>. [Accessed 2 September 2014].
- [55] "Pierce™ BCA Protein Assay Kit," Thermo Scientific, [Online]. Available: http://genome.yale.edu/resources/protocols/protein/685_162459_BCA.pdf. [Accessed 9 September 2014].
- [56] "Zygo NEw View 6300," Zygo, [Online]. Available: http://zeus.phys.uconn.edu/halld/diamonds/Zygo/MetroPro_docs/Basic%20NewView%206k%20Operator%20Training.pdf. [Accessed 10 September 2014].
- [57] M. Morlock, E. Schneider, A. Bluhm, M. Vollmer, G. Bergmann, V. Muller and M. Honl, "Duration and frequency of every day activities in total hip patients," *Journal of Biomechanics*, vol. 34, pp. 873-881, 2001.
- [58] M. V. Khariamova, V. N. Mochalin, M. R. Lukatskaya, J. Niu, V. Presser, S. Mikhalovsky and Y. Gogotsi, "Adsorption of proteins in channels of carbon nanotubes: Effect of surface chemistry," *Material Express*, vol. 3, p. 2158, 2013.
- [59] T. J. Joyce, P. Thompson and A. Unsworth, "The wear of PTFE against stainless steel in a multi-directional pin-on-plate wear device," *WEAR*, vol. 255, pp. 1030-1033, 2003.

- [60] M. J. Runa, M. J. Mathew, C. V. Nagelli, L. A. Rocha, M. Laurent, J. J. Jacobs and M. A. Wimmer, "Wear and Corrosion Synergism in a High-Carbon CoCrMo Alloy Used in Metal-on-Metal Hip Bearings," in *Orthopedic Reseach Society*, 2011.
- [61] M. Adams, "Aluminum Oxide, Al₂O₃ Ceramic Properties," Accuratus, 2013. [Online]. Available: <http://accuratus.com/alumox.html>. [Accessed 25 September 2014].
- [62] M. J. Stoddart, *Mammalian cell viability methods and protocols*, Davos Platz, Switzerland: AO Research Institute Davos, 2011.
- [63] ISO, *ISO document 10993. Biological compatibility of medical devices — Part 5. Tests*.

Eik Lang Lau

SUMMARY OF QUALIFICATIONS

- Fourteen years of hands on experience in pharmaceutical development (scale-up/ technology transfer/ optimization), manufacturing, and quality.
- Experience in leading cross functional team in developing new process and leading global team to address EMA/USP/ICH regulations and or requirements.
- Experience in conducting Quality by Design drug product development and writing CMC CTD sections.
- Details oriented and outstanding project management skills. PMP certified.
- Experience and proficient in experimental design, statistical data analysis, troubleshooting/continuous improvement using Six Sigma methodology; Lean Six Sigma Black Belt Certified.
- Effective communication and interpersonal skills, and highly motivated in either team or independent work.

EDUCATION

Doctor of Philosophy, Bioengineering (Fall 2012- Expected in spring 2015) University of Illinois at Chicago, IL, USA. GPA:4.00/4.00

Designing and evaluating nano-scale carbide-derive carbon as a novel biomaterial for biomedical application.

Master of Science, Chemical Engineering, (Fall 1999), Tennessee Technological University, Cookeville, TN, USA. GPA: 3.76/4.00

Bachelor of Science, Chemical Engineering, (Fall 1997), Tennessee Technological University, Cookeville, TN, USA, GPA: 3.12/4.00

PROFESSIONAL EXPERIENCE

Sr. Global QA Program Manager, AbbVie Quality Engineering (September 2012-present)

Responsible for managing, implementing and maintaining the effectiveness of the quality system and compliance projects. Uses engineering principles to conduct technical assessments involved with product performance, customer complaints and KPIs to design or development of new or improved products or processes. Conceives and plans continuous improvement projects to explore product or process problems and to identify areas of continual improvement and cost savings.

Technical Manager, Process Innovation, ANR&D ABBOTT NUTRITION (March 2011 – August 2012)

Key responsibility includes providing technical leadership and engineering/innovation services to the Abbott Nutrition research and development organization. These services include the design and development of new technologies, technology transfer of products and processes from concept stage to commercialization, and leading advanced independent or multidisciplinary research.

Technical Section Manager, GPO MS&T US/Puerto Rico Technical Center, ABBOTT (February 2009 – February 2011)

Key responsibility includes providing technical, regulatory, and quality documentation support to drug product manufacturing. These supports include 1) Providing scientific and technical leadership for projects, 2) Proposing and evaluating new technologies and process improvements for potential implementation into manufacturing, 3) Ensuring good technology transfers for both GPRD to GPO and Site Transfers, and 4) Managing project timelines, solving problems and managing resources to meet deadlines.

Principal Pharmaceutical Scientist II, GPO MS&T US/Puerto Rico Technical Center, ABBOTT (October 2007 – February 2009)

Responsible for providing technical, regulatory, and quality documentation support to drug product manufacturing. These supports include ensuring successful technology transfers for contract manufacturing product transfer, supporting plant work as needed, providing technical leadership in problem solving, and facilitating communication with M&ST staff management as well as other functional areas of interface.

Principal Process Development Engineer II, GPO MS&T Process Sciences & Engineering, ABBOTT (September 2004 – September 2007)

Responsible for providing technical, regulatory, and quality documentation support to drug substance manufacturing and third party manufacturing. Demonstrate scientific competency through laboratory/pilot plant and production experiments for process improvement/scale-up and validation; provide technical support to production and work on cost reduction and yield improvement projects.

Production Engineer, SPD Fermentation Recovery Finishing, ABBOTT (August 2003 – August 2004)

Provide Process/Project Engineering support for Fermentation production area. These supports include scoping, estimating, and executing under \$250M capital projects/capital plan development.

Process Development Engineer, SPD Technical Operations, ABBOTT (April 2001-July 2003)

Responsible for developing and implementing new and improved recovery and purification processes for drug substances from fermentation; coordinating and performing laboratory/pilot plant and production experiments for process development/scale-up and validation; providing technical support to production operations and work on cost reduction and yield improvement projects.

PUBLICATION AND PRESENTATION

Jenny Lau Eik Lang, Tapan Patel and F. Shutov, " Study of melt flow index and intrinsic viscosity properties of various virgin polymers and plastic scrap", Presented at the 108th Annual Tennessee Academic of Science Meeting, Cookeville, TN USA, November 11-13 (1998)

Jenny Lau Eik Lang, J. J. Biernacki, " Study of the reaction between fly ash and Calcium Hydroxide" Poster presentation submitted at the 109th Annual Tennessee Academie of Science Meeting, Memphis, TN USA, November 19 (1999)

PATENTS

Extruded Nutritional Powders Having Improved Emulsion Stability and Dispersibility and Methods of Manufacturing Same (Publication Number: WO/2014/066682, May 1, 2013)

Use of extrusion methods to improve heat labile vitamin stability (Publication Number: WO/2014/066680 A1, May 1, 2014)

Methods For Extruding Shaped Nutritional Products Using Vacuum Drying (United States 61/717,791; Filed October 24, 2012)